SPSD II

ANTARCTIC ICE-SHEET DYNAMICS AND CLIMATIC CHANGE: MODELLING AND ICE COMPOSITION STUDIES (AMICS)

H. DECLEIR, F. PATTYN, R. LORRAIN

PART 2

GLOBAL CHANGE, ECOSYSTEMS AND BIODIVERSITY

- ATMOSPHERE AND CLIMATE
- MARINE ECOSYSTEMS AND BIODIVERSITY
- TERRESTRIAL ECOSYSTEMS AND BIODIVERSITY
- NORTH SEA
- ANTARCTICA
- BIODIVERSITY

SCIENTIFIC SUPPORT PLAN FOR A SUSTAINABLE DEVELOPMENT POLICY
(SPSD II)

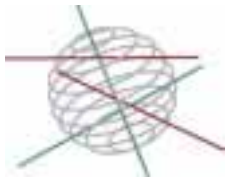

Part 2:
Global change, Ecosystems and Biodiversity

FINAL REPORT

ANTARCTIC ICE-SHEET DYNAMICS AND CLIMATIC CHANGE: MODELLING AND ICE COMPOSITION STUDIES (AMICS)

EV/08

R. Lorrain, R. Souchez, F. Debecker, D. Samyn, S. Sleewaegen, J-L. Tison -
ULB/Département des Sciences de la Terre et de l'Environnement (DSTE)

F. Pattyn, S. De Brabander, B. De Smedt, A. Huyghe, H. Decleir –
VUB/Vakgroep Geografie

January 2006

BELGIAN SCIENCE POLICY

D/2006/1191/8
Published in 2006 by the Belgian Science Policy
Rue de la Science 8
Wetenschapsstraat 8
B-1000 Brussels
Belgium
Tel: +32 (0)2 238 34 11 – Fax: +32 (0)2 230 59 12
http://www.belspo.be

Contact person:
Mrs Maaike Vancauwenberghe
Secretariat: +32 (0)2 238 36 13

'BELGIAN RESEARCH PROGRAMME ON THE ANTARCTIC, PHASE V'
BELGIAN FEDERAL SCIENCE POLICY OFFICE (BELSPO)

Research Project EV/03/08

Antarctic ice-sheet dynamics and climatic change: Modelling and Ice Composition Studies (AMICS)

REGINALD LORRAIN[1], FRANK PATTYN[2], ROLAND SOUCHEZ[1], FABIENNE DEBECKER[1], SANG DE BRABANDER[2], BERT DE SMEDT[2], ANN HUYGHE[2], DENIS SAMYN[1], SUZANNE SLEEWAEGEN[1], JEAN-LOUIS TISON[1] AND HUGO DECLEIR[2]

[1] Département des Sciences de la Terre et de l'Environnement (DSTE), CP 160/03, Université Libre de Bruxelles, Avenue F.D. Roosevelt 50, B-1050 Brussels
[2] Vakgroep Geografie, Vrije Universiteit Brussel, Pleinlaan 2, B-1050 Brussels

Final Report 2000–2005

Contents

ABSTRACT

The main objective of **AMICS** (**A**ntarctic ice-sheet dynamics and climatic change: **M**odelling and **I**ce **C**omposition **S**tudies) is to contribute to the international research effort leading to an improved understanding of the dynamic behaviour of the Antarctic ice sheet resulting from climatic change, through a better knowledge of the internal ice dynamics and the ice sheet's interactions with the subglacial environment.

To clarify the dynamic interactions between the ice sheet and the subglacial environment a new thermomechanical ice-sheet model was developed, including higher-order stress gradients. Such a model is capable of properly simulating the ice flow in areas characterized by complex basal interaction (ice streams, subglacial lakes, ...). As a contribution to the EPICA project, the model is imbedded in a large-scale model of the Antarctic ice sheet to determine the chronology and the origin of the ice within the EPICA DML ice core.

A comprehensive effort to improve our understanding of the physical processes at the interface between a frozen lake and a cold-based glacier explained the complex formation of the lake ice cover. It showed how sediments become trapped in lake ice and how this lake has contributed to the formation of the basal ice layer of the adjacent damming glacier. Moreover, an isotopic model has been elaborated for basal freeze-on associated with subglacial upward flow of pore water and tested against two Antarctic outlet glaciers by studying the δD-δ^{18}O relationships in the basal ice layers of these glaciers.

Investigation of the isotopic composition of the deepest part of the Vostok ice core shows the build-up of a highly deformed basal ice layer. Therefore, Lake Vostok's behaviour has been reassessed from new and existing ice core data. In view of these results, the higher-order model was applied to the area surrounding subglacial Lake Vostok. This showed for the first time that the surface flattening and turning of the ice flow across the lake are a direct consequence of the lack of friction at the ice-water interface, and that subglacial lakes can be at the origin of enhanced ice flow and the onset of continental ice streams. A detailed numerical investigation of such streams demonstrated that a large variability in glacier response can be expected when interaction with subglacial water flow is considered. Speedup and slowdown of such large flow features may be a result of ice piracy of neighboring streams.

The AMICS project has demonstrated that basal processes play an important – if not crucial – role in the ice flow of the vast interior of the ice sheet, a zone which was previously thought of being unconditionally stable. Subglacial interactions determine the onset of fast-flowing areas such as ice streams, which has its consequence for the stability of the Antarctic ice sheet with changing climate.

KEYWORDS: basal ice, cold-based glaciers, co-isotopic analysis, deep ice cores, EPICA, gas analysis, ice-sheet modelling, ice streams, lake ice, Lake Vostok, subglacial lakes

1 INTRODUCTION

Over the last decades, a number of deep ice-core drillings were carried out in Antarctica, such as Vostok, Dome Fuji and more recently Dome C. Analysis of these cores provides the scientific community with a continuous record of ice composition, which makes it possible to reconstruct climate and its variability over more than 800,000 years back in time. These data represent a time scale series of proxies of the most important climatic parameters, such as temperature, precipitation, atmospheric pressure, dust transport, and the corresponding atmospheric composition (in particular the concentration of greenhouse gases). This allows for a better insight in internal structure of the ice sheet, the deformation pattern and density. The relationships between climate fluctuations and the cryosphere can thus be investigated, which is essential for predicting future climatic changes. Interpreting an ice core – in terms of determining its chronology – demands a precise knowledge of the ice flow and dynamics of the inland ice sheet in the vicinity of the borehole, especially at depth and approaching the basal layers.

Recent investigations show that the inland ice flow is much more complex than previously thought (Bamber et al., 2000). Moreover, near the bottom of the ice core, a complex interaction of the basal layers of the ice sheet with the substratum is expected, further complicating its interpretation. These interactions, such as presence of liquid water and occurrence of melting and refreezing, play a major role in ice deformation and thus in ice flow, since they are to a large extent responsible for basal sliding which enhances ice flow. It is thus clear that the knowledge of the resulting flow pattern is essential not only in providing a correct age-depth relationship of the ice, but also in understanding the ice-sheet behaviour during past and future climatic changes.

Radio-echo-soundings in East Antarctica have revealed the existence of numerous areas of subglacial lakes. The largest one is Lake Vostok (14,000 km^2), near the homonymous Russian Station and drilling site. Smaller subglacial lakes are present in the immediate vicinity of Dome C, which is one of the EPICA[1] drilling sites. Understanding the ice flow over such a lake where the basal drag becomes zero, a situation comparable to ice shelves, opens up new research perspectives for understanding basal melting and accretion processes. In the case of the Vostok ice core, it was proved that ice below 3538 m is lake ice coming from Lake Vostok (Jouzel et al., 1999; Souchez et al., 2000b). This proved presence of lake ice under the East Antarctic Ice Sheet makes likely an entrainment of this ice by bottom deformation of the ice sheet. Since lake ice has properties completely different from glacier ice of meteoric origin, it can be recognized in a deep ice core and so used to study flow disturbances, for instance in the case of the EPICA basal sequence.

Over the last few years, the amount of data on the Antarctic ice sheet has increased tremendously, insofar that in some areas the data spreading is denser than the spatial resolution of most numerical models. Moreover, the data increase demonstrates a greater variability in ice sheet dynamics which cannot be explained by these models due to their lack of complexity. If we want to obtain accurate model predictions we should refine the models not only by increas-

[1] European Project for Ice Coring in Antarctica

ing the resolution but also by refining the physics involved. At present, most numerical ice-sheet models are based on the shallow-ice approximation, which determines the velocity field in an ice mass in a local way. However, the shallow-ice approximation is not valid near ice divides, nor for areas of fast ice flow or ice flow over subglacial lakes, where basal traction is very low or even zero. In such cases, the velocity is not a function of the local geometry of the glacier, but depends on the stress field up- and downstream. The ice mass will 'feel' what is happening up- or downstream through longitudinal coupling, and will react to this whenever basal traction is low. This non-local determination of the velocity and stress field complicates the 'ice-sheet' problem and demands a solution of the Stokes problem.

In Antarctica, basal interactions with the subglacial environment are not easily observed. Due to special environmental circumstances, the ice coming from the central part of the ice sheet does not completely fill the valleys of a marginal mountain range. Some of these valleys are even devoid of an ice cover and are called dry valleys. At the border of the ice sheet or at the margin of its outlet glaciers, basal ice is outcropping and can be sampled. Such a situation is encountered in the region called the Dry Valleys in South Victoria Land in the vicinity of the two permanent stations of McMurdo (USA) and of Scott Base (New Zealand). Interaction between these outlet glaciers and local glaciers with their beds or marginal lakes is of major interest. In this perspective there is a need for ice-composition studies relative to these contact zones

The importance of basal interactions is not limited to inland ice flow. The largest dynamical changes of the Antarctic ice sheet occur in the coastal area. According to the scientific recommendation of CLIC/WCRP,[2] we require a better knowledge on the present state of the mass balance of the Antarctic ice sheet. From a modelling perspective this requires an improved coupling of ice sheet/stream/shelf dynamics to further understanding of the stability of the ice sheet and to predict future change. Interaction between ice streams and their beds must be incorporated. In this perspective there is a need for ice-composition studies relative to the ice present and produced near grounding lines.

In the report we present our developments and findings with respect to a better understanding of the dynamic interactions of the ice sheet with the subglacial interface. Section 2.1 describes the development of a new thermomechanical ice-sheet model that solves the Stokes problem in an approximate fashion, i.e. by properly accounting for longitudinal and transverse stress gradients (so-called higher-order model). This model is capable of properly simulating the ice flow in areas characterized by complex basal interaction (ice streams, subglacial lakes, ...).

The higher-order model was applied to three distinct cases in which higher-order stress gradients play a dominant role. The first case being the transition zone between the ice sheet frozen to the bedrock and the ice flowing over a subglacial lake. Results are presented in section 3.4. The second case applies to the dynamic interaction of fast flowing outlet glaciers and/or continental ice streams that drain most of the ice flow from the interior of the Antarctic ice sheet. An analysis of the impact of basal water flow on the dynamics of such flow features is presented in section 3.5. In a third case, as a contribution to the EPICA project, the model is imbedded in a large-scale model of the Antarctic ice sheet to determine the chronology and the origin of the

[2]Climate and Cryosphere / World Climate Research Programme

ice within the EPICA DML ice core (see section 3.6).

Section 2.2 introduces the chemical and isotopic techniques which were applied to three case studies. The first one (section 3.1) is the study of a frozen lake into which a cold-based glacier is flowing. It shows that the way the ice cover formed is complex. It allows to explain how sediments become trapped in the lake ice and how this lake has contributed to the formation of the basal ice layer of the adjacent damming glacier. Moreover, an isotopic model has been elaborated for basal freeze-on associated with subglacial upward flow of pore water and tested against two Antarctic outlet glaciers by studying the δD-δ^{18}O relationships in the basal ice layers of these glaciers (section 3.3).

Investigation of the isotopic composition of the deepest part of the Vostok ice core shows the buid-up of a highly deformed basal ice layer. Therefore, Lake Vostok's behaviour has been reassessed from new and existing ice core data (section 3.2).

2 MATERIALS AND METHODS

2.1 Development of a new 3D thermomechanical ice sheet model including higher order stress gradients
(F. Pattyn)

Most ice-sheet models are based on the so-called 'shallow-ice approximation' or SIA (Hutter, 1983), which is valid for an ice mass with a small aspect ratio ($H \ll L$), where flow is dominated by internal shear deformation: ice flow is driven by gravity, and vertical shearing is concentrated close to the bedrock. Almost no shearing exists close to the surface. However, the SIA is not valid at all places in an ice sheet, such as at the ice divide or near the ice-sheet margin (Baral et al., 2001). Below the ice divide there is theoretically no shearing present. This would mean that – according to the SIA and for a Glen-type rheology – the effective stress becomes zero, implying an infinitely large viscosity so that the free surface is stiff against shearing. This is not realistic as longitudinal stresses must develop which enhance the effective stress and lower the viscosity. This effect goes beyond the lowest order of the shallow-ice approximation (Baral et al., 2001). A precise knowledge on the stress field underneath an ice divide is of importance to derive the vertical velocity, which determines age versus depth, thinning of the stratigraphic layers by vertical strain, and vertical advection of heat (Dansgaard and Johnsen, 1969). Numerical calculations have shown that the profiles of velocity versus depth have different shapes at divides compared to flank positions (Raymond, 1983; Schøtt Hvidberg, 1996).

Near the margin of ice sheets (which comprises grounding lines, transition zones, outlet glaciers and ice streams), all forces in the force balance become equally important, especially when basal sliding comes into play or even dominates the horizontal flow field. Longitudinal stretching and lateral shearing play an essential role in the dynamics of large outlet glaciers and major Antarctic ice streams. The governing processes near the margin involve a reduction of the basal drag, leading to significant basal motion (due to sliding and/or basal sediment deformation), which increases the complexity of the problem. Furthermore, thermomechanical control amplifies this complexity which might even lead to channeling of ice flow (Hindmarsh, 2001).

However, all these feedback processes are not clearly understood as thermomechanical models that solve the Stokes problem in three dimensions are not widely developed. Present-day three-dimensional numerical ice-sheet models including full thermomechanical coupling are those developed by Huybrechts (1990), Ritz et al. (1997), Greve (1997), or Marshall and Clarke (1997), to name a few. All these models have been successfully applied to simulate major present and palaeo ice-sheet behaviour on the globe. They are all based on the SIA and do not include longitudinal nor transverse stress gradients in a systematic way. The transition zone between different flow types (e.g. between ice-sheet and ice-shelf flow, or the onset regions of ice streams) is often not properly accounted for, even though all stresses and stress gradients are of equal importance in the force balance. Three-dimensional thermomechanically-coupled ice-sheet models including higher-order stress gradients are sparsely seeded. Among them are the models of Mayer (1996), Albrecht (2000) and Saito (2002), the latter two based on the model by Blatter (1995) and Colinge and Blatter (1998). The reason for this sparsity must be

sought in the complexity of the model description, the difficulty to obtain a numerically stable result, and the high computational cost, despite the exponential increase over time of computer power.

Within the AMICS framework, a new three-dimensional higher-order model (HO model; including longitudinal and transverse stress gradients) with full thermomechanical coupling is developed and briefly presented hereafter. A complete description is given in Pattyn (2003). It is based on a two-dimensional version developed earlier (Pattyn, 2000; Pattyn, 2002). Basic experiments with the model include the standard EISMINT I benchmark experiments (Huybrechts et al., 1996) as well the EISMINT II experiments with thermomechanical coupling (Payne et al., 2000).[3] Special attention is paid to the flow field underneath the ice divide and a comparison is made with a similar 3D model according to the SIA. An example of ice-stream development is given as well.

2.1.1 Brief model description

The model approach is based on continuum thermodynamic modelling, and encompasses balance laws of mass, momentum and energy, extended with a constitutive equation. Treating ice as an incompressible fluid with constant density, the equations for conservation of mass, momentum and energy are written as

$$\nabla \cdot \vec{\mathbf{v}} = 0\,, \tag{1}$$

$$\rho \frac{\mathrm{d}\vec{\mathbf{v}}}{\mathrm{d}t} = \nabla \cdot \sigma + \rho \vec{\mathbf{g}}\,, \tag{2}$$

$$\rho \frac{\mathrm{d}\,(c_p \theta)}{\mathrm{d}t} = \nabla \cdot k_i \nabla \theta + \Phi\,, \tag{3}$$

where ρ is the ice density, $\vec{\mathbf{g}}$ gravitational acceleration, $\vec{\mathbf{v}}$ the velocity vector, $[\sigma]$ the stress tensor, θ the ice temperature, c_p and k_i the heat capacity and thermal conductivity of the ice, respectively, and Φ internal frictional heating due to deformation. Values for constants are given in Table I.

Neglecting acceleration terms in (2) and considering the gravitational acceleration only important in the vertical direction, the linear momentum is solved in a somewhat reduced form. The major assumption to the force balance equations is to apply the hydrostatic approximation in the vertical. This implies that the variational stress is neglected, i.e. the resistance to a varying stress gradient in the direction of motion (the so-called T–term) in the vertically integrated force budget (Budd, 1971). This term is also known as the vertical resistive stress (Van der Veen and Whillans, 1989). Numerical calculations have shown that vertical resistive stress occurs in regions where the flow regime changes, such as near the ice divide or near the margin, but that this stress component is almost two orders of magnitude smaller than other normal and shear-stress components (Pattyn, 2000). Normal stress deviators are not neglected and accounted

[3] EISMINT = European Ice Sheet Modelling INiTiative

Symbol	Constant	Value	Units
β	Dependence of melting on pressure	9.8×10^{-8}	K Pa^{-1}
ρ	Ice density	910	kg m^{-3}
B_0	Flow-rate factor	2.207	Pa a$^{1/n}$
C	Flow-rate factor	0.16612	K^K
G	Geothermal heat flux	4.2×10^{-2}	W m^{-2}
K	Flow-rate exponent	1.17	
L	Specific latent heat of fusion	3.35×10^5	J kg^{-1}
Q	Activation energy for creep	7.88×10^4	J mol^{-1}
R	Universal gas constant	8.31	J mol^{-1} K^{-1}
θ_r	Limit temperature in flow-rate factor	273.39	K
c_p	Heat capacity of ice	2009	J kg^{-1} K^{-1}
g	Gravitational constant	9.81	m s^{-2}
k_i	Thermal conductivity of ice	6.62×10^{-7}	J m^{-1} K^{-1} a^{-1}
m	Enhancement factor in flow law	1	
n	Exponent in Glen's flow law	3	

Table I: *Constants used in the numerical model.*

for properly. The stress-deviator components are obtained by subtracting the amplitude of the hydrostatic pressure, or $\sigma'_{ij} = \sigma_{ij} - \frac{1}{3}\delta_{ij}\sum_k \sigma_{kk}$, where δ_{ij} is the Kronecker delta. Inserting the stress-deviator components and assuming a zero normal stress at the surface, the horizontal force-balance equations become after some algebraic manipulation

$$\frac{\partial}{\partial x}\left(2\sigma'_{xx} + \sigma'_{yy}\right) + \frac{\partial \sigma'_{xy}}{\partial y} + \frac{\partial \sigma'_{xz}}{\partial z} = \rho g \frac{\partial s}{\partial x}\,, \tag{4}$$

$$\frac{\partial}{\partial y}\left(2\sigma'_{yy} + \sigma'_{xx}\right) + \frac{\partial \sigma'_{xy}}{\partial x} + \frac{\partial \sigma'_{yz}}{\partial z} = \rho g \frac{\partial s}{\partial y}\,. \tag{5}$$

The constitutive equation governing the creep of polycrystalline ice and relating the deviatoric stresses to the strain rates, is taken as a Glen-type flow law with exponent $n = 3$ (Paterson, 1994)

$$\sigma'_{ij} = 2\eta\,\dot{\varepsilon}_{ij}, \quad \eta = \frac{1}{2}A(\theta^*)^{-1/n}\left(\dot{\varepsilon} + \dot{\varepsilon}_0\right)^{(1-n)/n}\,, \tag{6}$$

where $\dot{\varepsilon}$ is the second invariant of the strain-rate tensor, defined by $\dot{\varepsilon}^2 = \sum_{ij}\frac{1}{2}\dot{\varepsilon}_{ij}\dot{\varepsilon}_{ij}$ and η is the effective viscosity. $\dot{\varepsilon}_0$ is a small number (10^{-30}) to make the viscosity finite. The flow-law rate factor $A(\theta^*)$ is a function of temperature, where θ^* is the ice temperature (K) corrected for pressure melting, i.e. $\theta^* = \theta + \beta P$, and where P is the ice pressure ($P = \sigma'_{xx} + \sigma'_{yy} - \rho g(s-z)$). Following Hooke (1981), $A(\theta^*)$ is parameterized as an Arrhenius relationship:

$$A(\theta^*) = m\left(\frac{1}{B_0}\right)^n \exp\left(\frac{3C}{\left(\theta_r - \theta^*\right)^K} - \frac{Q}{R\theta^*}\right)\,. \tag{7}$$

Here Q is the activation energy for ice creep, R is the universal gas constant, and m is an enhancement factor (or tuning parameter). Another assumption made is that horizontal gradients of the vertical velocity are small compared to the vertical gradient of the horizontal velocity, or $\partial w/\partial x \ll \partial u/\partial z$ and $\partial w/\partial y \ll \partial v/\partial z$. This is a common assumption in ice-sheet modelling, and is valid for most of the ice sheet domain. Combining the flow-law equation (6) and the horizontal stress-field equation (4) and (5), and replacing the strain-rate components by velocity gradients, one obtains

$$\frac{\partial}{\partial x}\left(4\eta\frac{\partial u}{\partial x}+2\eta\frac{\partial v}{\partial y}\right)+\frac{\partial}{\partial y}\left(\eta\frac{\partial u}{\partial y}+\eta\frac{\partial v}{\partial x}\right)+\frac{\partial}{\partial z}\left(\eta\frac{\partial u}{\partial z}\right)=\rho g\frac{\partial s}{\partial x}\,, \tag{8}$$

$$\frac{\partial}{\partial y}\left(4\eta\frac{\partial v}{\partial y}+2\eta\frac{\partial u}{\partial x}\right)+\frac{\partial}{\partial x}\left(\eta\frac{\partial u}{\partial y}+\eta\frac{\partial v}{\partial x}\right)+\frac{\partial}{\partial z}\left(\eta\frac{\partial v}{\partial z}\right)=\rho g\frac{\partial s}{\partial y}\,. \tag{9}$$

where

$$\eta=\frac{1}{2}A(\theta^*)^{-1/n}\left\{\left(\frac{\partial u}{\partial x}\right)^2+\left(\frac{\partial v}{\partial y}\right)^2+\frac{\partial u}{\partial x}\frac{\partial v}{\partial y}+\right.$$
$$\left.+\frac{1}{4}\left(\frac{\partial u}{\partial y}+\frac{\partial v}{\partial x}\right)^2+\frac{1}{4}\left(\frac{\partial u}{\partial z}\right)^2+\frac{1}{4}\left(\frac{\partial v}{\partial z}\right)^2+\dot{\varepsilon}_0^2\right\}^{(1-n)/2n}\,. \tag{10}$$

Neglecting horizontal diffusion, the energy-balance equation (3) is written as

$$\rho c_p\frac{\partial\theta}{\partial t}=k_i\frac{\partial^2\theta}{\partial z^2}-\rho c_p\left(u\frac{\partial\theta}{\partial x}+v\frac{\partial\theta}{\partial y}+w\frac{\partial\theta}{\partial z}\right)+2\dot{\varepsilon}\sigma\,, \tag{11}$$

where σ is the effective stress or the second invariant of the stress tensor. The heat transfer is thus a result of vertical diffusion, horizontal and vertical advection, and internal deformational heating.

Using a kinematic boundary condition at the upper and lower surface of the ice mass (see below), the mass balance equation (1) is integrated along the vertical in order to obtain an expression for the change of local ice thickness in space

$$\frac{\partial H}{\partial t}=-\nabla\int_b^s\vec{\mathbf{u}}\,\mathrm{d}z+M_s-M_b=-\nabla\left(\overline{\vec{\mathbf{u}}}H\right)+M_s-M_b\,, \tag{12}$$

where $\vec{\mathbf{u}}$ is the horizontal velocity vector (m a^{-1}), H is the ice thickness (m), M_s is the local accumulation–ablation function (m a^{-1} ice equivalent), and M_b is the melting rate at the base of the glacier (m a^{-1}). Negative values of M_b imply refreezing, which is not considered here. Local ice thickness variations are thus in balance with the divergence of the ice flux and the net input of mass at the upper and lower surface of the ice mass.

In order to verify the results of the HO model, a 'shallow-ice' model was implemented as well. According to the SIA the horizontal velocity field is defined as (e.g. Huybrechts et al., 1996; Payne et al., 2000)

$$\vec{\mathbf{u}}(z) = -2\,(\rho g)^n\,|\nabla s|^{n-1}\,\nabla s \int_b^z A(\theta^*)\,(s-z)^n\;\mathrm{d}z + \vec{\mathbf{u}}_b\,. \tag{13}$$

Note that according to the SIA the velocity is obtained through vertical integration over the ice column and is only a function the local geometry of the ice mass.

Boundary conditions to the ice mass are zero ice thickness ($H = 0$) at the edges of the model domain, a stress-free surface and no-slip boundary condition at the base ($u_b = v_b = 0$). In some of the experiments hereafter a stress-free boundary condition was applied at some grid points of the numerical domain (free-slip condition or zero traction). These two treatments of basal conditions represent only the most extreme end members of reality and are not applicable to many natural situations (including ice streams, where basal drag is small but not zero). However, such conditions make it easier to compare the model with benchmark tests. Boundary conditions to the thermodynamic equation (11) follow from the mean annual air temperature at the surface. At the base, the temperature gradient is defined as

$$\frac{\partial \theta_b}{\partial z} = -\frac{G + \tau_{\mathbf{b}}\,\mathbf{u_b}}{k_i}\,, \tag{14}$$

where G is the geothermal heat flux. For numerical convenience a dimensionless vertical coordinate is introduced to account for ice-thickness variations, and which is defined as $\zeta \equiv (s-z)/H$, so that ζ = 0 at the upper surface and ζ = 1 at the base of the ice mass. More details on the numerical solution of the compete velocity field can be found in Pattyn (2003).

2.1.2 EISMINT experiments (Exp. A)

Basic experiments were carried out following the EISMINT benchmark for large-scale ice sheet models, more specifically the "moving margin" benchmark of Huybrechts et al. (1996). The model domain is 1500 $\times$ 1500 km in the horizontal. Following the EISMINT II experiments (Payne et al., 2000), a grid resolution of 25 km in both horizontal directions was taken, which corresponds to a numerical grid of 61 $\times$ 61 grid points. The accumulation / ablation rate M_s is a function of the distance from the ice divide, i.e.

$$M_s(x,y) = \min\left\{M_{\max}, S_b\left(R_{\mathrm{el}} - \sqrt{(x-x_{\mathrm{sum}})^2 + (y-y_{\mathrm{sum}})^2}\right)\right\}\,, \tag{15}$$

where $M_{\max}$ is the maximum accumulation rate and S_b the gradient of accumulation rate change with horizontal distance. The accumulation rate is zero at a radial distance R_{el} from the summit $(x_{\mathrm{sum}}, y_{\mathrm{sum}})$, where x and y are distance in km. At a distance larger than R_{el} from the summit,

Parameter	Value	Units
u_b, v_b	0	m a^{-1}
$A(\theta^*)$	10^{-16}	Pa^{-1} a^{-1}
$M_{\max}$	0.5	m a^{-1}
S_b	10^{-2}	m a^{-1} km^{-1}
R_{el}	450	km
$\theta_{\min}$	238.15	K
S_θ	1.67×10^{-2}	K km^{-1}
x_{sum}, y_{sum}	750	km

Table II: *List of parameters used for experiment* A.

surface mass balance becomes negative (ablation). The ice-surface temperature is also made a function of distance from the summit, according to the benchmark experiments by Payne et al. (2000):

$$\theta_s(x,y) = \theta_{\min} + S_\theta \sqrt{(x - x_{\mathrm{sum}})^2 + (y - y_{\mathrm{sum}})^2}\,, \tag{16}$$

where $\theta_{\min}$ is the minimum surface air temperature and S_θ is the gradient of air temperature change with distance form the summit. The model was run from zero ice thickness until a steady-state was reached (after 200 000 years of calculation). Two types of experiments were carried out with both the HO model (subscript 1) and the SIA model (subscript 0), similar to the experiments described by Saito et al. (2003). Experiment A is an isothermal experiment. Its numerical parameters are listed in Table II.

Figure 1 displays the surface topography of the ice sheet in steady state for A_1. This ice-sheet configuration is similar to the SIA solution A_0, as is expected, since the SIA is valid for large ice sheets resting on a flat bed. The difference between A_1 and A_0 amounts to 10 m. A_1 results in a somewhat smaller ice sheet and has a flatter ice divide. The differences at the divide are traced back to the effect of the inclusion of longitudinal stress gradients in the HO model, which is the only nonzero stress component at the symmetrical ice divide.

The vertical velocity field demonstrates the major difference between both models (Figure 2). A lower vertical velocity under the ice divide for A_1 results in a "bump" in the vertical velocity field, confined to the immediate region of the ice divide (Figure 2a). This corresponds to the so-called "Raymond bump" (Raymond, 1983; Schøtt Hvidberg, 1996), due to the fact that ice deep under an ice divide should be very hard and slow to flow, so that upper layers would tend to drape themselves over it. This anomaly in vertical velocity is a result of differences in the horizontal velocity field: close to the ice divide surface horizontal velocity is higher for A_1 compared to A_0. However, horizontal velocity at depth is lower than for A_0. This lower velocity is necessary to compensate for the higher surface velocity: as the surface mass balance is only a function of distance from the summit, the steady-state ice flux at any point should be the same for both A_0 and A_1. Since ice thickness is similar in both experiments (a difference of only ±10 m), the vertical integrated horizontal velocity should be the same for both models. Further away

from the ice divide, the difference in horizontal velocity between both models disappears. The divide anomaly is also observed in the basal temperature: a “hot spot” arises underneath the ice divide according to A_1 (Figure 3), due to the difference in vertical advection.

All these results – anomalies in vertical and horizontal flow field and temperature near the ice divide – are corroborated by the experiments carried out by Saito et al. (2003). However, their model results show a slightly thicker A_1 ice sheet, while the present study shows a thinner steady-state ice sheet compared to A_0. This difference is probably related to the type of nu-

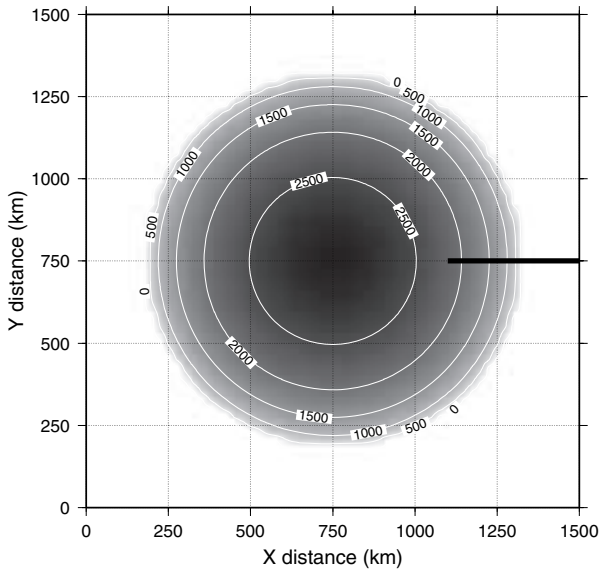

Figure 1: *Predicted surface topography of the steady-state ice sheet after 200 000 years of integration according to experiment* A_1. *The thick black line shows the position of the “ice stream” for experiment* B_1.

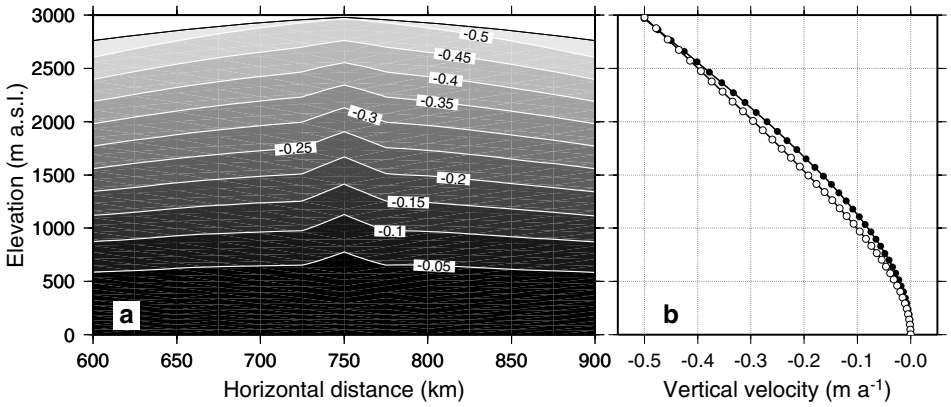

Figure 2: *Predicted vertical velocity: (a) near the ice divide for* A_1*; (b) at the ice divide for* A_1 *(black circles) and* A_0 *(white circles). Note the ‘bump’ in vertical velocity at the ice divide, which is not found in* A_0.

merical scheme used for the ice sheet evolution equation. The “hot spot” under the divide was determined previously by Dahl-Jensen (1989).

2.1.3 Ice stream evolution (Exp. B)

Starting from the steady-state ice-sheet conditions and temperature field from experiment A_1, an ice stream was generated by adjusting the basal boundary condition to a stress-free surface for the following coordinates: $i = 31$ and $j \geq 45$. The ice stream thus starts at a distance of 350 km from the ice divide and stretches to the edge of the model domain (Figure 1). The width of the ice stream is one grid point, or 25 km.

Figure 4 shows the evolution of the ice stream for the first 100 year after invoking the stress-free boundary conditions. Rather rapidly the ice velocity increases with almost two orders of magnitude, to reach maximum values of 2 500 km a^{-1}, a typical value for an Antarctic ice stream. Also, the surface topography changes dramatically to become almost flat over the whole length of the ice stream. Similar characteristics of ice-stream behaviour are shown in early flowline models of Van der Veen (1987). The major difference here is that both longitudinal stresses and transverse shear stresses are properly accounted and solved for in three dimensions.

The model result shows a concave inflection point at the onset of the ice stream, similar to the transition between an ice sheet and an ice shelf (Figure 4). It should be noted here that the basal boundary condition applied to our ice stream is similar to that of an ice shelf. Associated with the sudden increase in mass flux is a forward migration of the edge of the ice sheet, forming a frontal “bulge” (Figures 4 and 5a). Basal shear stress is zero along the whole length of the ice stream (Figure 5b). As a result, the surface velocity equals the basal velocity for the whole length of the ice stream (not shown). The longitudinal stress deviator reaches a maximum

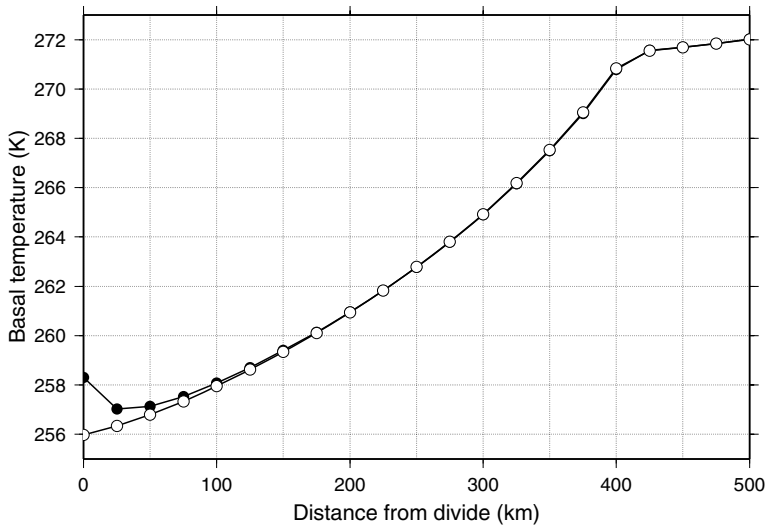

Figure 3: *Predicted basal temperature θ_b for A_1 (black circles) and A_0 (white circles). Note the “hot spot” under the ice divide.*

(extension flow) at the onset of the ice stream and a minimum (compressive flow) at the edge of the ice sheet (Figure 5c), but remains fairly low ($\sigma'_{xx} \sim 0$) along the whole length of the ice stream.

Transverse shear stress shows a pattern that is related to the existence of shear margins and is characterized by high positive values at the southern shear margin of the ice stream and high negative values at the northern shear margin. This results in an important lateral drag over the central part of the ice stream (not shown), which will – due to the absence of the basal shear as well as longitudinal stress gradients – balance the driving stress in the central part of the ice stream. The shear margins are a consequence of the rapid ice flow embedded in the slow-moving ice sheet. Both patterns of longitudinal and transverse shear stress are typical features for existing Antarctic ice streams, such as the Siple Coast ice streams (Whillans and Van der Veen, 1997), albeit that the magnitude of the marginal shear stress (20–80 kPa in Fig. 5) is relatively small compared to the magnitude of marginal shear stresses calculated for modern Antarctic ice streams.

2.1.4 Discussion and conclusions

The numerical model developed and presented here is a three dimensional thermomechanical ice-sheet model including higher-order (HO) stress gradients. Similar HO models exist, most of them solving for the stress field, using the method proposed by Van der Veen and Whillans (1989) and Van der Veen (1989). The uniqueness of this model lies in the fact that it solves the force-balance equations in their 'derivative' form, by formulating them in terms of velocity gradients (using Glen's flow law) and solving second derivatives analytically instead of numerically.

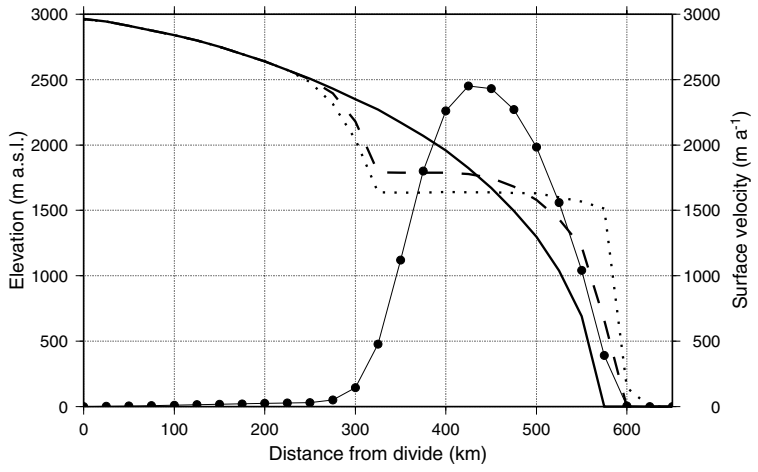

Figure 4: *Evolution of an ice stream (*B_1*) starting from the steady-state configuration of* A_1*. Predicted surface topography at* $t = 0$ *(solid line), at* $t = 50$ *year (dashed line) and at* $t = 100$ *year (dotted line) is displayed, after invoking a stress-free basal condition* $\tau_b = 0$ *along* $y = 750$ *km and between* $x = 350$ *km from the divide and the edge of the model domain. Predicted surface velocity at* $t = 50$ *year is given in solid circles.*

The resulting equations look rather cumbersome, but assure a high numerical stability.

Results of basic experiments are in agreement with results from Saito et al. (2003), and the solution under the ice divide ('Raymond bump' and 'hot spot') is confirmed by earlier flowline studies (Raymond, 1983; Dahl-Jensen, 1989). Two examples of prognostic model runs that can only be solved with a HO model are the ice-stream development and the ice flow over a

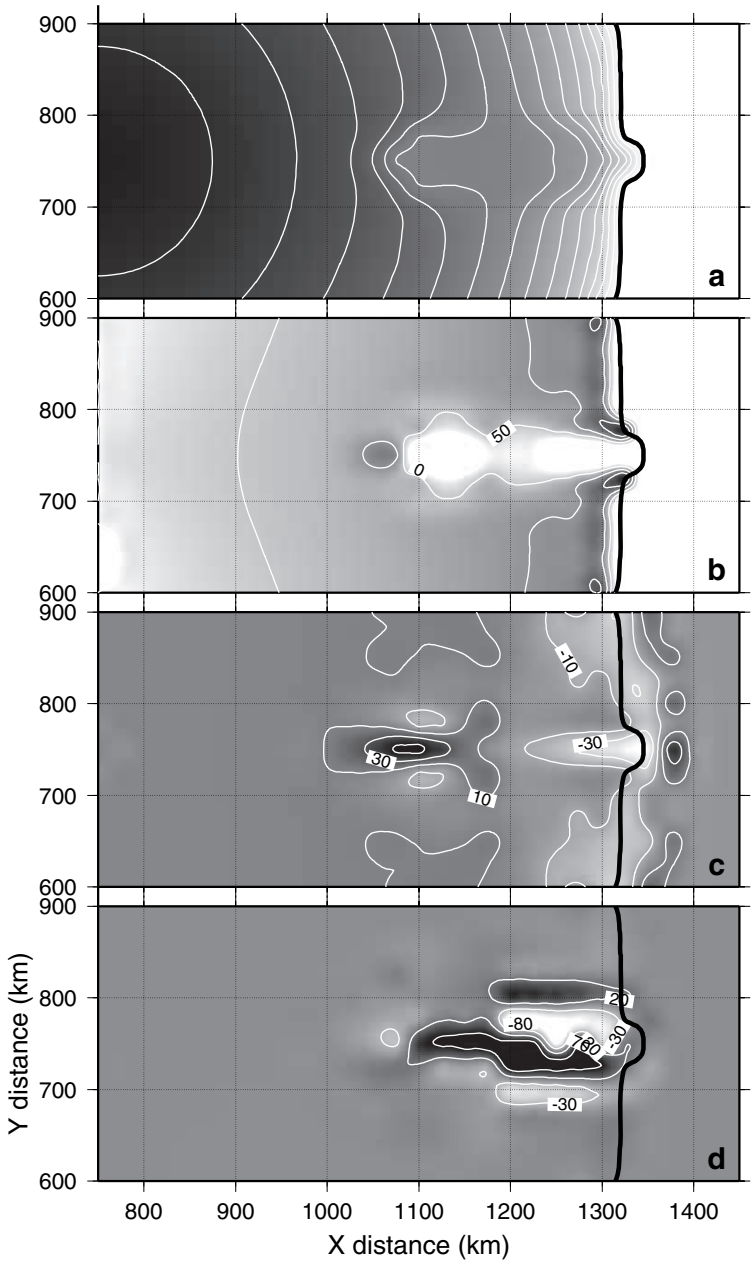

Figure 5: *Experiment* B_1. *(a) Predicted surface topography (m), (b) predicted basal shear stress* $\sigma_{xz}(b)$ *(kPa), (c) predicted surface longitudinal stress deviator* $\sigma'_{xx}(s)$ *(kPa), (d) predicted surface transverse shear stress* $\sigma_{xy}(s)$ *(kPa) at* $t = 50$ *year. The ice stream is situated at* $y = 750$ *km and stretches between* $x = 1100$ *km and the edge of the model domain* $x = 1500$ *km.*

subglacial lake, both simulated by considering locally a stress-free basal surface. Changing from a basal-stress dominated regime to a basal stress-free regime is similar to the ice-sheet / ice-shelf / grounding-line problem, which remains a hot topic amidst the ice-sheet modelling community. For instance, Marshall and Clarke (1997) solved this problem by treating the ice sheet area as a binary mixture of sheet ice (shallow-ice approximation) and stream ice (vertically integrated force-balance equations), which reduces the model complexity. In the present model a proper treatment of the transition zone is given, as the ice mass is considered as one single continuum. In reality, the reduction of basal drag in an ice stream is a complex process involving basal hydrology, sediment deformation, basal melting and sliding. Nevertheless, the simple basal boundary switch seems sufficient to explain major processes that are observed in real ice masses.

2.2 Ice composition studies
(R. Lorrain)

Ice samples are provided, either as ice cores by a drilling operation or as ice blocks using a chainsaw. They are stored in plastic bags and kept at a temperature below -18°C. Moreover, the samples cut for the analyses are retrieved in the cold room of the laboratory after shaving the walls of the cores or re-sawing a slice, 1cm thick, parallel to each side of the chain-sawed blocks. These subsamples are cut with a non contaminating band saw or, if they are rich in mineral particles, with a diamond wire saw (Tison, 1994).

The samples are studied for their gas characteristics using methods developed in our laboratory. CO_2, CH_4, O_2 and N_2 concentrations are measured by gas chromatography (Interscience Trace GC) using a crushing method to extract the gas (dry extraction) The procedure followed was fully described by Raynaud et al. (1982) and Barnola et al. (1983). The precision of the measurements is 2.5% for CO_2 and 0.4% for O_2 and N_2.

The CH_4 concentrations are also measured by gas chromatography (Chrompack CP 9001) but the gases are extracted using a melting-refreezing method (Blunier et al., 1993). Total gas content are determined by a melting-refreezing method using a Toepler pump. This method was fully described by Raynaud et al. (1988) and Blunier et al. (1993). The relative precision is better than 5% (Martinerie et al., 1994). The chemical analyses are carried out by atomic absorption spectrophotometry (Varian SpectrAA-300) for the major cations (Na, K, Ca, Mg) with a precision of 3% and by ion chromatography (Dionex DX-100 with conductimetric detector) for the major anions (Cl, SO_4, NO_3) with a precision of 5% for Cl^- and SO_4^{2-} for the concentration ranges encountered. NO_3^- was undetectable in most of our samples (detection limit = 0.2 ppm). The stable isotope measurements are performed at the Nuclear Research Center of Saclay (France), HDO and $H_2^{18}O$ concentrations are given in units versus VSMOW (Vienna Standard Mean Ocean Water) and expressed in per mil. The results obtained in δD and $\delta^{18}O$ on mass spectrometers have an accuracy of about 0.1‰ in δD and 0.05‰ in $\delta^{18}O$. Only a few milliliters are required to perform both analyses.

3 CASE STUDIES

3.1 Study of a dry-based Antarctic lake and implications for glacier-lake interactions *(R. Lorrain, S. Sleewaegen, F. Debecker, S. Fitzsimons, R. Souchez)*

3.1.1 Introduction

The McMurdo Dry Valleys region, an unglaciated area situated along the coastal regions of South Victoria Land (Antarctica), displays numerous perennially-frozen lakes, either in land-locked basins or dammed by local "alpine" glaciers. Such lakes contain liquid water beneath the ice cover (wet-based) or are frozen through to the bed (dry-based). In the latter case, as indicated by Chinn (1993), the ice thickness may far exceed those of the wet-based lakes. Once a lake is frozen to its bed, there is no more latent heat released by freezing at the base of the ice cover and a greater thickness of ice can be maintained under a given climatic regime.

The Dry Valleys lakes have been studied by numerous authors from the point of view of physical limnology, water chemistry or microbial ecology (see for example Chinn, 1993; Simmons et al., 1993; Spigel and Priscu, 1998; Priscu et al., 1998). The ice cover itself was much less studied, the more recent investigation being that of Adams et al. (1998) conducted on Lake Bonney. In another extensive study, Chinn (1993) shows that dry-based lakes are the most common types found at higher altitudes than the "regional snowline" or away from the arid Dry Valleys area.

In this section, we focus on a dry-based lake in order to study how sediments become trapped in the lake ice, and how the ice cover itself was formed. In the same way we show how this lake has contributed to the formation of the basal ice layer of the adjacent cold-based damming glacier. In a previous publication, Lorrain et al. (1999) concluded that water from that lake has played a major role in the formation of the stacked sequence of ice and sediment layers accreted at the glacier base. This conclusion was shown to be consistent with a previously proposed model of debris entrainment by cold-based glaciers flowing into lakes (Fitzsimons, 1996). This suggests a wet-based lake in the past and progression of the glacier above the lake margins. New fieldwork allowed to realize that the studied lake is frozen to the bed. The question of the origin of the liquid water considered in the model of debris entrainment has thus to be re evaluated.

The present study is based on data obtained not only from sedimentological investigations but also from ice composition analyses. Stable isotopes (δD and δ^{18}O), major ions, total gas content and gas composition analyses were performed; ice textural and structural studies were also carried out.

3.1.2 Site description

The dry-based lake investigated is Lake Popplewell (unofficial name), a small perennially frozen lake of Taylor Valley (Figure 6a) about 350m long and 150m wide, dammed by Suess Glacier descending on the slope of the eastern Asgard Range into the Taylor Valley.

The surface of Lake Popplewell, which is about 110 m a.s.l, appears bluish and very smooth, except where a few ice mounds are present (Figure 6b). The latter are less than 1 m high, have a diameter of about 10 m, and present some shallow radial cracks. During the summer, a narrow moat (1.5 m of mean width) of liquid water appears mainly along the southern shore. This moat is even narrower along the northern shore because this side is more frequently in the shadow of the steep slope which dominates the valley; sometimes, the moat does not form on the northern side.

The lake ice was drilled during the summer (January 1998) at four locations (points A to D in Figure 6a) with a SIPRE-type ice auger, 7.5 cm in diameter. All drilling was stopped when the auger was not able to go deeper. In each case, the ice was in contact with frozen sediments, which we consider to be the bottom sediments, indicating a dry based lake. The ice thickness varies between 2.47 and 4.76 m. Borehole temperature, measured a few hours after coring, was never lower than -0.5°C. Liquid water was not encountered except in one case, in a pocket about 40 cm thick located at about 280 cm deep. Similar water pockets have been observed by Chinn (1993) and Fritsen et al. (1998) in the ice covering neighboring lakes (Lake Bonney and Lake Hoare – see Figure 6a).

The ice cores retrieved from Lake Popplewell were transferred frozen to the laboratory in Brussels, where they were kept at -18°C. Close examination of the four cores was performed in the

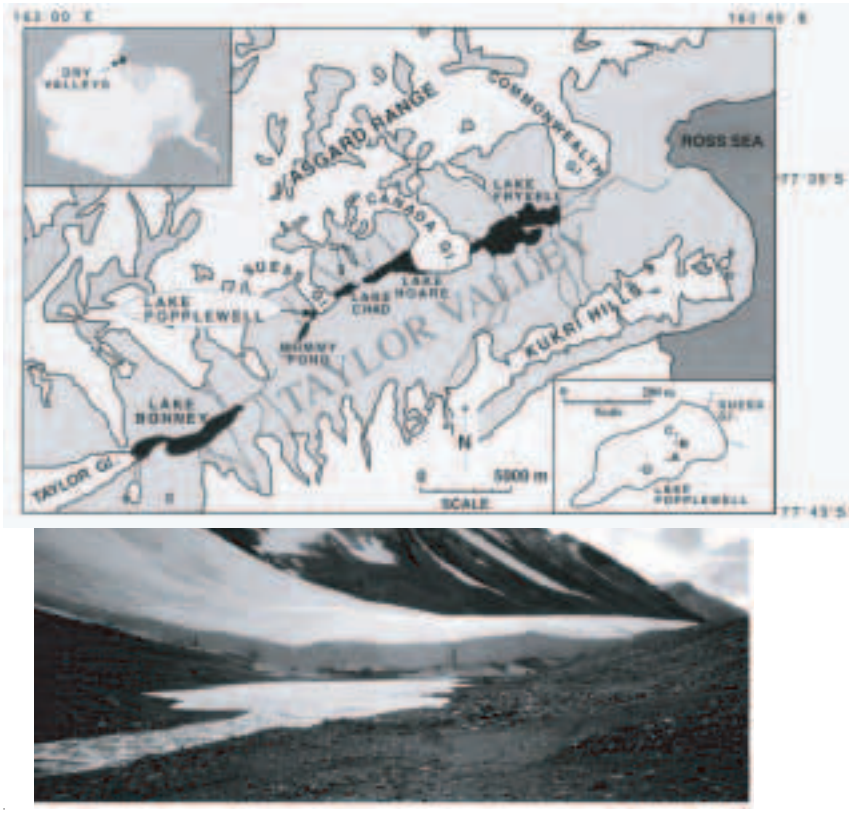

Figure 6: *(a) Location map of the perennially frozen lakes of Taylor Valley (dotted lines represent melt-streams). Close-up of Lake Popplewell showing coring sites, and location of the Dry Valleys in Antarctica. (b) Eastward view of Lake Popplewell with Suess Glacier in the background.*

cold room. Longitudinal thin sections were cut all along the cores and photographed between crossed polaroids allowing ice-texture observations and descriptions.

Sampling for isotopic, ionic and gas analyses was performed along the lines described in Section 2.2 of this report. The analytical techniques used as well as the related precision of the measurements are also given in this section. Moreover, samples for sedimentological analyses were also taken in the cold room. These samples were analyzed in the Blaustein Institute for Desert Research in Israel (Offer et al., 1993): data were obtained from grain size and micromorphological analyses (Sedigraph and Scanning Electron Microscope (SEM)), mineralogical investigations by X ray diffraction and elemental chemistry.

3.1.3 Results

It clearly appeared that the four cores retrieved from the lake ice were very similar except the basal part of the ice core A (Figure 6a). The particular situation encountered there explains why we concentrate our attention on that core: it is the longest, reaching the lake bed at a depth of 476 cm, and the only one containing in its deepest quarter well developed sediments layers a few centimeters thick interbedded with thicker ice bands. We also present the data obtained from the detailed sampling of core D.

3.1.3.1 Core A

Figure 7 gives the types of ice encountered in ice core A together with isotopic and chemical profiles. The upper part of the ice core down to a depth of 307 cm consists of lake ice with elongated crystals (about 40 cm long) having horizontal c-axes (Figure 8a). It is devoid of visible particles and contains vertical cylindrical bubbles about a few mm wide. At a depth of 347 cm, below a water pocket, there is a change in ice stratigraphy: a 5 cm thick ice layer with small crystals (a few mm long) and numerous small spherical bubbles is present, just above an ice cemented sediment layer about 9 cm thick. From the base of this latter layer, sediments penetrate underlying ice within narrow vertical pipes, which disappear below 365 cm (Figure 8b). From 361 cm to 423 cm, clear ice with clusters of particles is present. Ice crystals are still elongated but only a few cm long (Figure 8c). They show irregular boundaries and contain highly elongated bubbles. Below 423 cm, clear ice with spherical bubbles and sediment layers are interbedded until the lake bottom is reached at 476 cm. This ice shows polygonal crystals ranging from 0.1 to 1.3 cm in diameter (Figure 8d).

The isotopic and chemical profiles displayed in Figure 7 show striking features. The δD and $\delta^{18}O$ values become more negative downwards indicating an impoverishment in heavy isotopes down to 287 cm. This is followed by an enrichment between depths of 287 cm and 306 cm where impoverishment in heavy isotopes resumes, values as low as -286.7‰ in δD and -38.65‰ in $\delta^{18}O$ being reached at the lake floor. Concerning the chemical profiles, all exhibit low concentrations in Na^+, Ca^{2+}, Cl^-, SO_4^{2-} down to a depth of 355 cm i.e. at the level of the first sediment layer. Then the concentrations increase and reach the highest values for all the

elements measured at 434 cm. The concentration increase reaches more than 300 times the values measured at the top of the core.

Sedimentological investigations produced the following results. Grain-size analysis of the sediment layer at a depth of 352 cm shows a bimodal distribution with one peak in the sand class and the other in the fine silt class (Figure 9).

The intermediate class around 80 m is quite weakly represented. Observation by scanning electron microscope shows that most of the particles exhibit features characteristic of aeolian facies. Some diatoms are present among the particles. X-ray diffraction shows that quartz, feldspars and calcite are the dominant minerals with some kaolinite and montmorillonite in the finer fraction. Element chemical analyses reveal the relatively high abundance of calcium (up to 36%), iron (up to 13%) and sulphur (up to 2%). Since sulphur-bearing inorganic minerals (pyrite, mirabilite, gypsum) are not present, it seems that sulphur is bound to organic compounds.

Algal mats are present on the lake floor and as traces in the sediment layers within the ice core. A microbial activity based on the sulphur cycle in an oxygen-depleted environment could have been present at the bottom of the lake to explain the high sulphur and iron content of the

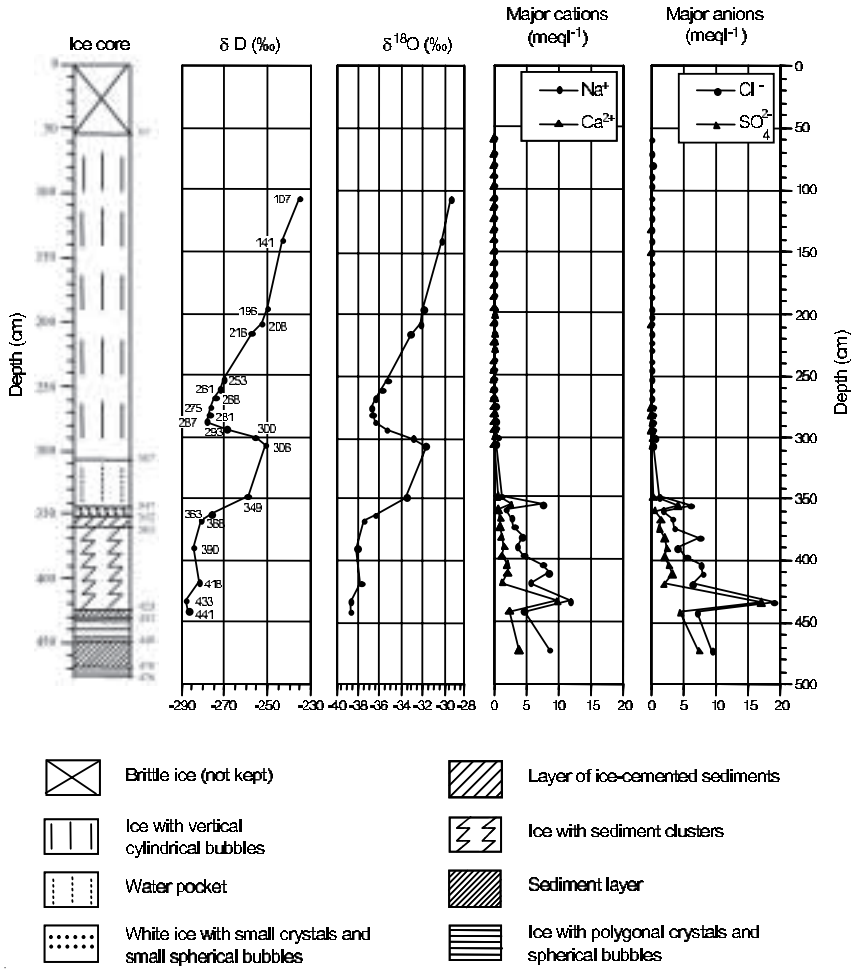

Figure 7: *Main characteristics of core A: types of ice, stable isotopes and major ions profiles.*

sediments. Abundant granules of iron and sulphur compounds have been reported in similar mats of the neighboring lakes Fryxell and Hoare (Simmons et al., 1993). In the ice with cylindrical bubbles present from the top to the depth of 347 cm, gas analyses performed on two samples give values of CO2 concentration ranging from 866 to 2250 ppmv and O_2/N_2 ratios ranging from 0.40 to 0.64. By contrast, the ice with spherical bubbles situated at the bottom

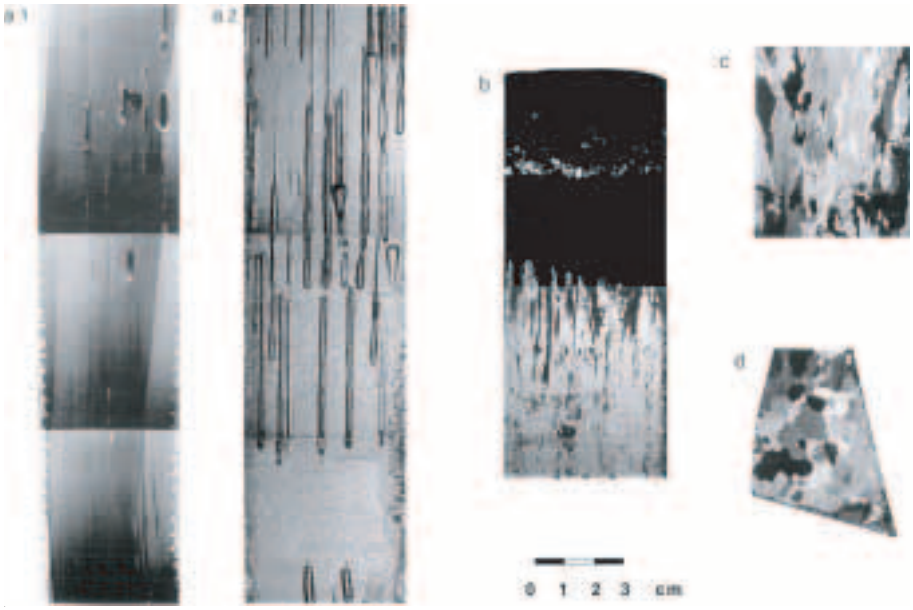

Figure 8: *Different ice facies encountered in core A: common elongated crystals (a1: thin sections between crossed polaroids) containing vertical cylindrical bubbles (a2: thick section in normal light); (b) sediment filled vertical pipes below the sediment layer present at a depth of 352 cm (normal light); (c) elongated crystals with irregular boundaries located at depths between 361 and 423 cm (thin section, polarized light); (d) ice with polygonal crystals near the lake bottom (thin section, polarized light).*

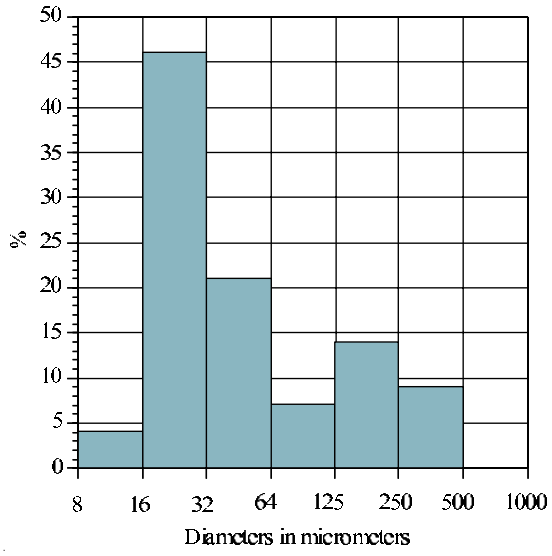

Figure 9: *Grain-size distribution of the 9 cm thick sediment layer present at a depth of 352 cm.*

shows a CO_2 concentration of 252076 ppmv and a O_2/N_2 ratio of only 0.12. This confirms the oxygen-depleted conditions at the bottom.

3.1.3.2 Core D

Figure 10a shows the different ice types observed in the ice core D. This core does not contain any water pockets or any visible mineral particles, except at its very bottom where the ice auger was able to obtain 1 cm of frozen sediments. Below this depth, the core shows columnar crystals, a few decimeters long (some of them reaching 1 m long), with vertical c-axes. This texture described as "candle ice" by Chinn and Maze (1983) is typical of lake ice. Cylindrical bubbles, 1 to 6 cm long and 1 to 3 mm wide, are present all along the core (Figure 11a). These crystal and bubble characteristics indicate downward progression of a freezing front through a water mass (Gow and Langston, 1977). The bubbles are produced by occlusion of gas within the ice during freezing and are oriented along the direction of ice growth (Adams et al., 1998). Close observation of the core, in particular between 110 and 180 cm depths, reveals that the shapes of the bubbles are highly variable (Figure 11b, c and d).

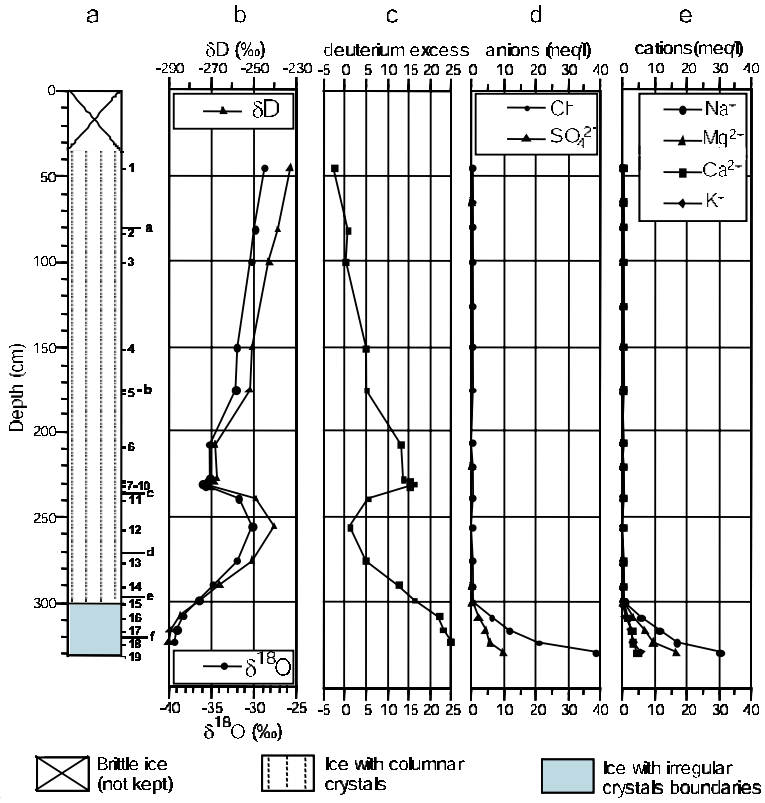

Figure 10: *Main characteristics of core D: (a) types of ice with locations of the isotopic and chemical samples noted 1 to 19 and of samples for gaseous analyses noted a to f; (b) δD and $\delta^{18}O$ profiles in ‰; (c) deuterium excess profile; (d) major anions profiles (Cl^-, SO_4^{2-} in meq L^{-1}); (e) majors cations profiles (Na^+, K^+, Ca^{2+}, Mg^{2+} in meq L^{-1}).*

In the bottom 30 cm of the core, the bubbles appear as vertically oriented filaments a few

millimeters to 1 cm long and with a diameter of the order of a tenth of millimeters (Figure 11e). The ice crystals are still vertically elongated, but with horizontal c-axes. However, in the last 10 cm, the ice crystals become relatively small (1 cm to a few centimeters long) with random c-axis orientation and with cylindrical bubbles situated along their boundaries (Figure 11f, 11g). In horizontal thin section, each individual crystal shows irregular boundaries and evenly spaced ice plates and brine lamellae (Figure 11h) which has been previously described in the case of certain types of sea ice as the "brine layer / ice plate substructure". This has been clearly illustrated by Gow et al. (1987). Moreover, small algal fragments are present within the last 1 cm of ice, and also in the frozen sediments, which constitute the very end of the core.

The isotopic profile shows clear trends (Figure 10b, 10c). The δD and $\delta^{18}O$ values become more negative with increasing depth indicating a depletion of heavy isotopes down to 230 cm. Below this depth, an inverse trend takes place until 256 cm where a new depletion is again displayed until the sediment is reached at 323 cm depth. Values are -232.8‰ in δD and -28.76‰ in $\delta^{18}O$ at the top of the profile and reach -290.0‰ and -39.33‰ respectively near the bottom. The deuterium excess profile ($d = \delta D - 8\ \delta^{18}O$) appears as a mirror image of the profiles.

The major ions profiles are simpler (Figure 10d, 10e). All of them have relatively low concen-

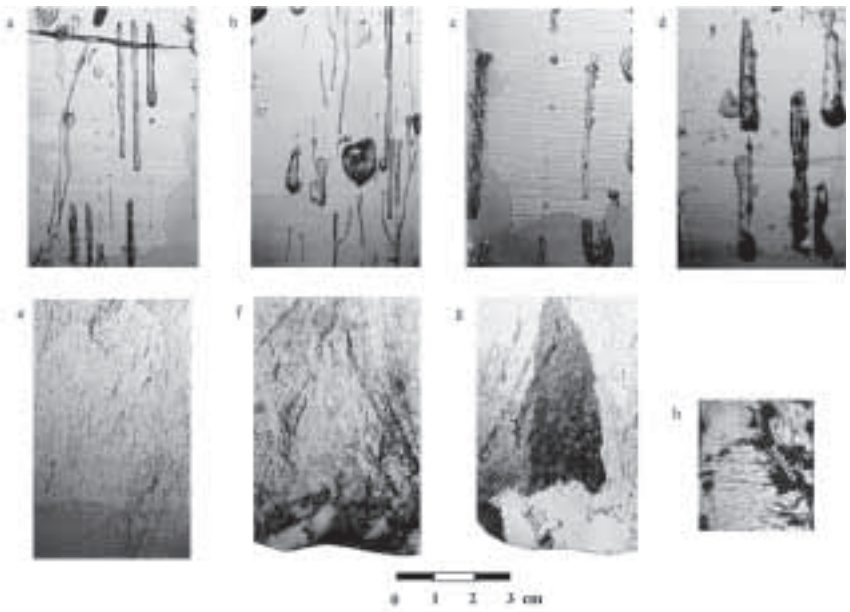

Figure 11: *Bubbles shapes displayed in vertical sections along core D and substructure: (a) common vertical cylindrical bubbles; (b) thin sinuous, sometimes dendritic, cylindrical bubbles and big nearly spherical bubble similar to an inverted teardrop bubble; (c-d) thick and irregular cylindrical bubbles; (e) very thin vertically oriented bubbles, appearing like filaments; (f) cylindrical bubbles situated along crystal boundaries of smaller crystals visible in vertical thin section on (g); (h) horizontal thin section of the basal part of the core showing crystals with striated surfaces similar to the "brine layer / ice plate substructure" developed in sea ice (Gow et al., 1987).*

trations all along the core except at its very bottom where they sharply rise, reaching higher values. Along the last 30 cm, chloride, the dominant anion, becomes 100 times more concentrated (from 0.39 to 38.49 meq L^{-1}) and sodium, the dominant cation, increases from 0.45 to 30.20 meq L^{-1}. The other ions analyzed exhibit the same trend but to a lesser extent.

Gas content and composition analyses were performed on six samples situated between 79 and 319 cm depth (Figure 10a). Gas content is always low (it ranges from 0.019 to 0.080 cm^3 g^{-1}). This range is clearly related to the bubble concentration, but it must be noted that some bubbles are so large that sampling necessarily implies the cutting of them, and thus loss of gases. The CO_2 concentration is relatively low all along the core (between 317 and 4557 ppmv) contrasting with nearly 700,000 ppmv near the bottom. The O_2/N_2 ratio gradually increases from top to bottom from 0.37 to 0.54.

3.1.4 Discussion

3.1.4.1 Isotopic data

When plotted on a $\delta D/\delta^{18}O$ diagram (Figure 12), the ice samples taken all along the two ice cores (A and D) show a linear relationship expressed by the equations:

$$\delta D = 5.4\,\delta^{18}O - 77 \qquad (r^2 = 0.996) \tag{17}$$

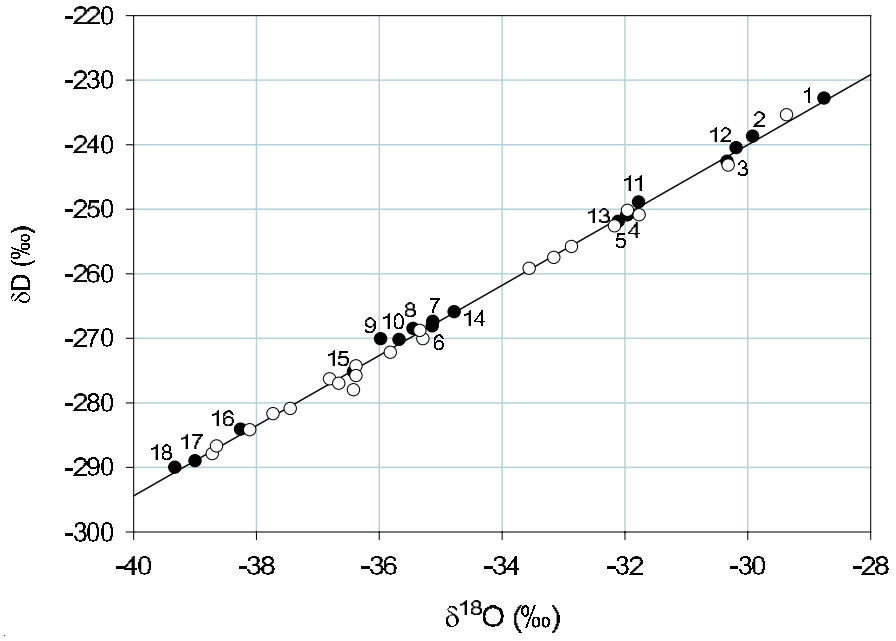

Figure 12: *$\delta D/\delta^{18}O$ diagram showing the 21 samples located all along core A (open circles) and the 18 samples located all along core D (black circles – numbers refer to those used in Figure 10a).*

The slope of this regression line (S = 5.4), called freezing slope, is an isotopic signature of ice formed by progressive freezing of a closed water reservoir, as explained by Jouzel and Souchez (1982) and Souchez and Jouzel (1984). As the freezing front moves, ice is enriched in heavy isotopes with respect to water. In a closed or quasi-closed reservoir, the residual water becomes more and more depleted in heavy isotopes and the successive ice layers formed are therefore depleted in heavy isotopes as well. The slope depends on the isotopic composition of the water at the beginning of freezing and on the ice-water equilibrium fractionation coefficient for δD and δ^{18}O. The following equation from Souchez and Jouzel (1984) can be used to compute this slope:

$$S = \frac{\alpha[(\alpha-1)(1+\delta i)]}{\beta[(\beta-1)(1+\Delta i)]} \tag{18}$$

where δi is the δD composition of the parent water, Δi its δ^{18}O composition, and α and β are the values of the ice water equilibrium coefficients for deuterium and for δ^{18}O, respectively (Souchez and Jouzel, 1984). The composition of the parent water, as suggested by Souchez and Jouzel (1984) is given by the intersection of the freezing slope with the local meteoric waterline. The latter has been obtained by Lorrain et al. (1999) from 25 glacier ice samples from the surface of Suess Glacier. These 25 samples have isotopic values ranging from -38.51 to -30.77‰ in δ^{18}O and from -307.4 to -248.6‰ in δD. This line has the following equation:

$$\delta D = 8.1\,\delta^{18}O + 9.4 \qquad (r^2 = 0.98) \tag{19}$$

The corresponding isotopic values of the parent water are δ^{18}O = -32.32‰ and δD = -252.38‰. Using them as δi and Δi in equation (18) with α and β taken as 1.0208 and 1.003, respectively (Souchez and Jouzel, 1984), we obtain a theoretical freezing slope of 5.5 which is in close agreement with the slope of 5.4 obtained from our samples.

It is also possible to estimate the isotopic composition of the ice formed when the freezing front has reached the bottom of the water reservoir. In a closed system, what mass is gained by the solid phase during freezing is lost by the liquid phase. Therefore, as demonstrated by Jouzel and Souchez (1982),

$$\delta_s = \alpha(1000+\delta_0)\left[\frac{N_0 - N_s}{N_0}\right]^{\alpha-1} - 1000 \tag{20}$$

where N_0 is the total number of moles in the system or the number of moles in the liquid when freezing begins, N_S is the number of moles in the solid phase at time t, δ_s is the δ value of the solid phase near the liquid-solid interface at time t, δ_0 is the δ value of the solution when freezing begins, and α is the equilibrium fractionation coefficient between solid and liquid. From equation (20), we can estimate the values of the ice corresponding to a given frozen fraction (N_S/N_0). For instance, at 97% freezing, the corresponding isotopic composition is δ^{18}O = 39.57‰ and δD = 290.5‰. These values are nearly the same as the ones of the deepest isotopic sample in core D (see in Figure 10, sample #18, 323 cm deep, δ^{18}O = -39.33‰ and δD = 290.0‰).

The impoverishment in heavy isotopes along the freezing slope observed in cores A and D between depths of 107 to 287 cm and down to 230 cm respectively (Figures 7 and 10) thus indicates that the lake has frozen from top to bottom as a closed water reservoir. The large elongated ice crystals with vertical cylindrical bubbles described from this upper part of core A (Figure 8a) are the fingerprint of that downwards freezing process (Adams et al., 1998). At first, the lake was wet-based. Progression of the freezing front in the liquid water body was possible because of surface ablation of the ice cover. The present day ablation rate is about 30 cm y^{-1} in the Dry Valleys (Chinn, 1993). Such a situation can be in a steady state if the water losses are compensated by inflow of melt water during the summer into the moat from surrounding areas of low albedo. However, if this water inflow markedly decreases, then the lake can become dry-based and, as indicated by Chinn (1993), cannot easily return to a wet-based situation.

Between 287 cm and 306 cm deep in core A and between 230 and 256 cm deep in core D, an enrichment in heavy isotopes with depth has been detected. This can be explained by mixing of the residual liquid water of the lake with water having higher isotopic values that plot onto the freezing slope cited above. Only on the latter condition can the isotopic values of the ice formed after mixing plot onto the same freezing slope (e.g. point 12 in Figure 12b). We think this mixing occurred when, during summer, the residual water situated at the lake bottom eventually made contact with moat water, and so diffusion of isotopes could take place (their diffusion coefficients in water is of the order of 10^{-5} cm^2 sec^{-1}). The fact that there is again an impoverishment in heavy isotopes with depth below 306 cm in core A suggests progressive closure of the residual water reservoir until the sediment layer present between the depths of 352 cm and 361 cm was reached.

3.1.4.2 Chemical data

The chemical results confirm the interpretation of the isotopic data. The ionic concentrations profile showing low values all along the ice cores, except at their bottom (especially in core A, where concentrations in major elements show a peak within the particle layer), expresses the chemical effects of the migration of the freezing front. During downward freezing of the lake water, most ions are expelled from the ice and diffuse into the residual water (Terwilliger and Dizio, 1970; Hallet, 1976). Near the end of the closed reservoir the ionic concentration become very high and, as a result, rises in the ice as well. Finally as the freezing front becomes grounded, the last ice increments must include most of the expelled ions.

The high final ionic concentration of this ice, although weaker than in the case of sea ice, is responsible for the presence of the brine layer / ice plate substructure of core D described above and which is typical in sea ice (Figure 11h). Regular elongated protuberances appear at the ice-water interface during ice growth and salts are present as liquid inclusions trapped along this substructure (Lofgren and Weeks, 1969).

Comparison of ionic profiles with the isotopic ones, raises the question of the lack of symmetry between them. One could indeed expect the latter be a mirror image of the former, since on the one hand ions are expelled from the growing solid phase and on the other hand heavy isotopes

are preferentially incorporated in the growing ice. In fact we observe different situations. Firstly the "end of reservoir" effect appears higher in the profile for isotopes than for ions. Secondly the isotopic enrichment detected between 210 and 240 cm depth in core D has no counterparts on the ionic profile. These differences can be explained as follows. The isotopic profile mainly describes the isotopic composition of the ice lattice of the crystals whereas the ionic profile mainly describes the brines present at the grain boundaries. Because the ice crystals are large in that core, the samples taken for ionic analyses have intersected only a small number of crystal boundaries where the brines are located. On the contrary, within the deepest ten cm of core D, as indicated above, the ice crystals are much smaller and the crystal boundaries intercepted more numerous.

In core A, a peak appears at the level of the sediment layer. Below it, chemical concentrations rise again until they reach a maximum near the bottom of the core where the lowest values were detected in the isotopic profiles. It is possible that the sediments contain soluble precipitates which can influence ice chemistry in the laboratory when the ice samples are melted for analysis. This is suggested by the fact that calcium is quite high in the ice close to the sediments. Calcium carbonate precipitation is a normal feature of closing reservoirs at the end of freezing (Hallet, 1976; Killawee et al., 1998) since its eutectic temperature is close to 0°C. The chlorine content however exhibits the same profile, while the eutectic temperatures of chlorine salts are much lower, in the order of -20°C. This last characteristic indicates that the increasing ionic concentrations observed below 361 cm in core A do not result from the sample treatment. The two concentrations peaks appearing at the bottom of the core and at the level of the first sediment layer thus both indicate the closing reservoir effect detected through the isotopic study.

3.1.4.3 Gas data

Results of the gas analyses give support to the interpretation of the other data. The total gas content is very low compared to values typical of polar meteoric ice, which is about 0.1 cm^3 g^{-1} of ice at standard temperature and pressure conditions (Martinerie et al., 1992). The values obtained from our samples in core D are around 0.02 cm^3 g^{-1} with one exception near the bottom of the core where there is a maximum of 0.08 cm^3 g^{-1}. These values are, however, higher than the normal gas content of bubble-free ice which usually is less than 0.00003 cm^3 g^{-1} (Berner et al., 1977). By comparison, the solubility of air in water at 0°C is about 0.03 cm^3 g^{-1}. Experiments of downward growth of ice from dilute solutions in a closed reservoir were carried out by Killawee et al. (1998). Some of these, conducted at constant linear rates of about 0.8 µm s^{-1} have lead to interesting conclusions which are relevant to our result. For instance, they have produced total gas contents reaching values between 0.05 and 0.06 cm^3 g^{-1} in their later stages, i.e. in the ice formed when the freezing front was approaching the bottom of the reservoir. Vertical trains of bubbles were observed and have been interpreted to be due to repeated nucleation of bubbles from particular points at the bottom of the reservoir. They are very similar to some observed in deep parts of ice core D (Figure 11).

Our results thus again reflect the progressive freezing from top to bottom of the lake water mass. During this process, gases become supersaturated in the region immediately below until

bubbles nucleate and form a gas phase. As freezing proceeds, gas is transferred from solution to the bubbles until finally the bubbles are entrapped in the ice (Craig et al., 1992).

The measured CO_2 concentration is generally higher than the present day atmospheric value all along core D (ranging from 564 to 4557 ppmv) but at the bottom it reaches the exceptionally high level of 695,000 ppmv which to our knowledge is the highest value ever reported for natural ice. Until now, the highest published values were 222,000 ppmv in the basal ice of Suess Glacier (Lorrain et al., 1999) and 135,000 ppmv in the basal ice of the GRIP core in Central Greenland (Souchez et al., 1995a). In the experiments of Killawee et al. (1998) cited above, CO_2 contents commonly reached 30%. In one of them, where the rate of freezing was about 2.2 µm s^{-1} and the calcium concentration of the ice from the last freezing stages was about 1.3 mmol L^{-1}, the CO_2 content peaked at about 63% (630,000 ppmv), which is close to our value of 695,000 ppmv obtained at the very bottom of core D. This experiment showed that this very high CO_2 concentration (much higher than the CO_2 concentration in air dissolved in water at 0°C and at atmospheric pressure) is explained by the addition of CO_2 produced by $CaCO_3$ precipitation (Ca^{2+} (aq) + 2 HCO_3 (aq) $\longrightarrow$ $CaCO_3$ (s) + H_2O (aq) + CO_2 (aq or gas)) and, indeed, calcite crystals were found within the ice produced in the last freezing stages.

In our case, the calcium concentration of the deepest ice samples of the core (2.187 mmol L^{-1}) is even higher than the values of the experiment reported above (1.3 mmol L^{-1}). This process of CO_2 enrichment is thus highly probable in the context of calcite precipitation in a eutectic calcite-ice-aqueous solution as described by Hallet (1976). The particle content of the ice from the very bottom of the core has been investigated by scanning electron microscopy. Calcite precipitates have been detected confirming the occurrence of the described process. Concentration of solutes by freezing thus leads to an increase in pCO_2 and supersaturation for calcite at the ice-water interface. When the solution becomes highly supersaturated for calcite, precipitation occurs and is associated with degassing of bubbles containing over 50% CO_2 which become trapped in ice.

3.1.4.4 Build-up of the ice cover of lake Popplewell

From the different aspects of the ice study developed above, it clearly appears that the ice retrieved from the "ice-block" Lake Popplewell has built up from a closed or quasi-closed water reservoir by progressive downward freezing until the lake bottom has been reached. However, no time scale can be provided. It is well known that a water body in contact with the atmosphere at this locality can form an ice cover about 3 m thick over the first year of its existence (T.J. Chinn, personal communication, 2001), but this does not help in this case. Indeed, due to superficial ablation, the 3.3 m thick ice core D we have sampled does not correspond necessarily to the whole thickness formed since the beginning of the process. This process may have lasted several years, so long as moat water has not been in contact with the water remaining at the bottom of the central part of the lake (except, as discussed above, when the ice between 230 and 256 cm deep formed). As pointed out by Chinn (1993), both the lake levels in the Dry Valleys and the equilibrium thickness of the ice covers have always fluctuated substantially. We think that during the history of the glacier-dammed lake, a floating ice cover eventually

grounded, except in the deeper central part of the lake, and that the climatic conditions allowed thickening of the ice until the bottom was reached in that part. The ice studied here was formed after the grounding event, probably due to a lowering of the lake level.

Following Chinn (1993), the dry-based lakes of the Dry Valleys have a thermal behaviour similar to that of glacier ice, with limited upward heat flow because, in contrast to what happens in wet-based lakes, once the lake has completely frozen, there is no further latent heat supply from freezing at the base. Once a lake becomes dry-based, it is unlikely for it to return to an ice-covered lake of water if the climate remains constant. A dry-based lake is fed only by flooding over the ice surface of glacier- or snowbank meltwater. The surficial alimentation-ablation balance governs the ice thickness. In the case of Lake Popplewell, a small stream which sporadically flows along the right side of Suess Glacier during the most sunny days of summer, eventually reaches the moat. On very rare occasions, this stream floods. As a result, a sheet of water spills on the ice cover of the lake and freezes on. The icings (aufeis) which are formed by this process are responsible for the bluish smooth surface of the ice cover. Some of us observed one of these phenomena in progress during the 1997-98 summer; in about five days, an icing, a few centimeters thick, froze completely solid on most of the surface of the lake ice.

Significantly, we do not find any trace of aufeis in any of the ice cores retrieved from the lake. Aufeis is usually laminated (Schohl and Ettema, 1986) and is generally characterized by small equigranular crystals that do not show discernible structure or c-axis orientation patterns (Pollard and Everdingen, 1992). Moreover, aufeis presents a specific isotopic signature: absence of correlation between δ and deuterium excess (d) values (Souchez et al., 2000a). This is the opposite of what we observe here (Figure 10b and 10c showing a clear δD-d relationship). We interpret the absence of visible aufeis as follows. On a mean annual basis, the icings are counterbalanced by the surface ablation loss, which ranges between 0.200 and 0.305 m yr^{-1} (Chinn, 1993). However Lake Henderson (also called Mummy Pond - see Figure 6), which is located a few hundred meters westwards of Lake Popplewell and is also dry based, has been reported as slightly rising (a few decimeters) between 1972 and 1990 (Chinn, 1993). Lake Popplewell should also have risen since it most probably behaves like its close neighboring Lake Henderson. We think that aufeis is probably present on top of the studied mass but has not been noticed because it corresponds to the top 57 cm / 35 cm which were discarded during sampling of cores A and D respectively since it was extremely brittle, as indicated above.

3.1.4.5 Implications for Suess Glacier – lake interactions

Chinn (1993) has extensively examined the possible interactions between Dry Valleys lakes and glaciers margins. He has considered configurations generated by equilibrium, advance or retreat of the glaciers and by static, rising or falling lake levels. Situations like lake ice moving over glacier ice or glacier ice extending out over lake ice are possible and point to the complexity of what can be found at the glacier base. In the present case, basal ice of the damming Suess Glacier has already been investigated (Lorrain et al., 1999). Although this glacier is cold-based (temperature lower than -17°C), it shows some blocks of undisturbed

lacustrine sediments within its basal part. The latter consists of a 3-5 m thick series of ice layers of variable thickness (1 cm to a few decimeters), interbedded with sand and fine gravel beds. Occasionally a thin organic mud layer or an algae layer (a few mm thick) is associated with a sand layer. The particle-size characteristics of the sediments are the same as those of the adjacent lacustrine environment (Fitzsimons, 1996). The well-preserved primary sedimentary structures of the blocks cited above suggest the sediments were frozen during entrainment. The analyses of stable isotopes and of gas content and composition of this basal ice have indicated that these blocks were formed by the freezing of water. The 85 ice samples taken from this basal ice have isotopic values ranging from -28.1 to -38.64‰ in $\delta^{18}O$ and -228.5 to -286.8‰ in δD. In a δD-$\delta^{18}O$ diagram, they show a regression line having the equation:

$$\delta D = 5.4\,\delta^{18}O - 79 \qquad (r^2 = 0.97) \tag{21}$$

which is practically the same as equation (17) obtained from the lake ice samples presented above. The gas analyses also have shown clear similarities with what is reported here for lake ice from core D : low total gas content (0.006 to 0.083 $cm^3\ g^{-1}$), high to very high CO_2 concentrations (446 to 222,900 ppmv) and O_2/N_2 ratios ranging from 0.25 to 0.52.

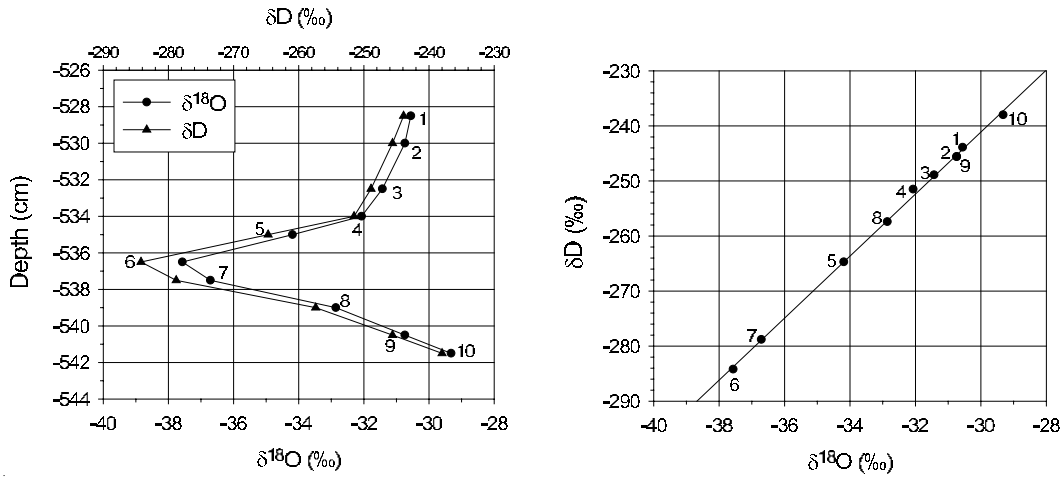

Figure 13: *δD and $\delta^{18}O$ diagram and profiles of one of the ice layers present in the basal part of Suess Glacier front.*

From these results Lorrain et al. (1999) concluded that the basal ice of Suess Glacier has been formed by freezing of water from the lake. It is now established that Lake Popplewell no longer has liquid water at its bottom. It is possible that the basal ice investigated has partly been formed by incorporation of lake ice at the glacier base, as in one of the situations envisaged by Chinn (1993). It is nevertheless a fact that some of the ice layers present in the basal ice of Suess Glacier confirm the local freezing of liquid water pockets. For instance, Figure 13 shows the variation of the isotopic composition in δD and $\delta^{18}O$ of one of these ice layers about 13 cm thick situated at the bottom of the basal ice sequence. One can observe isotopic shifts from -29.32 to -37.57‰ in $\delta^{18}O$ and from -238.0 to -284.2‰ in δD which are nearly as large as

what is observed through the whole thickness of the lake ice cover. Moreover, when plotted on a δD-δ^{18}O diagram these isotopic values show a linear regression line with the equation:

$$\delta D = 5.6\,\delta^{18}O - 72 \qquad (r^2 = 0.99) \tag{22}$$

which again is almost the same as equations (17) and (21). The fact that the isotopic shifts are nearly the same (in value and in range) as in the lake, but displayed on a very small thickness (about 12 cm) indicates that a water pocket of nearly the same isotopic composition as the lake water has frozen completely from both directions.

This interpretation is reinforced by the fact that the CO_2 composition varies from 1177 ppmv at one side to 11,306 ppmv in the middle of core D. The isotopic and gas characteristics are not compatible with what should be observed within a slab of lake ice about 12 cm thick incorporated solid at the glacier sole. In this latter case indeed, only a small isotopic shift would be displayed within a decimeter thick ice layer. Here the mean isotopic gradient in δD is about 8‰ cm^{-1} whereas the highest gradient within the lake ice studied is about 0.8‰ cm^{-1}. Moreover, similar isotopic shifts and gradients have been encountered higher up in the basal ice sequence, 35 cm, 270 cm and 290 cm above the ice layer described here in detail. The corresponding isotopic shifts are 40.7, 22.5, and 39.5‰ in δD and their gradients are about 9, 4, and 4‰ cm^{-1}, respectively. These ice layers, some of which containing sediment layers and algae fragments, clearly also result from freezing of liquid water of similar initial isotopic composition.

Pockets of lake water can be present at the glacier base if the glacier flows into a wet-based lake. The model proposed by Fitzsimons (1996) and confirmed by Lorrain et al. (1999), suggests that transient wet-based conditions can occur as the glacier flows onto the unfrozen sediments of the lake bottom, creating conditions favorable for the entrainment of sediments and organic debris and for ice accretion by water freezing. In the case of Suess Glacier, the isotopic data are compatible with that process. It is probable that the stacked sequence of ice and sediment layers accreted at the base and visible at the glacier front has been formed when Lake Popplewell was still wet-based.

3.1.4.6 Trapping of aeolian sediments

The sediment layer located at a depth of 352 cm in core A has most probably accumulated on top of a previous ice cover. It is unlikely that it was formed by progressive downward movement of particles into the ice as suggested by Nedell et al. (1987) and Squyres et al. (1991) for Lake Hoare. Indeed there are no visible particles within the 3 m thick lake ice present on top of it. Furthermore, the bimodal character of the grain size distribution in the sediment layer together with a paucity of particles around 80 m diameter is a feature well displayed in arid zones of the world. It is thought to be the consequence of saltation and sand movement by the wind (for an overview of some literature, see Pye, 1987; Offer et al., 1993). Large sand particles can be pushed by the wind and roll on the smooth surface of the lake ice cover. During transport, the finer particles in saltation are trapped in the interstices between the large sand particles, with

the larger particles in saltation bouncing, impacting the rolling particles and going farther. This results in the bimodal character observed. In such a scenario, the ice under the sediment layer represents an earlier ice-block phase of the lake which also resulted from complete freezing (as indicated by the isotopic impoverishment visible in Figure 7). The sediment layer can be considered as the record of strong winds in the history of the lake. Comparison with the other cores retrieved from the lake shows that the ice present under the sediment layer studied in core A is at a greater depth than the lake bottom encountered at these other drilling sites; this explains the unique characteristics of core A.

Sediments in lake ice of Dry Valleys lakes or on the lake floors are thought to be primarily of aeolian origin. Is the aeolian character displayed by some grains (roundness, pitted surfaces on electron microphotography) an acquisition during transport or is this character already present in the valley floor deposits? This question is difficult to answer. Two factors must be taken into account. Strong winds in the Dry Valleys were responsible for erosion and rounding of blocky material, development of stone pavements and presence of sand dunes (in Victoria Valley). At low temperatures, such as those prevailing in winter in the area (-20°C and lower), ice crystals have the same hardness as orthoclase grains and they can readily be in suspension or in saltation during high wind periods. Therefore micromorphology of grains is perhaps a less efficient discriminating tool in such an environment.

Sediment layers within lake ice from the Dry Valleys are considered to represent a dynamic equilibrium between downward movement as a result of melting during the summer and upward movement of ice from ablation at the surface and freezing at the bottom (Priscu et al., 1998). From different observations, it was also inferred that any sediment which was deposited on the ice cover could eventually make its way through the ice cover and settle in the water column below. Nedell et al. (1987) provided the first direct evidence of this by comparing the mineralogy and grain size distribution of sediment of different origins: from the surface of an ice cover, from the bottom of a lake and from adjacent melt streams. Developments along these lines by Wharton et al. (1989) and Squyres et al. (1991) put forward episodic point sources of sediment deposition through ice covers by way of cracks or gas bubble channels where ice covers are less than 3 m thick. More recently, Hendy (2000) proposed a model explaining how particles absorbing solar radiation can migrate through the ice cover or not, depending on their grain sizes. Such migration processes were probably effective in the lower part of the ice core beneath the sediment layer at a depth of 361 cm when the upper part of lake ice was not yet present. This is indicated by penetration of particles into the ice from the base of the sediment layer (Figure 8c). The sediment layer itself cannot however be the result of such processes since the upper lake ice is devoid of visible particles and since isotopic and chemical data favor a build-up of lake ice in two steps separated by a "wind event" responsible for the formation of the sediment layer.

Besides, Hendy (2000) developed a conveyor belt model for Trough Lake, another perennially frozen lake in South Victoria Land. In this model, the floating ice cover is pushed by a glacier across a proglacial lake towards the marginal moat where melting occurs. Depending on their grain size, the sediments present on the ice surface differentially migrate through the ice cover and eventually settle on the lake floor along their path to the moat. This model is not applicable

to the case studied here. Indeed, Lake Popplewell is presently dry-based, so that, due to the absence of liquid water at depth, the pressure exerted by glacier ice on the lake ice toward the moat does not exist. Such a situation could, however, have been present when the upper lake ice was constructed in wet-based conditions. But the absence of sediments in the upper lake ice rules out the set-up of the aeolian sediment layer by this process.

3.1.5 Conclusion

Isotopic analyses (in δD and δ^{18}O) of the ice of Lake Popplewell together with ionic and gas data, textural and structural investigations, strongly suggest that this ice-block lake has been formed by progressive freezing from top to bottom of the closed water reservoir remaining in the deepest part of the lake after the grounding of a floating ice cover probably due to a lowering of the lake level. The information retrieved confirms that the basal ice sequence, visible at the front of Suess Glacier, has been built up, at least partly, by freezing of bottom water from Lake Popplewell in a period during which the lake was wet-based. Furthermore, this study puts forward how a layer of aeolian sediments was trapped in the ice. On top of a shallow ice block lake, wind-blown sediments are deposited at the surface until liquid water invades the lake basin allowing subsequent formation of an upper layer of lake ice by complete freezing of this water.

3.2 Study of the basal part of Vostok ice core, Antarctica

3.2.1 Introduction and site description

Lake Vostok is a huge subglacial lake, one of the 70 lakes identified beneath the Antarctic Ice Sheet (Siegert et al., 2000). It is about 240 km long and 50 km wide and lies under 3750 m of ice in its southern part and under 4150 m of ice in its northern part. The ice ceiling is tilted, being at 750 m below sea level in the North and at 250 m below sea level in the South. The water depth near Vostok station in the southern part of the lake is about 680 m.

Interpretation of radio-echo-soundings (Siegert, 2000; Siegert et al., 2001) has promoted a lake system with melting occurring in the northern part of the lake while ice accretion characterizes the area around Vostok station in the southern part of the lake. Later radio-echo-sounding studies (Bell et al., 2002) have indicated that accreted ice is exported out of the lake system along with glacier flow at the south-eastern margin of the lake. Ice flowing above the subglacial lake is coming from the Ridge B area (Figure 14) and from Dome B in the northern part of the lake where subglacial melting is taking place.

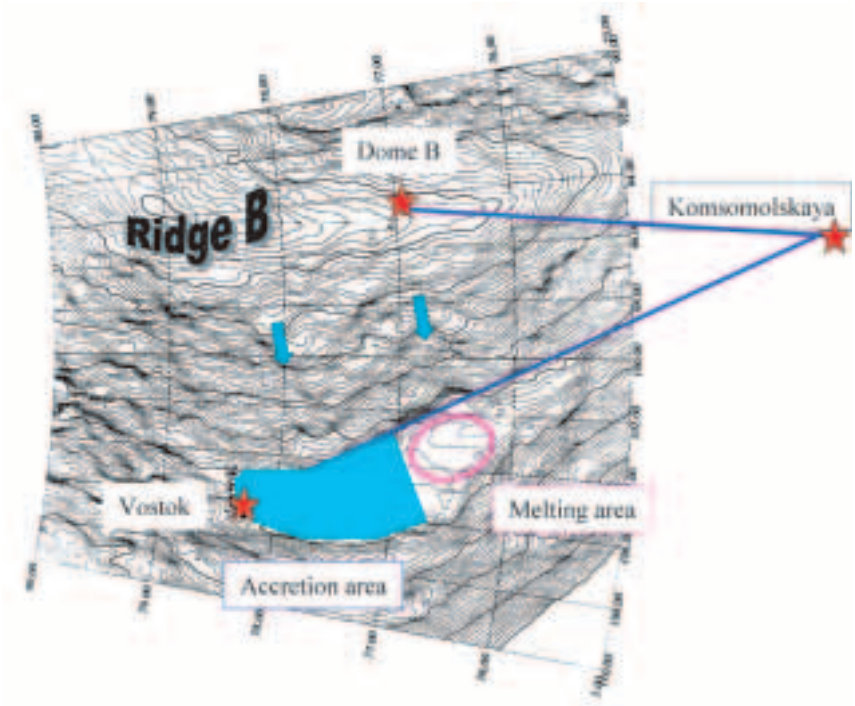

Figure 14: *The Lake Vostok environment with melting area and accreted ice formation area. Accretion area is derived from radio-echo soundings (Bell et al., 2002). Ice flow from Ridge B or Dome B is indicated by arrows. Traverse routes are shown by heavy straight lines and the stars are drilling sites. Surface contour lines are 5 m apart. The heavy isoline near Vostok station is 3500 m asl.*

The completion of ice drilling at the Russian Vostok station down to 3623 m, about 130 m above subglacial Lake Vostok, has allowed the extension of the record of atmospheric composition

and climate to the past four glacial-interglacial cycles. From the surface to a depth of 3310 m the Vostok ice core has given one of the most interesting palaeoenvironmental record at interglacial-glacial time scales (Petit et al., 1999). Below this depth, however, the climatic record cannot be directly deciphered : the ice core shows either evidence for the presence of dust particles coming from the ice-bed interface (Simoes et al., 2002) or ice properties indicating that the past-environmental record in the ice is lost (Petit et al., 1999). Below 3539 m depth, Jouzel et al. (1999) showed that the ice core consists of lake ice developed above subglacial lake Vostok. The mechanism of lake ice formation was further investigated by Souchez et al. (2000b). The ice is no more of meteoric origin (ice formed at the surface by snowfall) but is accreted ice produced by freezing of subglacial Lake Vostok waters (Jouzel et al., 1999; Souchez et al., 2000b).

Here we present two detailed investigations of a specific part of the Vostok ice core, respectively between 3311 and 3538 m depth and between 3539 m depth and the bottom of the core. The first interval is studied to document the build-up of the basal ice mainly on the basis of an isotopic composition investigation of the ice. The second interval is studied to reassess the isotopic properties of the accreted ice present below 3539 m depth and to develop the consequences for Lake Vostok's behaviour.

3.2.2 Highly deformed basal ice in the Vostok core

(R. Souchez, J.R. Petit, J. Jouzel, J. Simoes, M. de Angelis, N. Barkov, M. Stiévenard, F. Vimeux, S. Sleewaegen, R. Lorrain)

3.2.2.1 Ice composition characteristics

As indicated in Section 2.2 of the present report, the hydrogen and oxygen isotopic composition were determined with an accuracy of 0.5‰ in δD and 0.05‰ in $\delta^{18}O$. These accuracies give a one error on deuterium excess (d = δD - 8 $\delta^{18}O$) of ±0.7‰. Such a value makes possible an investigation of this parameter which exhibits much less variability than δD or $\delta^{18}O$. The sampling interval is 1 m.

Figure 15a gives the δD-$\delta^{18}O$ relationship for the basal part of the Vostok ice core between 3311 m depth and the lake ice at 3538 m depth. The regression line obtained has the equation δD = 8.06 $\delta^{18}O$ + 17.8 with r^2 = 0.99. This is not very different from the relationship obtained for the whole core down to 3310 m (Vimeux et al., 2001) on ice age interval 0–420,000 years (δD = 7.94 $\delta^{18}O$ + 11.33). Such similarity precludes any major change in isotopic composition for the basal ice due to phase changes between liquid water and ice.

Figure 15b gives the δD profile of the Vostok core between 3311 m and 3538 m. This profile shows a striking difference in amplitude of δ-variations from the top to the bottom. Down to 3346 m the δD values oscillate between -433‰, typical interglacial value, to -480‰, typical glacial value. This does not mean that older climatic cycles are displayed undisturbed since there is no lag between gas parameters and δ-values, a situation not present for the four climatic cycles identified higher up in the core (Petit et al., 1999). This can be interpreted as interbedding of

ice layers with different characteristics (either glacial ice or interglacial ice). The interbedding is most probably the result of large scale folding as indicated by inclined ash layers (up to 25° to the horizontal) in opposite directions (at 3310.6 and 3310.8 m depth). Such interbedding in top of the basal sequence was also found to be present at GRIP in Central Greenland (Souchez et al., 2000c).

After a decrease in the amplitude of δD values down to 3405 m, the isotopic signal oscillates quite regularly within a narrower range between about -450‰ and about -465‰. The deuterium excess provides insight that helps explain the situation. Vimeux et al. (1999) showed that, if deuterium excess is plotted against δD for the glacial-interglacial climatic cycles displayed in the Vostok core, a complex behaviour appears. During transitions from glacial to interglacial values, d remains quite stable. During glacial inceptions, there is an inverse relationship between d and δD. Finally during glacial stages, no definite trend is displayed.

In Figure 16, the two oldest glacial-interglacial climatic cycles from the Vostok ice core are displayed on a d-δD diagram. They represent ice between 2755 and 3108 m depth (black

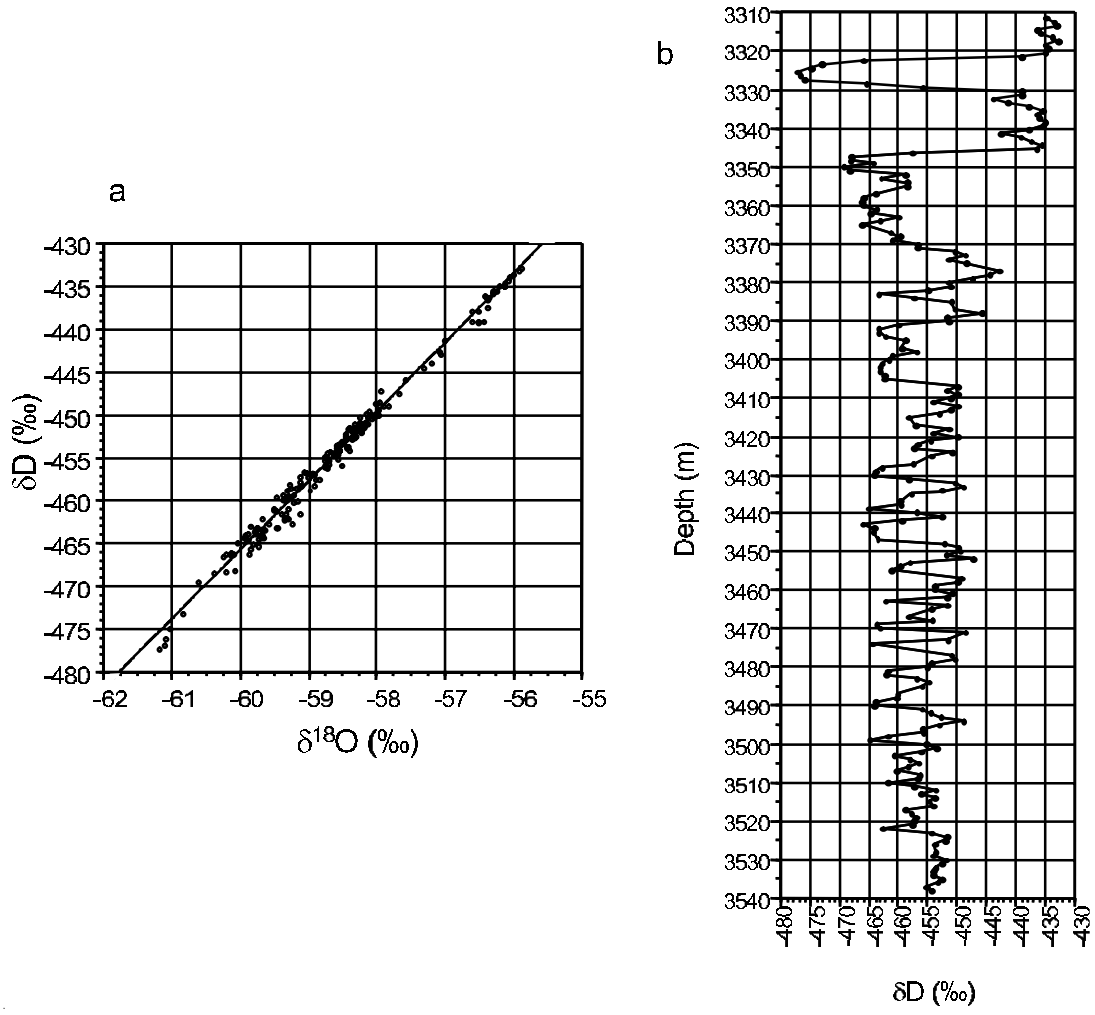

Figure 15: *(a) δD-$\delta^{18}O$ relationship in basal ice from the Vostok ice core (between 3311 and 3538 m depth); (b) The δD profile of the Vostok ice core between 3311 and 3538 m depth.*

circles) and between 3109 and 3309 m depth (open circles) respectively. Ice from these two cycles or from older ones is more likely to be affected by complex deformation (more complex than simple shear) than ice from the two last glacial-interglacial climatic cycles which is closer to the surface of the ice sheet. Now, samples of ice below 3405 m depth (crosses) are also indicated in Figure 16. The crosses representing such ice samples are mostly filling the central hole of the closed figure representing the distribution of sample points from the two oldest climatic cycles. Moreover, if a vertical line corresponding to the δD value of the middle of the maximum range for the climatic cycles is drawn in the figure (dotted line), most of the sample points from the two oldest climatic cycles are within the part containing the more negative values. Since one sample was measured per meter of core, this indicates that the colder periods are more developed in terms of ice thickness than the warmer ones. Now, the crosses representing ice samples below 3405 m depth are all included within this part containing the more negative values.

Such characteristics point to the occurrence of a folding/mixing process for the basal ice of the Vostok core. Folding/mixing will produce ice having an isotopic composition intermediate between those of ice layers before such a complex deformation, hence the distribution of the ice samples in a d-δD diagram in the hole described above. There is a higher probability that the intermediate isotopic compositions produced result from folding/mixing of ice more frequently present at depth. The distribution within the part containing the more negative δD values can

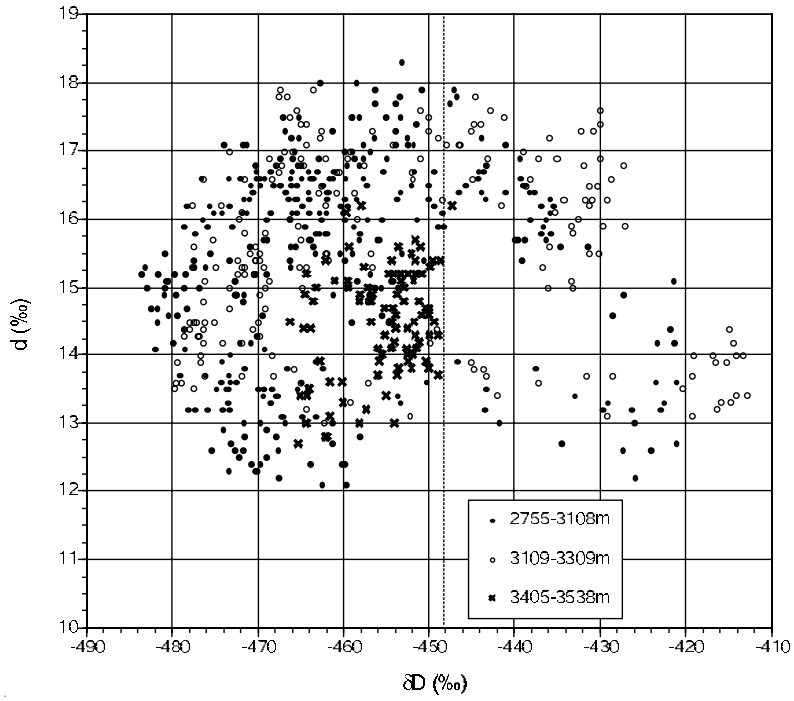

Figure 16: *Deuterium excess-δD diagram for ice of the Vostok ice core between 2755 and 3538 m depth. The black dots represent ice from the second oldest climatic cycle present in the Vostok core (2755-3108 m depth), the open circles the oldest climatic cycle (3109-3309 m depth) and the crosses basal ice between 3405 and 3538 m depth.*

so be understood. Within this context, the reduction in amplitude in the D variations with depth can be viewed as implying more complex ice deformation at depth, a very likely situation if one considers the uneven bedrock topography (Siegert and Ridley, 1998) where the ice is grounded upstream from Vostok station. Deformation more complex than simple shear is most pronounced close to the bed where ice viscosity is reduced by higher temperatures.

Since ice from the two climatic cycles considered here is most probably not deformed by such a process upstream from Vostok, it must be assumed that older climatic cycles which are presumably involved in basal ice deformation have the same general isotopic characteristics with a similar d-δD pattern. This is in our mind reasonable since all the four climatic cycles present in the Vostok ice core display such characteristics.

The damping of δD variations due to folding/mixing is also present in the trace impurities distribution. Marine (Na_m^+ , Cl^-) and terrestrial (non sea salt Mg^{++} and Ca^{++}) trace impurities have been studied in the basal ice below 3311 m depth by Simoes et al. (2002). The concentrations found are intermediate between those found in interglacial and glacial ice. The amplitude of the variations are between 30 and 50% lower than the ones observed between the Last Glacial Maximum and the Holocene and is further reduced below 3449 m depth. Total dust concentrations exhibit a similar pattern although below 3449 m depth the ice is loaded with particles coming from the bed which changes the picture. The above-cited properties reinforce the concept of folding/mixing at a submetric scale as indicated by the isotopic properties. Independently, below 3449 m depth, the presence of particles coming from the bed is associated with a layered ice structure characterized by interbedding of fine-grained and coarse-grained ice layers. Higher impurity content and single maximum fabric is associated with fine-grained ice while low particle concentration and girdle fabric is associated with coarse-grained ice. One section (3491-3492 m) was studied in detail in Simoes et al. (2002). It indicates most probably the presence of a major shear zone and will be considered below.

3.2.2.2 Mechanism of ice deformation

Underneath the basal sequence considered here, lake ice is present. This is the consequence of the fact that grounded ice upstream became floating on subglacial lake Vostok on its eastward journey. Arguments developed in Souchez et al. (2000b) indicate that freezing of lake water occurred along this flow line as soon as the ice overtakes the grounding line. It is therefore reasonable to assume that the basal sequence is complete with no ice loss from below by melting in contact with the lake waters. Melting is considered to only occur at the ice ceiling in the northern part of the lake.

Individual particles coming from the bed and present in the basal ice have a mode of 3.4 µm in diameter with a maximum size of about 9 µm. Larger particles up to 30 µm in diameter are aggregates. This raises the question of size-selective incorporation into the basal ice since it is quite improbable that only such fine particles are present at the ice-substratum interface. Amber ice consisting of silt-sized particles embedded in the ice, although in higher proportion, is shown to rest above a substratum with various and larger grain sizes at some glaciers in

South Victoria Land. In such cases, the ice-substratum interface temperature is also well below the pressure melting point.

Cuffey et al. (1999) and Cuffey et al. (2000) developed the role of interfacial water films at the surface of rock particles embedded in the ice for glacier sliding at -17°C. Interfacial films exist due to a reduction of the chemical potential of water very close to the surface of an embedded particle (Wettlaufer et al., 1996).

Pressure inequality between overlying ice and interfacial films at the ice-substratum interface may allow ice to penetrate a small distance into the inter-particle voids in patches of fine-grained sediment at subfreezing temperature. Such a process makes possible incorporation and entrainment of fine particles and adhesion to the glacier sole can promote the formation of aggregates. Fisher and Koerner (1986) found strain rates in an Agassiz Ice Cap core to be directly related to debris concentration and inversely related to ice crystal size. The non-homogeneity in ice properties induces differences in rheological behaviour and a small fold can be created. Simple shear close to the bed tends to rotate transverse structures such that folds become progressively recumbent and they ultimately approach parallelism with the flow lines. Shear zones can eventually occur in such conditions. Deformation is more pronounced in zones of strong longitudinal compression. This longitudinal compression is responsible for tectonic thickening of the deformed ice. There is a progressive build-up of the basal sequence upwards with more advanced deformation stages close to the bed. This explains the presence of the shear zone studied by Simoes et al. (2002) in the basal part of the sequence, followed higher up by recumbent folding at the submetric scale propagating first in the ice layers containing rock fragments from the bed and then through ice devoid of such particles. A change in ice properties indeed often results in a change in ice viscosity.

Interbedding of ice layers at a larger scale which is present in top of the basal sequence is most probably related to large scale rock protuberances at the bed.

3.2.3 Reassessing of Lake Vostok's behaviour
(R. Souchez, J.R. Petit, J. Jouzel, M. de Angelis, J.L. Tison)

3.2.3.1 Stable isotopes in accreted ice

Previous interpretation of the isotopic data

Major shifts in deuterium and deuterium excess are observed at the 3539 m transition. Within less than 50 cm, deuterium values increase by about 10 per mil (‰) and deuterium excess d (d = $\delta D - 8\,\delta^{18}O$) values shift from around 14‰, a value typical for meteoric ice in the Vostok area, to 7 or 8‰ (Souchez et al., 2002; Jouzel et al., 1999). In a δD-$\delta^{18}O$ diagram, data points above 3539 m lie on the Vostok precipitation line with a slope of 7.93 calculated over the past 420,000 years. In contrast, data from the zone below 3539 m depth cluster to the right side of this precipitation line (Figure 2 in Jouzel et al., 1999). Other ice properties also drastically change at this 3539 m transition (Figure 17). These isotopic characteristics have been interpreted

as a clear fingerprint of the isotopic modifications resulting from a freezing process (Jouzel et al., 1999; Souchez et al., 2000b) in accordance with fractionation effects occurring during this phase change (Jouzel and Souchez, 1982; Souchez and Jouzel, 1984). In such a view, the explanation for the clustering point data being on the right side of the precipitation line is that accreted ice was formed by freezing of water from the subglacial lake. The lake water isotopic composition corresponds to the intersection of the freezing slope passing through the average point of the cluster and of the precipitation line. The theoretical freezing slope equals 3.98, which is about half the precipitation slope. Consequently, lower deuterium excesses are displayed in this ice.

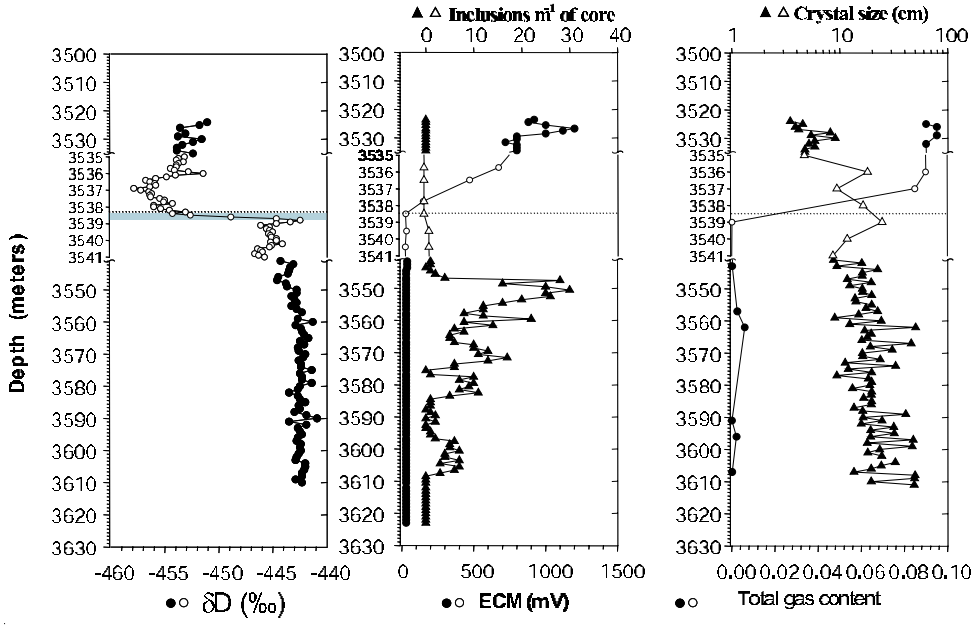

Figure 17: *The isotopic composition, ECM values and mineral particle aggregate (inclusion) numbers profile, crystal size and total gas content in the basal part of the Vostok ice core. Open symbols are used for the depth range 3535-3541 m where the resolution for isotopic measurements is 0.1 m. Samples in the shaded area of the isotopic profile have been used for the δD-$\delta^{18}O$ diagram shown in Figure 20. The dotted line is considered as the contact between meteoric ice and accreted ice. Note that the ECM and inclusions number profiles are now prolonged to 3623 m depth.*

The deuterium and oxygen 18 enrichment of the accreted ice in comparison to lake water is however only about 60% of the corresponding isotopic equilibrium. After considering different possibilities to explain such a situation, Souchez et al. (2002) and Souchez et al. (2000b) developed arguments for a lake ice origin by accretion of frazil ice crystals at the bottom of the ice cover followed by slow freezing of the host water present between the frazil ice crystals.

This overall process, based on the freezing slope concept, is still valid in a general way but, as shown below, recent developments on Lake Vostok's dynamics call for a reassessment of this isotopic interpretation. Firstly, subglacial melting at the ice-lake interface is limited to the northern part of the lake where glacier ice can be aligned on another meteoric water line in a δD-$\delta^{18}O$ diagram than that of Vostok station. This will affect the lake's isotopic composition.

Secondly, the inclined ice-lake interface must be considered as the result of a dynamic equilibrium. Melting in the North of the lake and freezing in the South are conducive in the long run to an horizontal interface but, in the mean time, accreted ice is exported out of the lake by glacier movement, maintaining the inclination of the interface. Thirdly, the lake is geologically old – most probably several millions years old – and there is evidence from the chemistry of the accreted ice that an ancient evaporitic-type reservoir contributed to its chemistry (Angelis et al., 2004). The lake must so be considered as having been several times renewed. These considerations are taken into account in the new isotopic model developed hereunder.

A new isotopic model

Accreted ice sampled in the Vostok ice core was formed in the postglacial period. Because of ice flow (3 m per year) older accreted ice, if present, was exported out of the lake system. Within this timescale with no significant climatic change, the lake can be considered as having a constant volume ($dV = 0$). This assumption is perhaps questionable at glacial-interglacial timescale where climate and ice sheet configuration have changed. Even at this timescale, it still represents a reasonable first approximation for an isotopic model in view of the huge dimensions of the lake and of its tectonic setting regulating subglacial water collection.

With $dV = 0$, the water discharge brought into the lake as a result of ice melting (Q_{in}) is equal to the water discharge (Q_{out}) exported out of the lake system in the form of accreted ice. If C is the concentration of an isotopic species in the lake water with the index "in" for meltwater and index "out" for accreted ice, the isotopic mass balance of the system can be written as:

$$V dC = Q_{in} C_{in} dt - Q_{out} C_{out} dt = Q_{in} \tau dC \tag{23}$$

where τ is the residence time of lake water. Since there is fractionation on water freezing, $C_{out} = \alpha C$ with α being the fractionation coefficient for deuterium or oxygen 18 between ice and water, and:

$$\frac{dt}{\tau} = \frac{dC}{C_{in} - \alpha C} \tag{24}$$

Integrating (24) gives:

$$C = \frac{C_{in}}{\alpha} + \left(C_0 - \frac{C_{in}}{\alpha} \right) \exp\left(-\frac{\alpha t}{\tau} \right) \tag{25}$$

where C_0 is the initial C value at $t = 0$. It can easily be shown that, for $t \geq 3\tau$, $C = C_{in}/\alpha$ and $C_{in} = C_{out} = \alpha C$. The isotopic composition of the accreted ice is the same as the isotopic composition of the meltwater produced. For deuterium as an example, the evolution in time follows the equation:

$$1 + \delta \mathrm{D}_{\mathrm{lakewater}} = \left(1 + \delta \mathrm{D}_{\mathrm{meltwater}}\right)/\alpha + \left(\delta \mathrm{D}_0 - \delta \mathrm{D}_{\mathrm{meltwater}}/\alpha\right) \exp\left(-\frac{\alpha t}{\tau} \right) \tag{26}$$

If δD is expressed in per mil, then 1 has to be replaced by 1000 in equation (26). See also Figure 18.

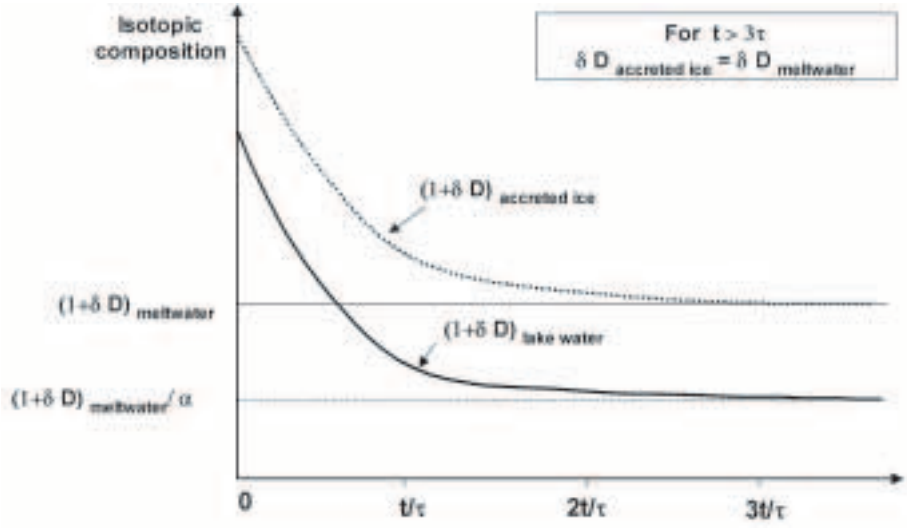

Figure 18: *Schematic diagram showing the evolution of the deuterium composition of lake ice and water in the course of time.*

The time required for ice to cross the lake and reach Vostok station is about 16000 years so that the uppermost accreted ice cannot be older than this, while the ice at the bottom of the accreted layer is probably very recent. Within this time scale, the isotopic composition of the accreted ice is nearly constant, reflecting the steady-state situation reached by the lake system (Figure 17). The isotopic composition of the meltwater produced gives the mean isotopic composition of the glacier ice subjected to melting since there is no fractionation in water isotopes on ice melting. This model considers the evolution in isotopic concentration through time. No effort has been devoted yet to model the spatial distribution of stable isotopes in the lake system.

Reassessment

What are the consequences of this model on the interpretation of the isotopic data?

A first problem concerns the deuterium values. In Figure 19, the deuterium concentration in surface snow samples is given along traverses Vostok-Komsomolskaya (a station north of the lake) and Dome B-Komsomolskaya as a function of the distance from Vostok station (upper straight line). Assuming that the mean deuterium concentration for meteoric ice of the four climatic cycles shows the same geographic variation than present-day snow, a parallel is drawn passing through the point representing the mean deuterium concentration for a complete interglacial-glacial climatic cycle at Vostok (or for the four climatic cycles). A δD value of -442.5‰, the mean value observed in the accreted ice, is reached at a distance about 200 km north from Vostok i.e. along the northern shores of the lake. Although the authors are fully aware that extrapolating the present surface isotope gradient over an entire interglacial-glacial cycle or over four climatic

cycles is questionable, notably because of change in ice sheet configuration in such a long time period, at least the results indicate that it is possible for the subglacial meltwater in the North of the lake to have the isotopic composition of the accreted ice. Furthermore, similar variations in stable isotopes are observed in Dome B and Vostok from the LGM to the present-day while accumulation and surface configuration have probably varied.

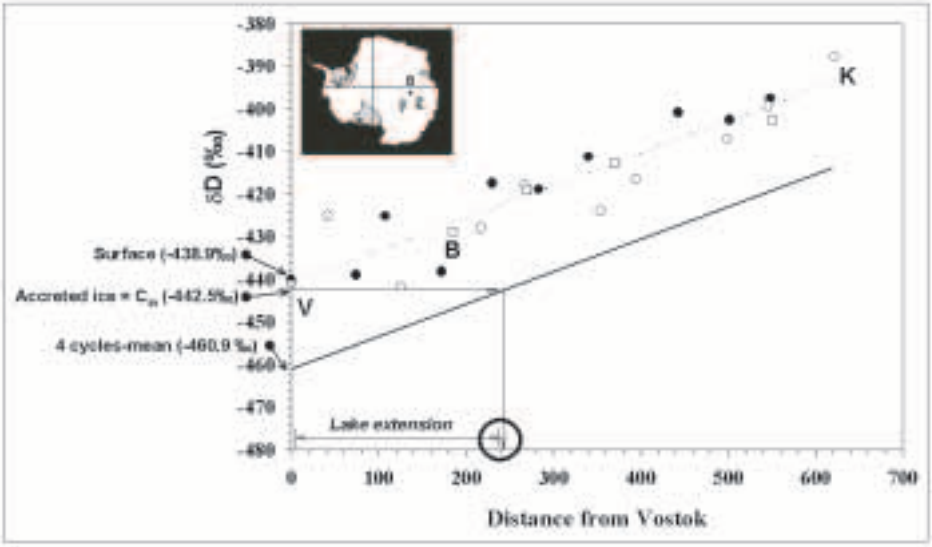

Figure 19: *Use of the δD surface distribution between Vostok (V), Dome B (B) and Komsomolskaya (K) to infer the melting source for the accreted ice. Solid line is drawn parallel to the regression line for surface points through the 4 cycles - mean value at Vostok (see text for details). Open squares = surface snow samples between B and K (Vaikmae, personal communication) ; open and black circles = surface snow samples between V and K for two different traverses.*

A second problem concerns the deuterium excess. Deuterium excess varies between 12 and 18‰ along the four glacial-interglacial climatic cycles at Vostok station (Vimeux et al., 1999). Accreted ice has a mean deuterium excess of 7.5‰. The implications of the model developed are that the latter value of deuterium excess will also be that of glacier ice melting in the northern part of the lake. This ice is coming from the Dome B area. But deuterium excess values of 7-7.5% are only present in some ice from the Last Glacial Maximum in the Dome B core. It is thus unlikely that a mean deuterium excess value of 7.5‰ be reached by melting a substantial part of ice coming from the Dome B area. There is however another possibility. The weak deuterium excess in accreted ice could result from the influence of hydrothermal waters. In hydrothermal areas, spring waters are known to be enriched in oxygen 18 with respect to precipitation supplying the system (Clayton and Steiner, 1975; Craig, 1963). Oxygen shift with respect to the Meteoric Water Line results from isotopic exchange with δ^{18}O-rich rocks at high temperature. From helium studies in the accreted ice (Jean-Baptiste et al., 2001; Jean-Baptiste et al., 2003), a crustal hydrothermal contribution to Vostok lake water probably occurs in connection with a seismo-tectonic activity of the area (Jean-Baptiste et al., 2003; Studinger et al., 2003). A reasonable shift of δ^{18}O = 0.5‰ due to this effect will permit the deuterium

excess of the accreted ice to reach values as low as 7‰.

A third problem is related to the frazil ice hypothesis since effective freezing at a level of 60% equilibrium value cannot be considered anymore. But, as developed below, thermodynamic considerations can help to solve this problem.

A somewhat weak salinity (between 0.1 and 1‰) is suggested for Lake Vostok from chemical studies on the accreted ice in the Vostok ice core (Souchez et al., 2000b; Priscu et al., 1999). Even with such a weak salinity, because of the high pressure (about 337 bars), a thermohaline circulation can occur if lower density waters are produced by melting in an area where the ice ceiling is at lower altitude like in the northern part of the lake. Siegert et al. (2001) showed the water circulation pattern if a weakly saline water is considered. The meltwater produced will progressively form a plume propagating in the upper water column along the inclined ice-water interface. Along this path, supercooling occurs and frazil ice crystals are generated (Souchez et al., 2000b). A loose accreted frazil ice crystals layer is formed; the liquid water initially present decreases as a result of progressive freezing downwards of the host water.

Based on radio-echo-soundings, Bell et al. (2002) suggest an ice accretion rate in subglacial Lake Vostok of 0.7 cm per year for Vostok station. Now, there is a thermal gradient in the bottom of the drilling hole of 0.02°C m^{-1} which corresponds to 45 mW m^{-2}. If this amount of heat is the one released by freezing of ice at the ice-water interface, only 0.45 cm of ice is produced in one year. In perspective of a process where ice originates as frazil crystals within the upper water column, the following reasonable assumption can be proposed. While the latent heat produced by the formation of the frazil ice crystals themselves is released into the lake water, the heat conducted upwards through the solid ice corresponds to freezing of the host water present between the accreted frazil crystals leading to the consolidation of the loose bottom ice layer. Then, the percentage of ice resulting from host water freezing would represent 64% of the accreted ice layer. Another way to approach the problem is to consider that the accreted ice layer, although having a nearly constant isotopic composition (Jouzel et al., 1999), is in fact composed of two different layers (Figure 17). The upper layer consists of ice loaded with solid mineral particles usually aggregated (inclusions); it is about 69 m thick and is most probably formed in the shallow western embayement of the lake discovered by Bell et al. (2002). The lower layer devoid of solid mineral particles (inclusions) has now been sampled to 3623 m depth and is supposed to be about 141 m thick (if it extends to the ice-water interface); it is formed in an area where the lake is deeper. If the transit time for ice from the bedrock ridge separating the shallow embayement from the deep lake to Vostok is taken as 15000 years (annual ice velocity: 3 m per year), freezing of host water would represent 48% of the accreted ice layer at Vostok station. Let us use a value of 50% as a rule of thumb. Such a value is comparable to those obtained in experimental and field studies of frazil ice formation (Souchez et al., 2000b).

Given reasonable apparent fractionation coefficients for frazil ice crystals and frozen host water (Souchez et al., 2000b), the lake's deuterium composition could be calculated but, due to the relative importance of mixing processes in the lake, such a value is not well constrained. It is however, in a δD-$\delta^{18}O$ diagram, on the freezing slope for the accreted ice but not necessarily at the intersection with the Meteoric Water Line defined for Vostok station as previously suggested.

3.2.3.2 Special features in the transition zone

A study of ice properties in the transition zone between meteoric ice and accreted ice in the Vostok core supplies additional information in the context of this chapter. Figure 17 gives the ECM (Electrical Conductivity Measurements), mineral particle aggregates (inclusions) number, gas content and crystal size at a 1 m sampling length across the meteoric ice - accreted ice contact. Also shown is the δD profile with a 0.1 m sampling length between 3535 and 3541 m depth. A striking feature of this figure is that the transition in ECM values from 800 mV, a value typical for meteoric ice, to the detection limit (30 mV) in accreted ice lies above the isotopic transition. Furthermore, gas content is nil at the level of and below the isotopic transition. Gases and impurities are indeed expelled in ice resulting from water freezing. This is the main reason for the total absence of gases in the accreted ice. The isotopic transition is developed along an ice core thickness of about 0.7 m. If this is considered as the length over which diffusion is noticeable, then solid state diffusion is excluded as the main mechanism to explain the situation. It can indeed be computed that, with a solid state isotopic diffusion coefficient in ice of 10-15 $m^2\ s^{-1}$, diffusion will only be discernible on a distance of 0.1 m in 16000 years, the maximum age for the accreted ice as seen above. Therefore, diffusion within the host water surrounding the accreted frazil ice crystals must be considered.

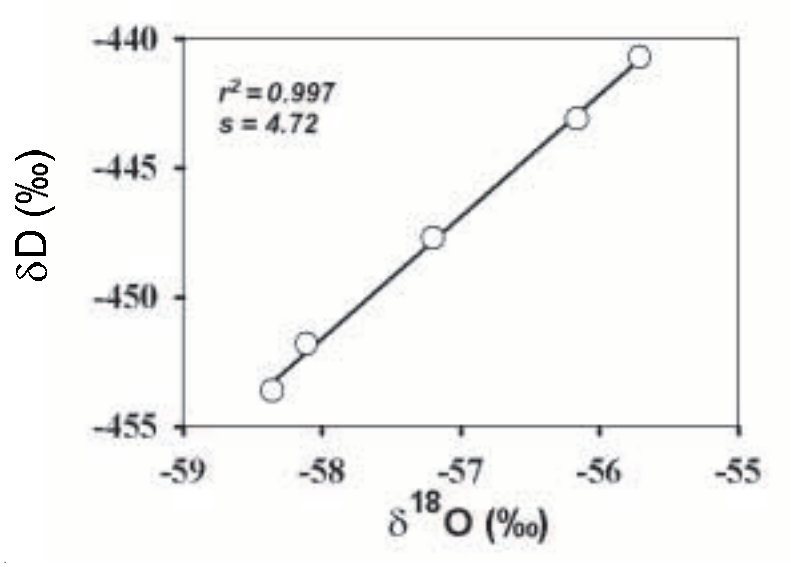

Figure 20: *δD-δ^{18}O diagram for the isotopic transition zone to the accreted ice. S is the slope of the regression line.*

The progression of the freezing front in this host water consolidating the accreted ice is to be viewed as the resultant of a continuous exchange liquid water solid ice, a consequence of thermal agitation and heat transfer. The isotopic composition in the transition zone represents a combined signal of the initial isotopic composition in the accreted ice and that of the influence of diffusion in liquid water during consolidation of the accreted frazil and recrystallisation. A similar process was invoked to explain the transition between glacier ice and marine ice present in a former crevasse of an ice shelf Souchez et al. (1995b). In a δD-δ^{18}O diagram (Figure 20),

the points representing the samples of the isotopic transition zone are well aligned on a slope joining a point representing the lowest meteoric ice sample in the core to a point representing the upper unmodified accreted ice sample. This can be considered as a mixing line although mechanical mixing of the two end members is not considered.

3.2.4 Conclusions

A detailed investigation of ice properties, mainly the isotopic composition, was conducted on at the basal part of the Vostok ice core.

Complex ice deformation developed in the lower 228 m of the ice sheet (3311m to 3538m depth) has resulted in folding and intermixing of ice, at two distinct scales. A size-selective entrainment of bed material into basal ice has most probably occurred. The basal layer has built upwards through longitudinal compression and complex deformation associated with inhomogeneities in the ice and with bedrock protuberances. This first conclusion is relevant to ice core paleoclimatology and to ice sheet modelling. It suggests that it is unlikely to find very old ice with a proper chronology.

Secondly, the physical environment of Lake Vostok is primarily the consequence of the kind of thermohaline circulation implying ice formation in the upper water column of the lake. In a lake system having been renewed several times, owing to meltwater input and accreted ice export, the isotopic concentration of the accreted ice is shown to be the same as that of the glacier ice subjected to melting. The dual origin of the accreted ice layer – frazil ice crystals and frozen host water – is supported by thermodynamic considerations. Furthermore, a detailed survey of the transition zone between meteoric ice and accreted ice adds further weight to the suggested processes.

3.3 An isotopic model for basal freeze-on associated with subglacial upward flow of pore water

(R. Souchez, D. Samyn, R. Lorrain, F. Pattyn, S. Fitzsimons)

3.3.1 Introduction

There are numerous cold-based glaciers at temperatures several degrees C below the pressure-melting point in polar environments. Some of these glaciers are resting on subglacial sediments and exhibit stratified basal ice layers more or less loaded with debris. Such debris-bearing ice testifies for the action of basal freeze-on.

Soft-bedded ice streams are the main control on ice discharge of some important sectors of ice sheets. Lubrication by build-up of pore-water pressure in subglacial sediments results in low effective stress and allows fast flow in these ice streams (Tulaczyk et al., 2000). Basal freeze-on can induce water-pressure changes that result in fast flow stoppage because of till consolidation. Basal freezing may result from climatic cooling, ice thinning or change in basal shear heating. Christoffersen and Tulaczyk (2003a) indicate that in such circumstances subglacial upward pore water flow occurs as a consequence of ice-water interface curvature and surface tension effects. These effects and the progression of the freezing front downward lead to the construction of a stratified basal debris-bearing ice.

In this chapter, we investigate from an isotopic point of view the upward pore-water flow model and the consequent ice segregation giving rise to a basal ice accretion layer. An isotopic model for stable isotopes composition, both in δD and $\delta^{18}O$, is developed predicting the hydrogen and oxygen isotopic composition of the ice segregated by such a mechanism. Examples of isotopic composition of basal ice layers from some Antarctic glaciers matching the predictions of the model are then described. Such ice layers are supposed to be built by the subglacial process invoked by Christoffersen and Tulaczyk (2003a).

3.3.2 Freeze-on thermodynamics

The temperature of the freezing point is depressed by an increase in fluid pressure and by an increase in solute concentration. In some circumstances, ice-water interfacial effects arising from interface curvature have also to be taken into account. This is the case in pore spaces of fine-grained subglacial sediments. The pressure difference across the ice-water interface when supercooled liquid pore water is present gives rise to a lowering of the pore water pressure at the freezing interface. This drop of pressure induces an hydraulic gradient driving water flow toward the freezing interface where a layer of segregation ice is accreted. Building up on the analogy between frost heave phenomena and debris-bearing basal ice formation, Christoffersen and Tulaczyk (2003a) develop a high-resolution numerical model that is able to understand the freeze-on mechanism and to trigger ice stream stoppage.

In their study, these authors consider either a closed water system where water driven to the freezing interface is only pore water of the subglacial sediment or an open system where water

is supplied from beneath the subglacial sediment. In both situations the upward flow of pore water leads to ice formation. Since the freezing front is moving into the subglacial till, successive layers of segregation ice are produced and the observed stratification of debris-bearing basal ice is so developed. Figure 21 visualizes the process.

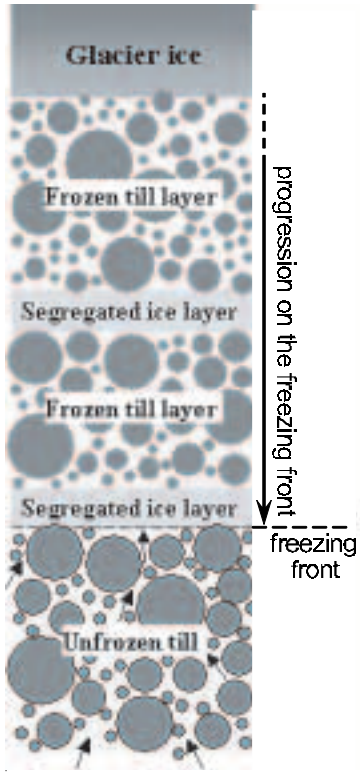

Figure 21: *Schematic diagram showing pore water flowing within subglacial sediments towards the freezing front at the base of a glacier and producing accretion ice (modified from Christoffersen* and *Tulaczyk (2003b). Either frozen till or segregated ice layers are produced, depending on the physical conditions.*

3.3.3 The isotopic model

The upward flow of pore water toward the freezing interface through the subglacial fine-grained sediment is considered to occur as water migration along thin liquid films surrounding the sediment particles. Let us consider a specific path and define the liquid film along this path. The same reasoning will apply to the other paths.

Let N be the number of water molecules presenting a specific isotopic composition in $H_2^{18}O$ or HDO (D = deuterium), then:

$$N = CV \tag{27}$$

where C is the concentration of such an isotopic water molecule in the liquid film and V, the volume of this film. It follows that:

$$dN = d(CV) = CdV + VdC \tag{28}$$

The volume of the water film is supposed to be constant in time, the amount of liquid water driven into the film at the base of the subglacial sediment being equal to the amount of film water frozen at the freezing front (open system). Thus, $dV = 0$.

Therefore $dN = VdC = Q_{in}C_{in}dt - Q_{out}C_{out}dt$ where Q_{in} and Q_{out} are the water flux entering the film (with isotopic concentration C_{in}) and the water flux leaving the system by refreezing and ice export (with isotopic concentration C_{out}), respectively.

Now, the model described in section 3.2.3.1 (see therefore equation (25)) can be adapted as it has been developed in Souchez et al. (2004). So it can be shown that the composition of the ice formed by freezing is the same as the one of the water entering the pores of the fine-grained subglacial sediment after a period longer than 3 times the water film renewal time.

Considering that the water film has been renewed at least three times in the process of ice segregation is most probably correct in view of the micrometric thickness of the film and of the commonly observed thickness of segregation ice layers in debris-bearing basal ice and of the subglacial till.

3.3.4 Discussion

The water present in the pores of the subglacial sediment has most probably a composition in stable isotopes very close to that of glacier ice. This is supported by a fractional melting experiment that has been performed on polar meteoric ice sample. In a δD-δ^{18}O diagram, points representing the successive melt samples taken during the experiment appear tightly clustered (Souchez et al., 1988). The extreme range is only 0.2‰ in δ^{18}O. This implies, as suggested by Moser and Stichler (1980), the absence of fractionation during ice melting. It follows that the isotopic composition of segregation ice originating by the above-described process is also that of the overlying meteoric glacier ice. Since different meteoric ice samples are aligned in a δD-δ^{18}O diagram on a Meteoric Water Line with a slope close to 8, debris-bearing basal ice produced by upward pore water flow in subglacial sediment would also plot on the same line. This prediction can be tested and will be considered below.

The study of fractionation by freezing has led to the freezing slope concept (Souchez and Jouzel, 1984) in closed as well as in open systems. Samples of ice due to freezing of water are aligned in a δD-δ^{18}O diagram on a slope lower than the one of the Meteoric Water Line. The value of the freezing slope can be calculated from knowledge of the isotopic composition of initial water at the onset of freezing and from the equilibrium fractionation coefficients between ice and water for deuterium and oxygen 18. Freezing slopes implying an inverse relationship between deuterium excess (d = δD - 8 δ^{18}O) and δ-values are displayed in lake ice (see section 3.1.3), in some basal stratified ice from polar glaciers (Souchez et al., 1988; Sleewaegen et al., 2003) and also in ice due to regelation past grains at the glacier bed (Iverson and Souchez, 1996). By contrast, amber ice (Cuffey et al., 1999; Cuffey et al., 2000) and basal ice with

fine dispersed debris facies (Knight, 1997) do not exhibit freezing slopes but are produced by completely different mechanisms. Dealing with basal stratified ice, how can the apparent fractionation be explained, while in the isotopic model apparent fractionation does not occur at steady state?

3.3.5 Basal stratified ice with no apparent fractionation

Figure 22 shows in different δD-δ^{18}O diagrams the position of samples of debris-bearing basal ice layers (black triangles) together with layers of glacier (meteoric) ice (open circles) from two Antarctic outlet glaciers. In Figure 22a are represented samples from Mackay glacier, an outlet glacier from the East Antarctic ice sheet crossing the Transantarctic Mountains and reaching the Ross Sea. The samples were taken from two overturned icebergs from that glacier, exhibiting a basal sequence tens of meters thick. In 1998, these icebergs were located at 76°57.5'S, 162°20.5'E and at 76°57.4'S, 162°20.1'E, respectively. In Figure 22b are represented samples from Taylor glacier, an outlet glacier from the East Antarctic ice sheet ending in the Dry Valleys area of South Victoria Land. The samples were taken in a tunnel excavated in the basal sequence in the left margin of the glacier, about 1 km from the snout.

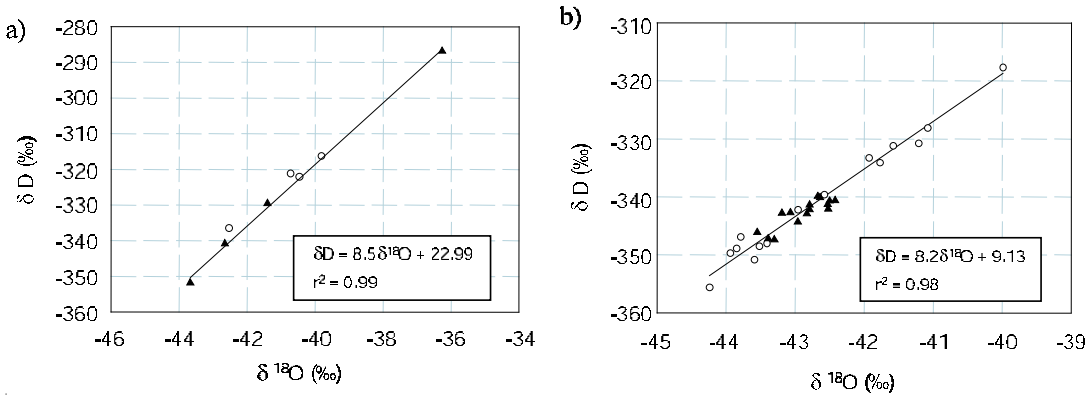

Figure 22: *δD-δ^{18}O diagrams showing different samples from two Antarctic glaciers - Mackay (a) and Taylor (b) glaciers. Black triangles stand for debris-bearing basal ice layers. Open circles represent layers of glacier (meteoric) ice. The equations of the regression lines are given with their respective correlation coefficients.*

In both situations, samples from the debris-bearing ice are aligned on a Meteoric Water Line; the slope being 8.5 for Mackay glacier and 8.2 for Taylor glacier. If the middle point of the range of δ-values were considered as representative for glacier melt in the area, the calculated freezing slope from Souchez and Jouzel (1984) would be 4.94 and 4.87 respectively. This is strikingly different from the values given above. There is thus no apparent fractionation in these debris-bearing ice layers. Thus, isotopic composition of the debris-bearing ice layers from these two Antarctic glaciers strongly suggests that they result from ice segregation by upward pore water flow in the subglacial fine-grained sediments.

3.3.6 Contrasting basal ice isotopic signatures

While freezing slopes are displayed in a δD-δ^{18}O diagram for some debris-bearing basal ice layers of polar glaciers, none are present in the two examples given above. The question then arises: what are the conditions required for a freezing slope to be developed and to what extent are such conditions fulfilled.

Since equilibrium fractionation always occurs at the ice-water interface, distribution of stable isotopes of oxygen or hydrogen in ice during water freezing is related to compositional variations in the liquid adjacent to the freezing front. These compositional variations depend on mixing in the liquid water that occurs by diffusion and by convection. A zone in which transport takes place by diffusion only always exists as a boundary layer adjacent to the ice-water interface. If the boundary layer is sufficiently thick so that the role of convection can be ruled out, a steady-state is developed in the ice in which the isotopic composition is the same as that of the initial water at the onset of freezing (Souchez et al., 1987). The lower the isotopic diffusion constant in the water, the best developed is the steady state in the ice.

Now, in the thin water films surrounding the grains of the subglacial sediment, diffusion must be particularly slow because of the tortuosity of the path and of the reduced thickness of the water film. Therefore, the isotopic model described above most probably applies and the debris-bearing ice shows no apparent fractionation. The suggested isotopic distribution in Christoffersen and Tulaczyk (2003b) is not very likely because diffusion cannot compensate sufficiently rapidly the impoverishment in heavy isotopes of the water adjacent to the ice-water interface.

By contrast, if convection occurs in the water reservoir or if diffusion is facilitated, the ice will exhibit an isotopic composition different from that of the liquid water. Depending of the freezing rate, on trapping of unfractionated water pockets during ice accretion or on a reservoir effect – in a closed system, the enrichment of the ice produces an impoverishment of the residual water –, the amount of observed fractionation is variable. This leads to the development of a freezing slope in a δD-δ^{18}O diagram. The same is true for regelation past grains in the subglacial sediment (Iverson and Souchez, 1996) in which multiple melting and freezing events and a loss of liquid water progressively produce an enrichment in heavy isotopes of the ice along the freezing slope.

Varied isotopic responses result from different freeze-on processes in the subglacial environment. The isotopic composition can thus be an interesting tool for a better understanding of the mechanisms involved.

3.3.7 Conclusion

Upward pore water flow in subglacial sediments as a consequence of ice-water interface curvature and surface tension effects can be at the origin of the formation of segregation ice at the glacier sole and of debris-bearing basal ice layers. A simple isotopic model indicates that no apparent fractionation will be detected in this case. Isotopic analyses, both in δD and in δ^{18}O, of basal ice layers from two Antarctic outlet glaciers give weight to this assertion.

3.4 Ice flow over subglacial lakes: the Lake Vostok case *(F. Pattyn, B. De Smedt and R. Souchez)*

As mentioned in section 3.2, radio echo sounding in East Antarctica has revealed the existence of numerous subglacial lakes (Oswald and Robin, 1973; Siegert et al., 1996). The largest one is Lake Vostok (14 000 km^2) and is associated with a prominent morphological surface feature within the Antarctic ice sheet. The ice-sheet surface above the lake is rather flat and featureless, consistent with the surface of an ice shelf. Ice flow over a large subglacial lake should be analogous to the flow of an ice shelf, where the lack of basal shear stress prevents deformation of internal layers (Siegert et al., 2000). Ice flows over the lake in a general west-east direction (Figure 23). Once over the lake the ice flow in the south is diverted towards the southeast (Kapitsa et al., 1996), a feature that is confirmed from an analysis of internal radar reflection layers (Bell et al., 2002). Moreover, this along-lake flow component seems persistent since the Last Glacial Maximum (Bell et al., 2002). On the contrary, velocity vectors derived from interferometry show a different direction, i.e. more towards the east (Kwok et al., 2000). The northern part of the lake is largely unexplored and velocity measurements are lacking (Figure 23).

Although the ice surface above the lake is relatively flat, an along-lake north-south slope is prominent, tilting 60 m over a horizontal distance of more than 250 km. Over the lake, the ice is thicker in the north (up to 4300 m) and thins to 3700 m in the south (Studinger et al., 2003). Lake Vostok has an ice-water interface sloping at eleven times the ice surface gradient (but in the opposite direction), which indicates that the overlying ice is in hydrostatic equilibrium (Siegert et al., 2001). According to Souchez et al. (2004), the inclined ice-lake interface should be considered as the result of a dynamic equilibrium: melting in the north of the lake and freezing in the south are conducive in the long run to a horizontal interface but, in the mean time accreted ice is exported out of the lake by glacier movement, maintaining the inclination of the surface. This refreezing is due to a well developed water circulation in the lake (Souchez et al., 2000b; Wüest and Carmack, 2000; Williams, 2001; Siegert et al., 2001; Mayer et al., 2003). Lake Vostok is thus quite unique in an ice-dynamical way, encompassing a variety of ice-deformational features in a nutshell.

A comprehensive understanding of the ice flow across Lake Vostok demands the use of a so-called higher-order ice-sheet model, i.e. a model that besides deformation due to vertical shearing, takes into account normal stress components as well. Mayer and Siegert (2000) investigated the ice flow along a longitudinal transect with a 2D higher-order flow line model, but these experiments were carried out in a diagnostic fashion (ice-sheet geometry was kept fixed). Here, the ice flow across Lake Vostok is investigated using a dynamical 3D thermomechanical higher-order ice-sheet model (see section 2.1), which shows – for the first time – the major ice-dynamical features of this area in a prognostic fashion. The purpose of the experiments is to determine the ice flow field across the whole lake and to *identify* the processes responsible for the flat surface topography, the along-lake slope component, the ice flow turning across the lake, and Lake Vostok's influence on the regional dynamics of the East-Antarctic ice sheet.

3.4.1 Experimental setup

The modeled domain consists of the East-Antarctic catchment area between Dome Argus, Ridge B, the Transantarctic Mountains and the Southern Ocean (Figure 24). Present ice ge-

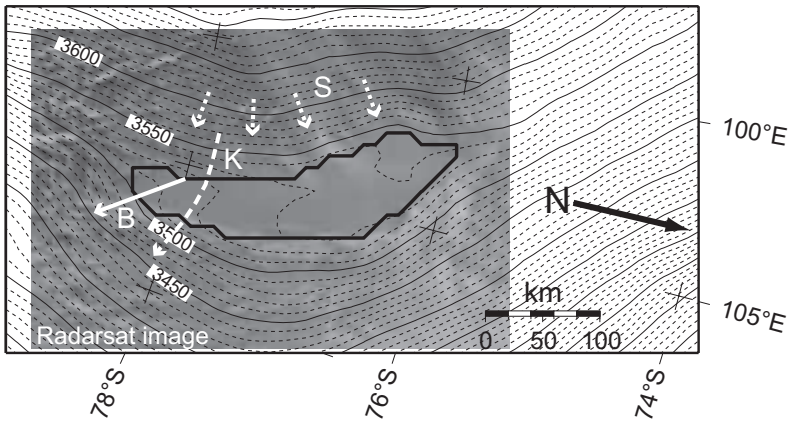

Figure 23: *Surface topography near Lake Vostok, determined from satellite altimetry (Liu et al., 1999), superposed on a RADARSAT image. A general situation of the area is given in Figure 24. White vectors show different observed flow directions: B = ice flow across the southern part of the lake according to Bell et al. (2002); K = ice flow across the lake according to Kwok et al. (2000); S = grounded ice flow according to Siegert et al. (2001).*

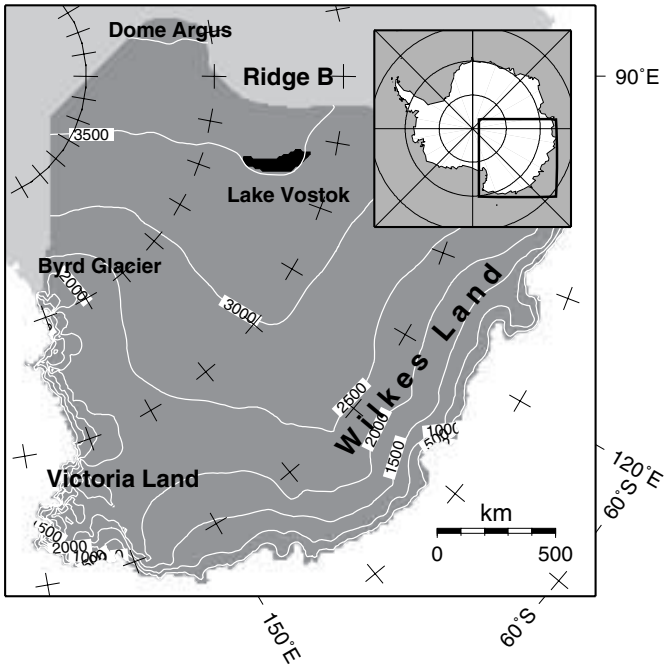

Figure 24: *Situation map of the modeled domain (dark gray). The position of Lake Vostok is shown in black. For this black zone the condition* $\beta^2_{\text{lake}} = 0$ *is fulfilled.*

ometry (ice thickness, bedrock elevation) is taken from the BEDMAP datasets (Liu et al., 1999; Lythe and Vaughan, 2001). Surface accumulation is obtained from Vaughan et al. (1999). Data were resampled to a grid of 10 by 10 km, leading to 251 by 251 grid points in the horizontal, and 40 layers were considered in the vertical. The position and size of Lake Vostok are derived from Studinger et al. (2003) (Figure 24). Lake Vostok is implemented in the model as a zone with a frictionless base, i.e. $\beta^2_{\text{lake}} = 0$. The assumption is made that the pressure of the water at the bottom of the ice is equal to the hydrostatic pressure necessary to float the ice mass.

A first series of experiments are diagnostic, i.e. the velocity field is calculated based on the present observed ice-sheet geometry that was kept fixed. This involves a 'no lake' (DNL) and a 'lake' (DLE) experiment, where for the latter a stress-free basal surface was considered within the lake boundaries ($\beta^2_{\text{lake}} = 0$). The prognostic experiments start from the present-observed ice geometry, and the model is run forward in time for 10,000 years to reach a situation close to steady state. There is no explicit treatment of the lake/bed or the lake/ice interface, nor is there any treatment of water circulation. Our sensitivity analysis consists of three prognostic experiments, a 'lake' experiment (LE), where the lake is determined as a stress-free spot or $\beta^2_{\text{lake}} = 0$, a 'no lake' experiment (NL), and a 'lake' experiment with buoyancy (LBE). For the LE experiment, the ice/water interface was kept fixed in time and only the ice/air surface changed in time. In the LBE experiment, both ice/water and ice/air interfaces were altered to fulfill buoyancy.

3.4.2 Diagnostic experiments (DNL and DLE)

Ice flow in a grounded ice sheet will generally follow the steepest surface gradient, as in the absence of a significant longitudinal stress contribution, the driving stress is balanced by the basal shear stress and hence directly dependent on the surface slope and direction. This notion is confirmed by the DNL experiment (Figure 25), accounting for a general west-east ice flow over the grounded ice sheet, perpendicular to the surface contours. The surface of the ice above Lake Vostok, however, is very flat and slightly tilted in a north-south direction, which deviates the bulk ice flow to the southern sector of the lake area. The basal and surface velocity are lowest across the lake, as the area is nearly flat. This is not a realistic case, as it implies that the eastern margin of the lake receives no ice flux. The higher-order model solution (DNL) is very similar to the solution according to the *shallow-ice approximation* (SIA). In large ice sheets, the SIA is perfectly valid as long as surface and bedrock slopes are relatively low (typical interior ice flow) and basal friction is high. As shown by Pattyn (2003), the major difference between the SIA and a higher-order model solution occurs under the ice divide, in areas with pronounced bedrock variability and in zones of low basal friction. As long as Lake Vostok is considered as a high-friction area, both model results will be complementary.

Treating the lake area as a stress-free basal spot within the ice sheet results in an ice flow pattern that exhibits a general west-east flow component, also for the ice that crosses the lake. Experiment DLE puts a higher weight on the horizontal stress gradients as – due to the lack of basal friction – vertical shearing vanishes across the lake. While the ice flow is perpendicular to the surface contours for the grounded ice sheet, the ice flux at the lake margins controls the ice flow across the lake, which is in the direction of the highest ice flux and not necessarily in the

direction of the steepest surface slope (e.g. an ice shelf). Contrary to experiment DNL basal velocity is highest across the lake: due to the drag-free basal boundary condition there is no shear stress gradient near the ice base over the lake, so that basal velocity is a direct indication of the column velocity. The flow direction in the southern part of the lake is towards the east, in agreement with the flow pattern by Kwok et al. (2000).

3.4.3 Prognostic experiments (NL, LE and LBE)

Figure 26 shows the surface elevation and surface slope according to the three prognostic experiments. Both LE and LBE experiments exhibit a distinct surface flattening across Lake Vostok, which is – as demonstrated by Pattyn (2003) – associated with the stress-free base ($\beta^2_{\text{lake}} = 0$). Such a feature is not observed in the NL experiment. The surface topography according to LBE fits better the observed situation OBS across the lake.

The ice flow direction across Lake Vostok is highly dependent on the position of the local ice divide that – according to present observations – crosses the lake from west to east and divides the ice flow towards the Transantarctic Mountains from the ice flow towards Wilkes Land. As this series of experiments are dynamic, we have no control on the exact position of this ice

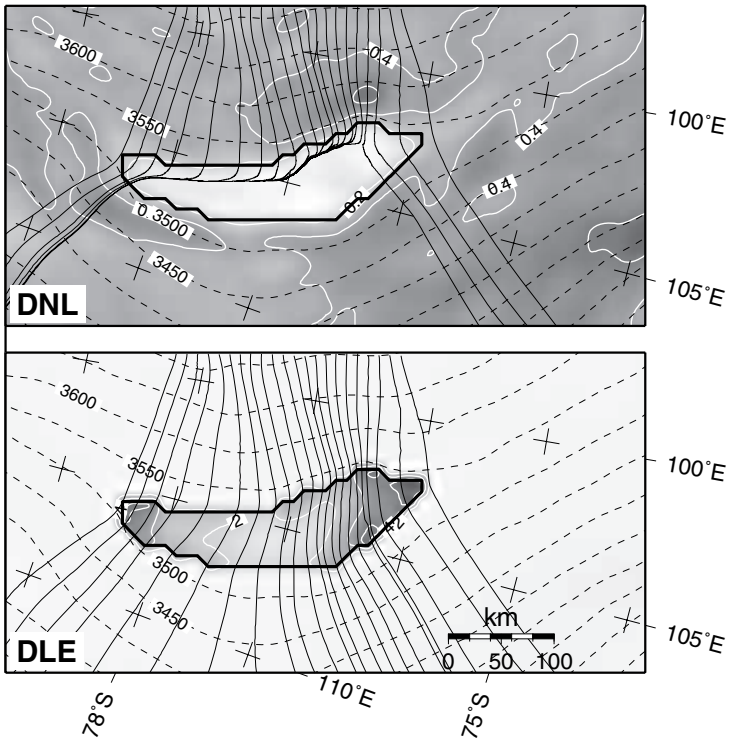

Figure 25: *Predicted basal velocity (m a^{-1}, gray shaded and white contours), surface topography (m a.s.l., black dashed contours), and flow lines across Lake Vostok for the* DNL *and* DLE *experiment. The position of Lake Vostok is given by the thick black line. A different gray scale is used for both panels.*

divide and its position will depend on the overall geometry of the drainage basin as well as local characteristics of the Lake Vostok area. In a near steady-state situation, this divide lies

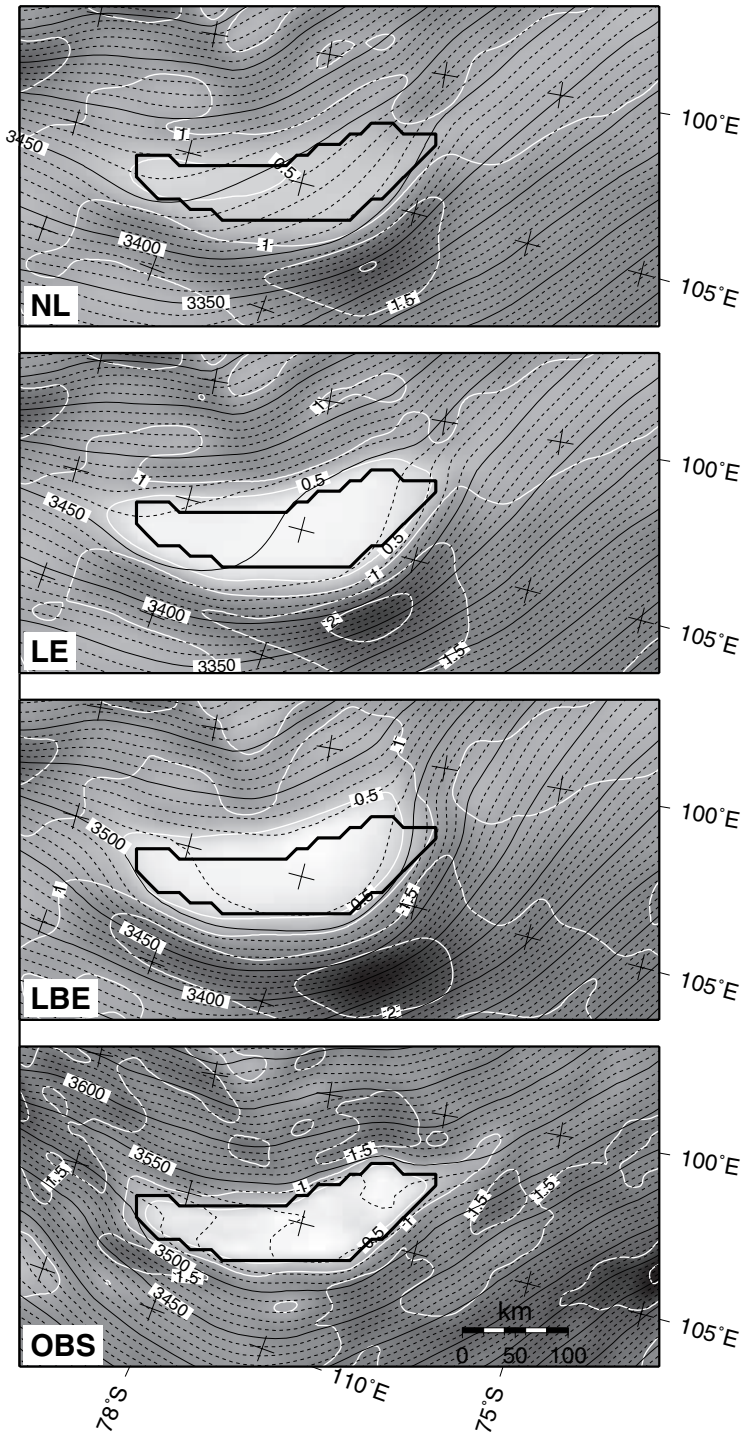

Figure 26: *Predicted surface slopes (gray shaded and white contours every 0.5 $\times$ 10^{-3} rads) and surface topography (m a.s.l., black contours) for the* NL*,* LE *and* LBE *experiment, as well as the altimetric observations (*OBS*). The position of Lake Vostok is given by the thick black line.*

to the south of Lake Vostok, giving rise to a northward along-lake slope component (Figure 27, experiments NL and LE). Only when taking into account buoyancy (LBE experiment) the local divide lies across the lake, diverting the ice flow to the southeast in the southern sector of the lake, and to the northeast in the northern part. The flow pattern in the south is in accord with the findings of Bell et al. (2002). Also, the velocity magnitude and direction is in accord with the observations of Kapitsa et al. (1996). A prominent feature, however, is the turning of the ice flow across the lake, as shown in both LE and LBE experiments, while without the presence of a lake a steady west-east flow pattern is observed (panel NL in Figure 27).

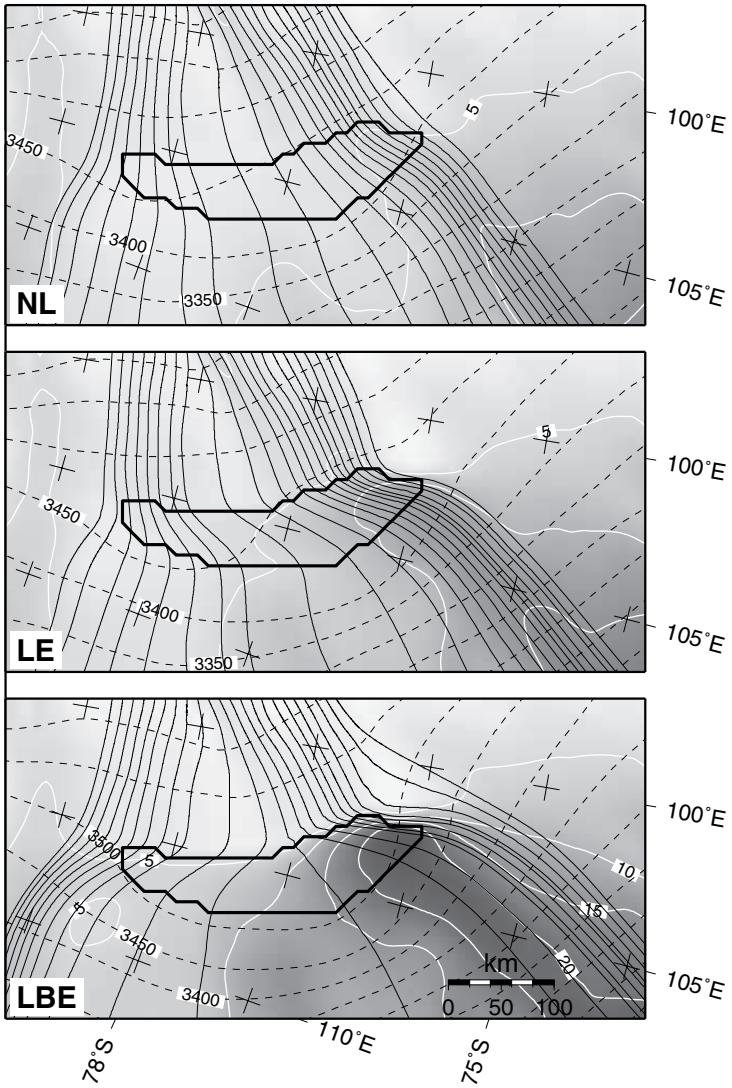

Figure 27: *Predicted surface velocity (gray shaded and white contours every 5 m a^{-1}), surface topography (m a.s.l., black dashed contours), and flow lines across Lake Vostok for the* NL*,* LE *and* LBE *experiment. The position of Lake Vostok is given by the thick black line.*

From the pattern of the modeled flow lines and ice velocity it is evident that an important amount of ice is transported along the northern margin of the lake. LE and LBE experiments show the

highest velocity in the northern part, which is also the area where prominent basal melting at the ice/water interface occurs (Siegert et al., 2001). The local speedup over the lake is more pronounced in the LBE experiment, but visible in the LE experiment as well. In a region of 40 km downstream of the western grounding line, the ice speeds up. Further downstream, it slows down towards the eastern grounding line. The speedup is a direct consequence of the lack of basal drag when the ice crosses the grounding line and flows across the lake. The slowdown is due to the backstress exerted by the grounded ice at the eastern margin of the lake. The ice speedup is more pronounced in the north as here (i) the ice flux across the western margin is larger than in the south, (ii) the ice is thicker, (iii) the along-flow surface slope across the margin is steeper than in the south, and (iv) the lake (hence the frictionless area) is wider as well. All these factors lead to a higher ice flux in the northern sector of the lake. According to the LBE experiment the ice in the northern sector is somewhat thinner compared to the LE experiment. At first sight, this should reduce the ice speed as the ice flux becomes smaller. However, the reverse is true and the reason probably lies in the fact that the northeastern lake margin is less steep than in the LE experiment as the ice/water interface is situated higher within the subglacial trench (due to the floatation criterion). This would eventually reduce the amount of backstress so that the ice can flow faster.

For both LE and LBE experiments, this higher ice flux in the north seems to start an enhanced flow feature in the direction of Totten Glacier in Wilkes Land. The onset of enhanced flow of ice in East Antarctica is believed to be associated in a number of cases with the presence of subglacial lakes (Siegert and Bamber, 2000). Storage of subglacial water has the potential to control the ice flow of the interior ice sheet and several lakes lie at the onset of major enhanced ice-flow features such as those feeding into Byrd Glacier (Siegert and Bamber, 2000). However, their analysis is based on flux calculations, leading to so-called balance velocities (Budd and Warner, 1996). Since balance velocities are directly derived from surface slopes, they infer a flow mechanism that is based on gravitational downward motion. Ice flow over subglacial lakes is similar to the flow of ice shelves and thus flux-driven, which is not accurately represented using the technique of Budd and Warner (1996). This is probably the reason why Lake Vostok – lying relatively far inland – is not associated with any enhanced flow feature derived from balance velocities.

When buoyancy forces and hydrostatic equilibrium are taken into account, the along-lake surface slope is preserved, which is not the case for the LE experiment. Due to hydrostatic equilibrium, this tilted surface slope is also responsible for a tilted ice/water interface in the opposite direction. In the long run, however, when the LBE experiment is run forward for another 10,000 years, even the tilted surface disappears. The ice divide, however, remains more or less across the center of the lake so that the southeastern flow pattern in the south is maintained. These findings corroborate the results of Bell et al. (2002) that the flow pattern did not change during the last 10,000 years. The leveling of the ice/water interface in the long run is due to a thinning of the ice across the lake in the northern sector – as the ice flux in the north is higher – and does not influence any other part of the ice sheet in the vicinity of Lake Vostok. This means that the present tilted surface is either a transient feature or (more likely) controlled by the dynamic equilibrium between melting and accretion processes at the ice/water interface due to the lake

circulation (Souchez et al., 2004).

The lack of comprehensive velocity measurements in the northern part of the lake prevents a proper validation of the above model results. Ice velocities in the northern part are probably slightly overestimated according to the LBE experiment as anisotropic effects are not taken into account in the model description: crystal orientation in ice shelves is distinctly different compared to that in ice sheets, which has its impact on deformation rates (Paterson, 1994).

3.4.4 Conclusions

For the first time, a dynamical 3D thermomechanical simulation of the ice flow across Lake Vostok is presented. The model results show that by treating the ice/lake interface as a stress-free surface (similar to an ice shelf), major ice-dynamical features such as the surface flattening and turning of the ice flow across the lake, are accurately reproduced, even though subglacial lake dynamics are not treated explicitly.

A relatively stable velocity pattern – with a local ice divide that crosses Lake Vostok – is obtained when taking into account buoyancy effects. This also assures an along-lake southward slope, maintaining the tilted ice/water interface. However, the tilted ice/water interface shows the tendency to level when the model is allowed to run on a longer time scale, which indicates that the lake water circulation plays a decisive role in balancing melting in the north and accretion in the south. Only when coupling a model of lake water circulation to the ice sheet model, a more comprehensive insight in these processes might be obtained.

According to the experiments, ice velocities are the highest in the northern sector of the lake. Lake Vostok can therefore be considered as the onset of an enhanced ice-flow feature, more precisely the onset of the Totten Glacier catchment.

3.5 Dynamics of continental ice streams: influence of subglacial water flow *(F. Pattyn, S. De Brabander and A. Huyghe)*

The East Antarctic ice sheet is traditionally considered a stable feature characterized by slow moving interior ice with drainage through ice shelves across a grounding line and by a few faster moving outlet glaciers. This view is now challenged by new evidence coming from balance velocities (the depth-averaged velocity required to keep the ice sheet in steady state for a given net surface mass accumulation) obtained from radar altimetry and radio-echo sounding, as well as surface velocities obtained from interferometric synthetic aperture radar (Bamber et al., 2000). Complex ice flow (a combination of ice flow due to internal deformation and basal motion) was already observed within the West Antarctic and the Greenland ice sheets (Joughin et al., 1999; Joughin et al., 2001), and recent studies confirm a similar complexity within the East Antarctic ice mass (Pattyn and Naruse, 2003; Rippin et al., 2003). Balance velocity maps reveal a complex network of enhanced flow tributaries penetrating several hundred kilometers into the ice sheet interior (Bamber et al., 2000; Testut et al., 2003). Here, we investigate such features observed in Dronning Maud Land, East Antarctica and try to disentangle the mechanisms that control their existence and behaviour with a three-dimensional thermomechanically coupled ice-sheet model including higher-order stress gradients, coupled to a steady-state model of basal water flow.

3.5.1 Data

The Ragnhild glaciers are three – as yet nameless – ice-flow features situated between the Sør Rondane and Yamato Mountains in eastern Dronning Maud Land, Antarctica. They are clearly identified as enhanced ice flow features in maps of balance fluxes of the Antarctic ice sheet. The largest feature – here referred to as West Ragnhild Glacier or WRG – penetrates almost 400 km inland (Figure 28). Radarsat imagery reveals distinct flow lines along the ice surface, but they are less apparent compared to those of other large ice streams and outlet glaciers of East Antarctica. A comparison between 1937 Norwegian maps and 1960 Belgian maps permitted Nishio et al. (1984) to determine the horizontal movement of the ice shelf front along the Princess Ragnhild Coast. Derwael Ice Rise is situated directly in front of WRG, and therefore most of the ice flow is diverted around this buttressing feature. The maximum flow speed occurs at the western side (350 m a^{-1}), while flow velocities to the east of Derwael Ice Rise are somewhat lower. A comparison between 1965 Belgian maps and Radarsat imagery (Jezek and RAMP Product Team, 2002) shows an acceleration in the west and a deceleration towards the east along the Princess Ragnhild Coast (Table III). The latter might indicate an eventual stoppage of the glaciers in the center and the east of the catchment area. Ice flow measurements in the interior of the drainage basin are sparser, but clearly mark a velocity of 100 m a^{-1} on WRG between the Sør Rondane and the Belgica Mountains (Figure 28; Takahashi et al., 2003). This is relatively fast for typical ice-sheet flow so far inland. According to Bindschadler et al. (2001), 100 m a^{-1} can be considered as the lower limit of ice-stream flow in Antarctica. Ice speed on Central Ragnhild Glacier (CRG) is distinctly lower.

If these stream features exist, they are to a certain extent topographically controlled.[4] Airborne

[4]Additional evidence for the existence of these glaciers stems from an aerial survey to the west of the Sør

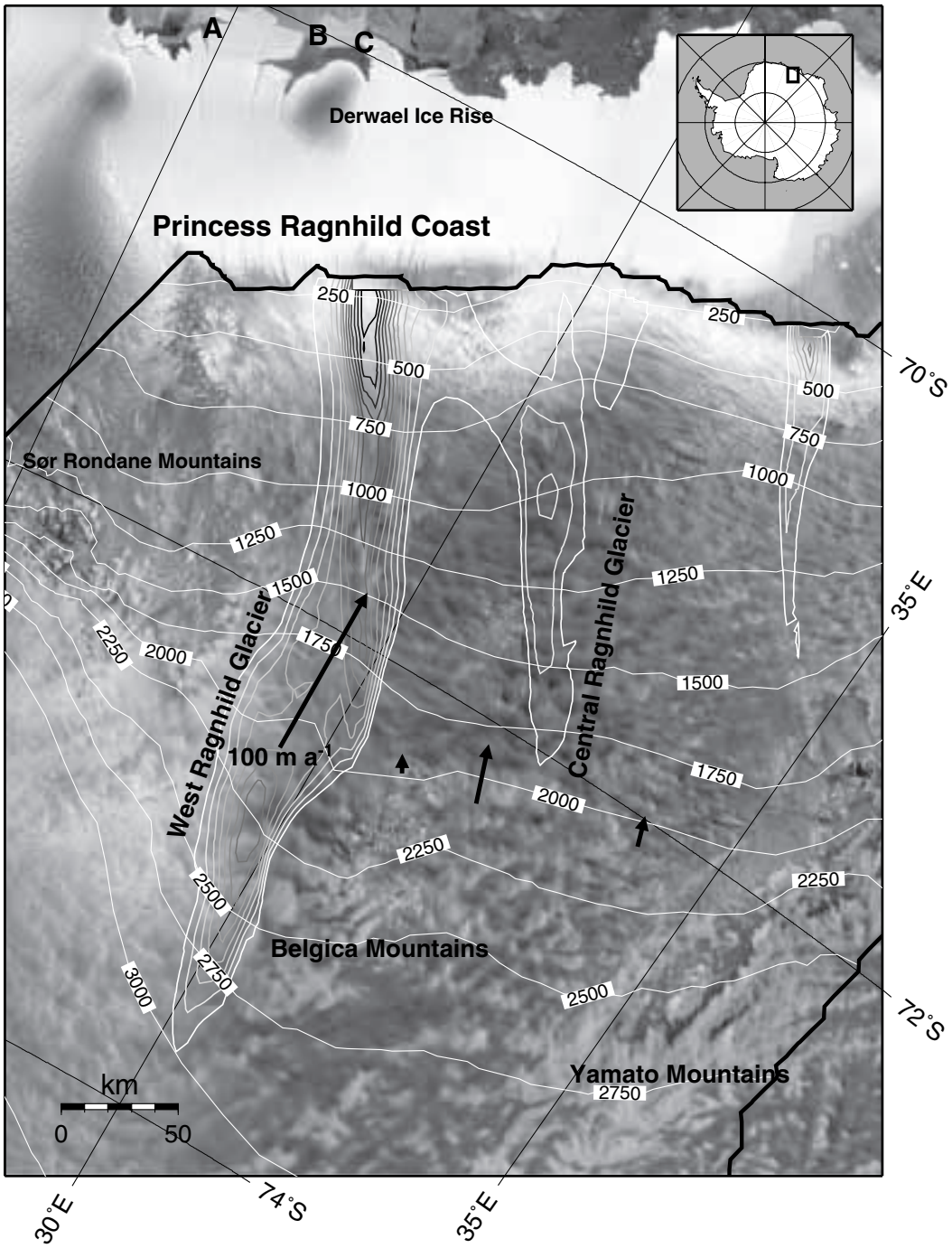

Figure 28: *Satellite image map based on Radarsat–RAMP imagery (Jezek* and *RAMP Product Team, 2002). The thick black line delimits the modeled drainage basin (only part of the catchment is shown). Measured velocities (arrows) are taken from Takahashi et al. (2003). Calculated balance fluxes are shown in gray-shaded contours (unlabeled); surface topography (m a.s.l.) in white contours.*

Marker	1937–1960	1965–1997
A	350	382
B	300	218
C	205	127

Table III: *Velocity estimates (m a^{-1}) of the ice shelf along the Princess Ragnhild Coast between 1937 and 1960 (Nishio et al., 1984) and between 1965 and 1997 (this study). Markers correspond to positions in Figure 28.*

radar surveys reveal that the coastal mountain blocks are interspersed by large subglacial valleys with their floors lying below sea level (Nishio et al., 1995). These ice-thickness measurements, included in the BEDMAP database (Liu et al., 1999; Lythe and Vaughan, 2001), form the major source material for the numerical experiments carried out below. For the prognostic experiments, surface mass balance was taken from Vaughan et al. (1999). Instead of modelling the whole Antarctic ice sheet, the model domain is limited to a regional catchment area between the Dome Fuji ice divide and the Princess Ragnhild Coast (Figure 28). Boundary conditions on the model are a fixed ice thickness at the grounding line and a zero surface slope across the ice divide. Grounding-line motion and ice shelf dynamics were not included, as this study focuses on the inland part of the ice sheet and the ice stream. To create the input files, the BEDMAP data were resampled to a grid of 10 by 10 km, leading to a model domain of 86 by 86 grid points in the horizontal, and 41 layers in the vertical.

3.5.2 Subglacial water and basal sliding

In the model, basal hydrology is represented in terms of the subglacial water flux, which is a function of the basal melt rate. A continuity equation for basal water flow is written as

$$\frac{\partial w}{\partial t} = -\nabla \cdot (\mathbf{v}_w w) + \dot{m}_b \tag{29}$$

where w is the thickness of the water layer (m), $\mathbf{v}_w$ the vertically integrated velocity of water in the layer (m a^{-1}) and $\dot{m}_b$ the basal melting rate (m a^{-1}). If we consider steady-state conditions, the basal melting rate must balance the water flux divergence, or $\dot{m}_b = \nabla \cdot (\mathbf{v}_w w)$. Basal melting occurs when the ice base reaches the pressure melting point, and is defined as

$$\dot{m}_b = \frac{1}{\rho_i L}\left(k_i \frac{\partial \theta_b}{\partial z} + G + v_b \tau_b\right) \tag{30}$$

where L is the latent heat flux, G is the geothermal heat flux, taken as 54.6 mW m^{-2} (Huybrechts, 2002), v_b is the basal ice velocity, τ_b the basal drag, and θ_b the basal ice temperature.

Rondane Mountains during BELARE 2004 (Belgian Antarctic Research Expedition – December 2004), where a distinct crevasse pattern and associated flowlines were observed corresponding to enhanced ice flow, similar to the enhanced ice flow east of the mountain range (Ragnhild glaciers).

Subglacial water tends to move in the direction of decreasing hydraulic potential ϕ (Shreve, 1972). If we assume that basal water pressure is equal to the overlying ice pressure, the hydraulic potential gradient (or water pressure gradient) is written as $\nabla\phi = \rho_i g \nabla z_s + (\rho_w - \rho_i) g \nabla z_b$, where ρ_w is the water density, and z_b is the lower surface elevation of the ice mass. The steady-state basal waterflux $\psi_w = (\mathbf{v}_w w)$ is obtained by integrating the basal melt rate $\dot{m}$ over the whole drainage basin, starting at the hydraulic head in the direction of the hydraulic potential gradient $\nabla\phi$. This is done with the computer scheme for balance flux distribution of ice sheets described in detail by Budd and Warner (1996).

In large-scale ice sheet modelling, basal sliding is often taken as being proportional to the basal drag (or driving stress) and inversely proportional to the effective pressure, which is defined as the ice overburden pressure minus the basal water pressure. Weertman (1964) relates basal sliding velocity to the driving stress and a roughness factor. The presence of a thin water film underneath an ice sheet will reduce friction and thus bed roughness, hence facilitating basal sliding. In that sense it is possible to involve basal water layer thickness as inversely proportional to roughness (Johnson and Fastook, 2002). However, water layer thickness can only be determined if the subglacial water velocity is known. For sake of simplicity, we assume water velocity constant over the whole drainage basin, so that the subglacial water flux ψ_w can be inversely related to bed roughness. Although we are aware that in some limit cases – such as a subglacial lake where $\mathbf{v}_w = 0$, but the ice velocity across the lake differs from zero – the above relation breaks down, the model results show that ψ_w generally increases towards the grounding line. As such, we obtain a sliding law, in its most simple form (linear) written as

$$\mathbf{v}_b = A_b \psi_w \tau_b \exp\left[-\gamma\left(\theta_{\mathrm{pmp}} - \theta\right)\right] \tag{31}$$

where A_b is a sliding constant and θ_{pmp} is the pressure melting temperature. The exponential term in Equation (31) allows for basal sliding at subfreezing temperatures over a range of $\gamma = 1$K (Hindmarsh and Le Meur, 2001). Since basal sliding $\mathbf{v}_b$ also appears in the determination for the basal melt rate (Equation 30), Equation 31 is solved iteratively within each time step. Basal sliding due to subglacial meltwater is likely to occur in the Ragnhild catchment as evidence of subglacial water flow is found in deglaciated areas in the coastal part of the adjacent drainage basin (Sawagaki and Hirakawa, 1997).

3.5.3 Standard experiments

A first series of experiments are diagnostic in nature, i.e., the velocity, stress and temperature fields were calculated by keeping the glacier geometry (ice thickness) fixed. Four experiments were carried out: an isothermal experiment DI where the flow parameter $A(\theta^*)$ was kept constant at 2 $\times$ 10^{-17} Pa^{-n} a^{-1}, a model run where the temperature field was coupled to the velocity (DC), and two model runs where basal sliding was included (DIS and DCS).

As seen from Figure 29, the isothermal ice-sheet model is not capable of explaining the observed surface velocities. Introducing thermomechanical coupling and/or basal sliding based

on the subglacial water model results in a channeled flow pattern of enhanced ice flow. Both sliding and/or coupling result in a similar pattern of ice flow, i.e. a concentration of the ice flux in the topographic lows, hence forming an elongated pattern penetrating far inland for the major ice streams in the area (Figure 30). The basal temperature pattern (not shown) is quite similar, and reaches pressure melting point within these channels. Introducing basal sliding or temperature coupling leads to a similar pattern in ice flow with comparable velocities. Cumulating these effects does not alter this pattern nor the magnitude of the surface velocity, although basal sliding is relatively important. The reason for this convergence lies in a negative feedback where increased basal sliding increases the advection of colder ice from above and reduces the amount of vertical shear, hence reducing the thickness of the highly deforming basal ice layer that is at pressure melting point.

3.5.4 Sensitivity of the Ragnhild glaciers

The effects of basal sliding on the dynamic behaviour of the model are assessed in a series of four prognostic experiments in which the value of parameter A_b in Equation (31) is gradually increased, i.e. A_b = 1.3, 2.0, 3.3, and 5.0 $\times$ 10^{-3} Pa^{-1} m^{-1}. All experiments are run to a steady-state. In each of the experiments a final time-independent solution is achieved. Increasing the basal sliding parameter A_b leads to an acceleration of WRG and a deceleration of CRG (Figure 31). The origin of this dynamic behaviour lies in ice piracy by WRG (Figure 30). Increased basal sliding allows WRG to drain more ice from the upper part of the drainage basin. The surface topography lowers within the fast-flowing corridor, so that surface slopes at the edge with the slower-moving ice increase and both ice and basal water are drawn towards this fast-flow corridor, which also narrows to compensate for the high ice flux in the center (Figure 31 and 30). Although CRG could potentially exhibit a similar behaviour, the larger WRG grows

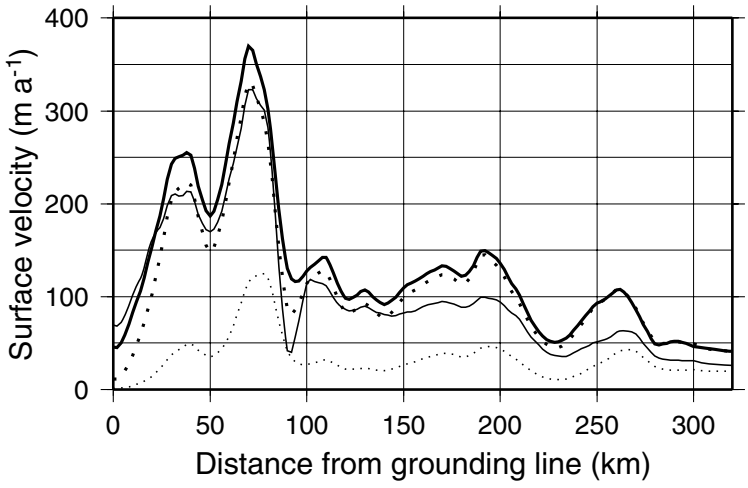

Figure 29: *Predicted surface velocity (m a^{-1}) according to the four diagnostic experiments* DI *(small dots),* DC *(large dots),* DIS *(thin line), and* DCS *(thick line).*

faster than the smaller CRG. Therefore, the drainage zone of CRG gradually decreases in size, decreasing the local ice flux, so that CRG eventually shuts down. Anandakrishnan and Alley (1997) showed that the slowdown of Ice Stream C occurred because of loss of lubrication at the bed, due to a bump in the glacier bed that has directed lubricating water to the neighboring Whillans Ice Stream. For the Ragnhild glaciers, water piracy is more a result of the ice piracy, as the direction of the subglacial water flow – governed by the potential gradient – is largely determined by the surface slope of the ice sheet.

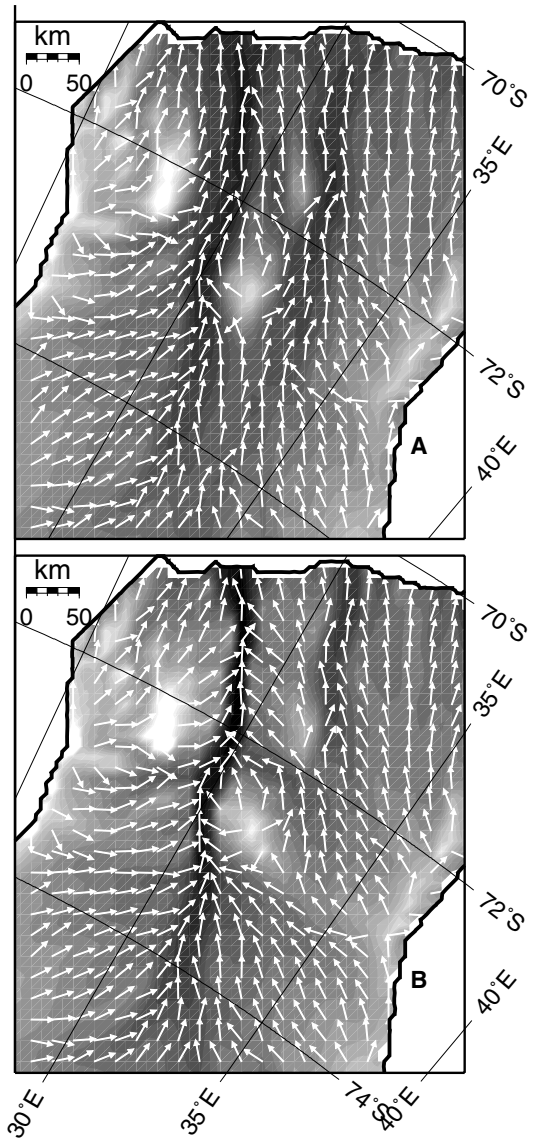

Figure 30: *Predicted steady-state ice flux according to the basal sliding experiment with* $A_b = 1.3 \times 10^{-3}$ *(A) and* $A_b = 5.0 \times 10^{-3}$ *(B). Arrows show the direction of basal water flow.*

3.5.5 Discussion and conclusions

Stokes and Clark (1999) make a distinction between pure and topographic ice streams, because an outlet glacier does not need to be associated with enhanced flow rates. Bentley (1987), however, claims that topographically controlled ice streams or outlet glaciers are associated with enhanced flow velocities as there is a tendency for ice flow to accelerate within topographically constrained corridors. The main reasons for occurrence of enhanced ice flow in topographic ice streams are summed up by Bennett (2003): higher temperatures leading to enhanced ice flow are likely to occur as the ice is thicker, which allows for better isolation. Thicker ice also leads to higher driving stresses, hence higher velocities, which results in increased strain heating. Finally, most of the meltwater will be produced in these topographic lows at pressure melting point, enhancing basal sliding. However, the whole process does not necessarily need to turn into a feedback system that leads to flow acceleration and (partial) disintegration of the ice sheet (Clarke et al., 1977). The combined effect of basal sliding and ice softening due to thermomechanical coupling results in a relatively stable ice-sheet configuration. Even a prescribed increase in lubrication (through parameter A_b) does not lead to a periodic switch between fast and slow ice flow (e.g. limit cycles as described in Payne, 1995; Pattyn, 1996), nor does it lead to a switching behaviour between ice streams in a time-dependency, as reported by Payne (1998) for the Siple Coast ice streams.

Comparison of Norwegian and Belgian maps with Radarsat imagery point to a speedup of the ice in the western part of the Ragnhild Coast and a slowdown to the east. Although the dynamic experiments and balance flux estimates clearly show the presence of at least two ice streams, the diagnostic experiments fail to reproduce CRG or other flow features in the east of the drainage basin. Observed inland ice velocities also show a much higher flow speed for WRG than for the adjacent CRG. Sensitivity experiments demonstrate that a speedup of

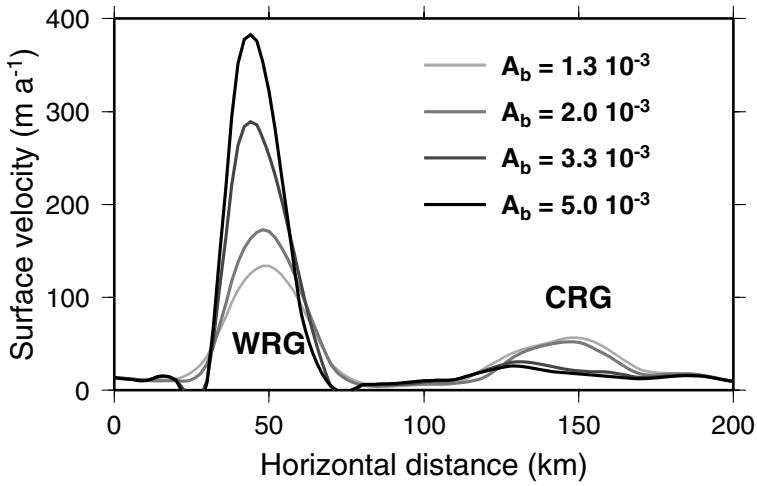

Figure 31: *Cross section through West and Central Ragnhild Glaciers of predicted surface velocity, according to different basal sliding parameterizations.*

WRG causes ice piracy which eventually leads to a stoppage of CRG. In view of the above observations, such a process might already be underway.

One major distinction between an outlet glacier and the enhanced flow zone of WRG is that the latter is not flanked by surrounding mountains. Rutford Ice Stream, for instance is at one side flanked by mountains (and hence a real outlet glacier) but flanked by slower moving ice at the other side (Bentley, 1987). WRG on the contrary lies in a broad valley, but the fast moving ice is flanked by surrounding slower moving ice and distinct shear margins can be traced all along the glacier within the ice. The fast flow zone is not wider than 30 km within a valley that is more than 100 km in width. The narrowing gets more pronounced as basal sliding increases (Figure 30).

In conclusion, ice flow within the East Antarctic ice sheet seems rather complex, and the interior plateau is drained by large elongated features of enhanced ice flow. The Ragnhild glaciers are such features penetrating several hundred kilometers inland. Enhanced ice flow is due to thermomechanical effects and the role of basal sliding in topographic lows. Although the position of these glaciers is topographically controlled, these fast flow zones are not flanked by rock outcrops at the surface. Hence they differ from outlet glaciers by the presence of shear margins *within* the ice sheet penetrating far inland. An increased lubrication of these glaciers results in ice piracy by West Ragnhild Glacier which leads to a progressive stoppage of Central Ragnhild Glacier, a process that in view of observations might already be underway.

3.6 Modelling ice flow near ice divides in support for dating the EPICA–DML ice core *(F. Pattyn, P. Huybrechts, O. Rybak and D. Steinhage)*

Over the last decades, a number of deep ice-core drillings were carried out in Antarctica, such as Vostok, Dome Fuji and more recently Dome Concordia and Dronning Maud Land (DML), the latter two forming part of EPICA.[5] Analysis of these cores provides the scientific community with a continuous record of ice composition, which makes it possible to reconstruct climate and its variability over more than 800,000 years, in the case of Dome Concordia, back in time. These data represent a time scale series of proxies of the most important climatic parameters, such as temperature, precipitation, atmospheric pressure, dust transport, and the corresponding atmospheric composition (in particular the concentration of greenhouse gases). This allows for a better insight in internal structure of the ice sheet, the deformation pattern and density. The relationships between climate fluctuations and the cryosphere can thus be investigated, which is essential for predicting future climatic changes. Interpreting an ice core – in terms of determining its chronology – demands a precise knowledge of the ice flow and dynamics of the inland ice sheet in the vicinity of the borehole, especially at depth and approaching the basal layers.

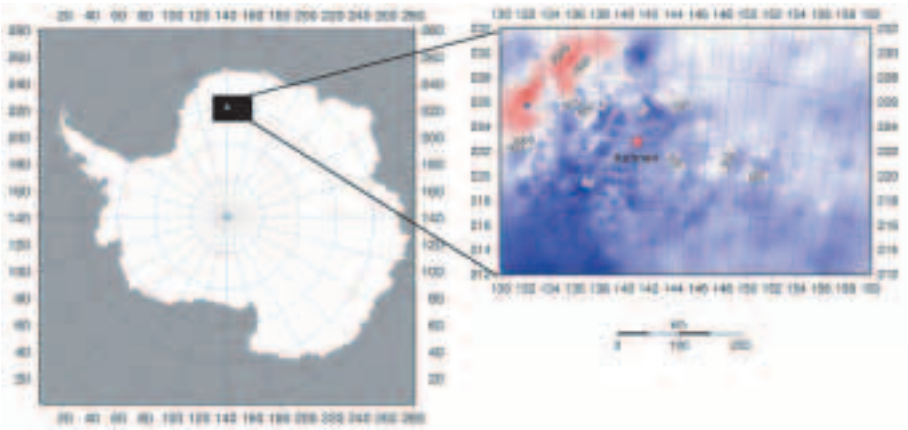

Figure 32: *Left: modeled domain of the Antarctic ice sheet with the large-scale model of Huybrechts (1992) on a 20 km grid; Right: modeled subset of the area around the DML drilling site on a 2.5 km grid with the model of Pattyn (2003).*

For a correct dating and interpretation of the EPICA DML ice core at Kohnen Station one needs to take into account the effects of horizontal advection. That is because the ice core is being drilled on a flank position, implying that the ice was not deposited locally. The deeper in the ice core, from the further and higher inland the climatic information was transported with the ice flow. A potentially complicating factor is that individual ice particles may have encountered different strain and thermal regimes along their respective trajectories as the ice sheet geometry changed during the total period covered by the ice core. These issues are addressed with a

[5]EPICA: European Project on Ice Coring in Antarctica

comprehensive three-dimensional thermomechanical ice-sheet model of the Antarctic ice sheet (Huybrechts, 1992) nested with a detailed higher-order ice-flow model (Pattyn, 2003) for the area around the drill site. The large scale model is based on the shallow ice approximation, considers coupling with an ice shelf and a variable grounding-line, and is implemented on a 20 km grid. The local model includes all stress gradients in the force balance and makes use of the most recent ice-thickness and accumulation data provided on a 2.5 km grid (Figure 32).

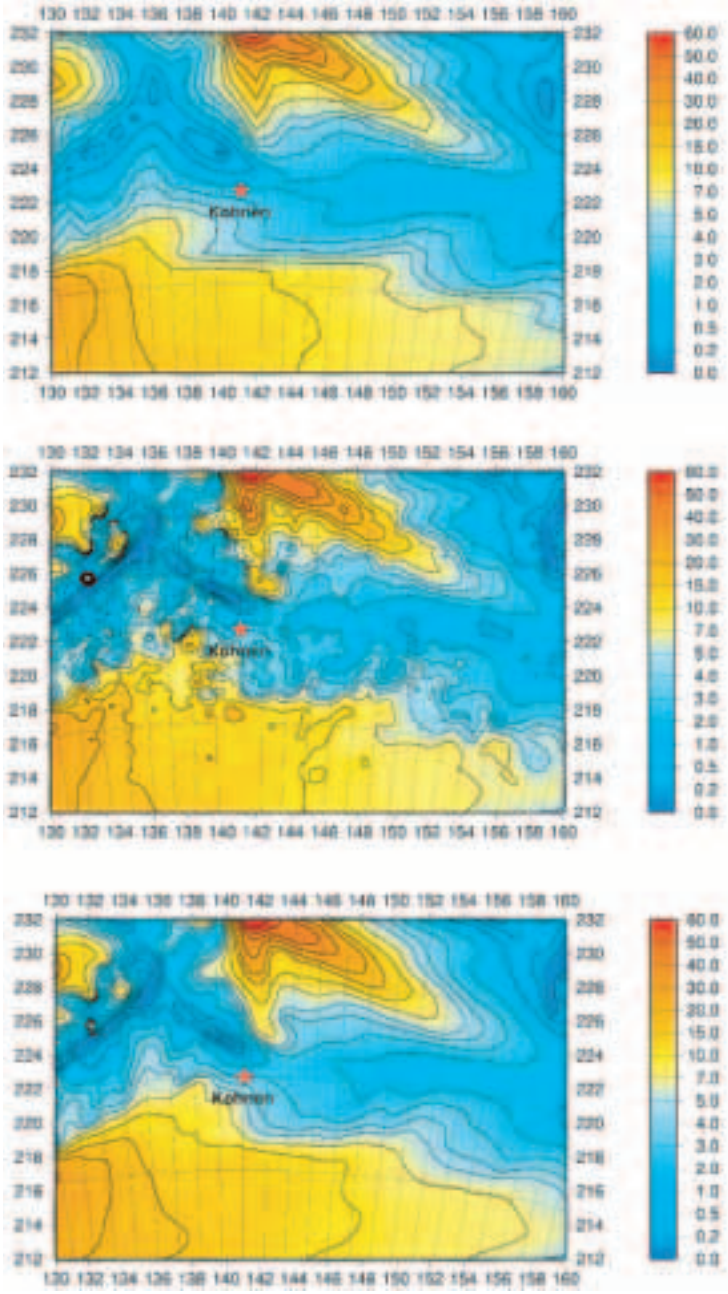

Figure 33: *Modeled surface velocity field near the EPICA DML drilling site with the shallow-ice model on a 20 km grid (top) and a 2.5 km grid (center), as well as with the higher-order model on a 2.5 km grid (bottom).*

The effect of including higher-order stress gradients in the model setup is clearly depicted in

Figure 33. First of all, shallow-ice approximation is valid for grid sizes that are relatively large (20 km as shown here) and for areas with a low variability in basal topography. Obviously, increasing the resolution leads to a velocity field that shows too much variability. This is due to the local definition of the shallow-ice approximation, where the velocity is a function of local surface slope and ice thickness to a certain power. A higher resolution inevitably leads to higher surface slopes, as the distance over which the gradients are calculated are smaller. This velocity variability is an artifact, as high slopes in surface and bedrock will develop longitudinal stress gradients which result in a longitudinal coupling and hence a non-local determination of the velocity field. This is demonstrated by the higher-order model result in Figure 33, which leads to a smoothing of the velocity, even though the topography is accidented.

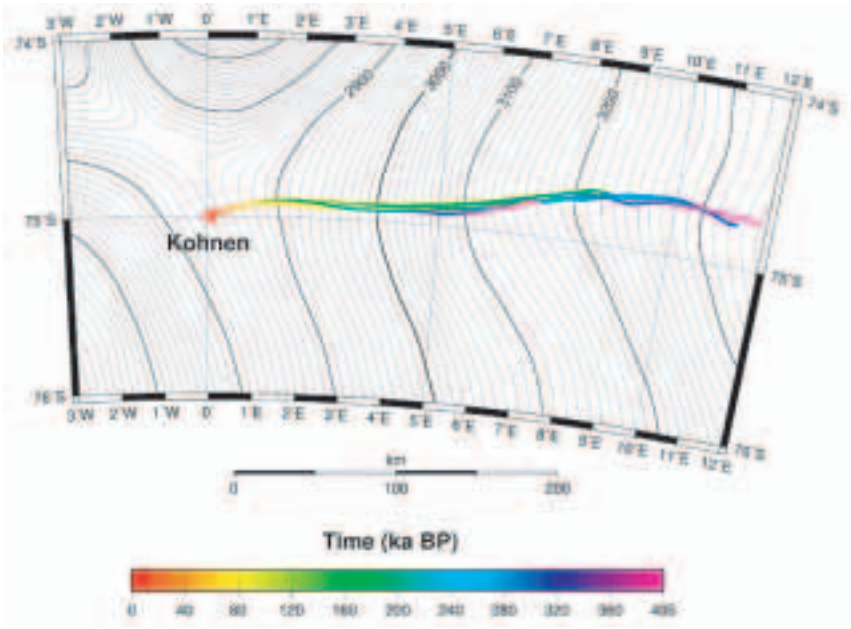

Figure 34: *Origin and age of particles within the EPICA DML ice core over the last 405 ka according to different model experiments.*

The EDML ice core is dated by Lagrangian backtracing carried out by consecutive cubic spline interpolation of a particle's location using the reversed 3D velocity field obtained from forward experiments (Figure 34). This procedure fully accounts for time-dependent changes in ice thickness, flow direction, flow velocity, accumulation rate, basal conditions, etc. An important output is the palaeo-location of the origin of individual particle paths. This information is needed to assess the temperature bias introduced by flow effects, which needs to be separated from the ice core record to extract the climatic information.

The main conclusions so far are that there are no stratigraphic distortions expected in the EPICA DML ice core from large irregularities in the strain history along particle paths, and that for a geothermal heat flux smaller than 56 mW m^{-2}, basal melting does not occur at any time at the drillsite nor along any particle path. This means that the ice is likely older than 400 ka below 98% depth.

4 CONCLUSIONS AND RECOMMENDATIONS

With the **AMICS** project (**A**ntarctic ice-sheet dynamics and climatic change: **M**odelling and **I**ce **C**omposition **S**tudies) it was aimed to clarify the dynamic interactions between the ice sheet and the subglacial environment, based on analysis of ice from the basal part of the Antarctic ice sheet and ice-sheet modelling. It was envisaged that results from the ice analyses would constrain the basal boundary conditions of the numerical model and would make validation of the model possible with regard to the melting and refreezing processes at the base.

For this purpose, a new three-dimensional thermomechanical ice sheet model was developed, including higher-order stress gradients (a so-called higher-order model; Pattyn, 2002; Pattyn, 2003). Such a model is capable of properly simulating the ice flow in areas characterized by complex basal interaction (ice streams, subglacial lakes, ...). As a contribution to the EPICA project, the model is imbedded in a large-scale model of the Antarctic ice sheet to determine the chronology and the origin of the ice within the EPICA DML ice core, since this is an area of high topographical variability (Huybrechts et al., 2004).

With the numerical model it was expected to translate the results of the ice-composition analyses into physical processes, hence providing the scientific community with a model tool of complex basal interaction. The development of an isotopic model is an example of such gained insight (Souchez et al., 2004): it explains the basal freeze-on associated with subglacial upward flow of pore water and is fully tested against two Antarctic outlet glaciers by studying the δD-δ^{18}O relationships in the basal ice layers of these glaciers. An adaptation of this model also allowed for a better understanding of the refreezing processes at the ice water interface of subglacial Lake Vostok, the largest subglacial lake underneath the Antarctic ice sheet.

Ice composition analyses remains a key issue in understanding subglacial processes and interactions: it emphasized on the importance of liquid water in constructing the basal part of the Antarctic Ice Sheet, even at temperatures well below the pressure melting point (Lorrain et al., 1999; Sleewaegen et al., 2002; Sleewaegen et al., 2003). The results proved to be valuable in constraining ice-sheet flow models, since the presence of liquid water strongly influence the dynamical behaviour of the ice (see below). Moreover, the detailed composition study of the deepest part of ice cores or/and of ice sections at the margin of outlet glaciers, has shown the widespread occurrence of complex ice deformation even at the sub metric scale, at the base (Souchez et al., 2002). Taking this complex basal ice flow into account is a prerequisite for a more thorough modelling of the ice sheet. Among the processes discovered by these ice composition studies is the importance of lake ice entrainment either in the central part of the ice sheet (Vostok ice core) or in its marginal areas (Dry Valleys). This provides a means for a better knowledge of the physical processes involved in fast flowing ice streams that play a paramount role in evacuating ice from the Antarctic Ice Sheet.

As basal processes play an important role in the onset of fast-flowing areas such as ice streams, the role of these drainage features in the stability of the Antarctic ice sheet and their influence on the variability of the ice sheet with changing climate has been investigated. Dynamic ice-stream development was simulated by implementing a stress-free basal surface within the ice sheet.

Changing from a basal-stress dominated regime to a basal stress-free regime is similar to the ice-sheet / ice-shelf / grounding-line problem, which remains a hot topic amidst the ice-sheet modelling community. The experiment could explain all major processes that are observed in real ice-stream development, such as the forward bulging, high longitudinal stress gradients at the onset and the development of shear margins (Pattyn, 2003).

In reality, the reduction of basal drag in an ice stream is not based on a simple basal boundary switch, but is a complex process that involves basal hydrology, sediment deformation, basal melting and sliding. A new sliding relationship was developed and implemented, taking into account basal hydrology in terms of the subglacial water flux, which is a function of the basal melt rate (Pattyn et al., 2005). Results underscore that ice flow within the East Antarctic ice sheet is rather complex, and the interior plateau is drained by large elongated features of enhanced ice flow. The Ragnhild glaciers (Dronning Maud Land) are such features penetrating several hundred kilometers inland. Although the position of these glaciers is topographically controlled, they differ from outlet glaciers by the presence of shear margins *within* the ice sheet penetrating far inland. Increased lubrication of these glaciers results in ice piracy, thereby accelerating the major ice drainage features and slowing down neighboring streams.

Interaction of the ice sheet with subglacial lakes is another issue addressed by the AMICS project. For the first time, a dynamical 3D thermomechanical simulation of the ice flow across Lake Vostok is carried out (Pattyn et al., 2004). Results show that by treating the ice/lake interface as a stress-free surface (similar to an ice shelf), major ice-dynamical features such as the surface flattening and turning of the ice flow across the lake, are accurately reproduced, even though subglacial lake dynamics are not treated explicitly. Experiments taking into account buoyancy effects underline that lake water circulation plays a decisive role in balancing melting in the north and accretion in the south. Furthermore, it has been shown that subglacial lakes and Lake Vostok in particular, can be the onset of an enhanced ice-flow feature or a major ice stream.

Recommendations

Evaluating the importance of phase changes at the base of the Antarctic Ice Sheet and its occurrence either by ice composition studies in deep ices core or in marginal areas is required for a better understanding of the complex ice flow recently recognized. Within this context a better modelling of the basal ice composition will give an added value to this methodology. Complex ice deformation at depth can be tackled, as shown in this report, by the study of isotopic and chemical properties of the basal ice. This is an important step for constraining the physics of basal ice flow.

The Antarctic ice sheet is drained by outlet glaciers and ice streams that evacuate the grounded ice towards the ocean. Increased mass loss at the ice-ocean boundary results in anticipated eustatic sea-level rise. Although basal processes and enhanced ice-flow onsets are better understood today, dynamical processes at the grounding line[6] are hardly understood at all.

[6]the boundary between the grounded ice sheet and the floating ice shelf

Especially with the recent dramatic retreat of the grounding line of Pine Island Glacier in West Antarctica (Shepherd et al., 2004; Payne et al., 2004), the call for a comprehensive insight into the processes of grounding line retreat, such as the response to mass balance and sea-level change as well as stress transfer across the grounding line, is ubiquitous.

Understanding the interactions with subglacial lakes and other complex environments calls upon an interdisciplinary approach in which modelling acts as the cement between the different building blocks of nature. Coupling different models and systems will become more and more essential; a model of lake water circulation coupled to a higher-order ice sheet model, for example, will ultimately lead to a comprehensive insight of the processes and interactions of the Antarctic ice sheet and its subglacial environment.

ACKNOWLEDGEMENTS

Thanks are due to Antarctica New Zealand for providing the logistical support of the field work in the Dry Valleys area as well as to the Marsden Fund and the University of Otago for financial support.

The AMICS team is grateful to Dr. Fitzsimons for associating its members to different field parties he organized in the Dry Valley and for his direct contribution to field work and related research. The team is indebted to Drs. J. Jouzel and J.R. Petit for including its members within the Vostok ice core project.

Dr. M. Stiévenard from LMCE-Saclay (France) is gratefully acknowledged for dealing with the isotopic measurements.

Drs. P. Huybrechts, O. Rybak and D. Steinhage from the Alfred-Wegener Institute, Germany, are acknowledged for their contribution to the research presented here. This research is part of the EU Framework V project "European Project on Ice Coring in Antarctica (EPICA)" 2001-2004 (Work Package WP7) and EU Framework VI project "EPICA-MIS: New paleoreconstructions from Antarctic ice and marine records" 2004-2007 (Work Package WP7).

We also want to express our gratefulness to all other members of the laboratories, especially S. Elamri and C. Lelouchier for their work and strong support.

This report is a contribution to the Belgian Antarctic Research Programme (BELSPO – Science Policy Office).

REFERENCES

Adams, E.E., Priscu, J.C., Fritsen, C.H., Smith, S.R., and Brackman, S.L. 1998. Permanent ice covers of the McMurdo Dry Valleys lakes, Antarctica: Bubble formation and metamorphism. In Priscu, J.C. (Ed.), Ecosystem Dynamics in a Polar Desert: The McMurdo Dry Valleys, Antarctica. Antarctic Research Series 72. American Geophysical Union. Washington D.C, 281–295.

Albrecht, O. 2000. Dynamics of Glaciers and Ice Sheets: a Numerical Model Study. PhD Thesis, ETH No. 13278, Swiss Federal Institute of Technology, Zurich, Switzerland.

Anandakrishnan, S. and Alley, R.B. 1997. Stagnation of ice stream C, West Antarctica by water piracy. Geophys. Res. Lett., 24(3): 265–268.

Angelis, M. De, Petit, J.R., Savarino, J., Souchez, R., and Thiemens, M. 2004. Contribution of an ancient evaporitic-type reservoir to lake Vostok chemistry. Earth and Planetary Science Letters, 222(3–4): 751–765.

Bamber, J.L., Vaughan, D.G., and Joughin, I. 2000. Widespread complex flow in the interior of the Antarctic ice sheet. Science, 287(5456): 1248–1250.

Baral, D.R., Hutter, K., and Greve, R. 2001. Asymptotic theories of large-scale motion, temperature, and moisture distribution in land-based polythermal ice sheets: a critical review and new developments. Appl. Mech. Rev., 54(3): 215–256.

Barnola, J.M., Raynaud, D., Neftel, A., and Oeschger, H. 1983. Comparison of CO_2 measurements by two laboratories on air from bubbles in polar ice. Nature, 303: 410–413.

Bell, R.E., Studinger, M., Tikku, A.A., Clarke, G.C.K., Gutner, M.M., and Meertens, C. 2002. Origin and fate of Lake Vostok water frozen to the base of the East Antarctic ice sheet. Nature, 416: 307–310.

Bennett, M.R. 2003. Ice streams as arteries of an ice sheet: their mechanics, stability and significance. Earth-Science Reviews, 61: 309–339.

Bentley, C.R. 1987. Antarctic ice streams: a review. J. Geophys. Res, 92: 8843–8858.

Berner, W., Bucker, P., Oeshger, H., and Stauffer, B. 1977. Analysis and interpretation of gas content and composition in natural ice. IAHS Publication, 118: 272–284.

Bindschadler, R., Bamber, J., and Anandakrishnan, S. 2001. Onset of streaming flow in the Siple Coast region, West Antarctica. In Alley, R. and Bindschadler, R. (Eds.), The West Antarctic Ice Sheet: Behavior and Environment, volume 77 of Antarct. Res. Ser. AGU, Washington D.C., 123–136.

Blatter, H. 1995. Velocity and stress fields in grounded glaciers: a simple algorithm for including deviatoric stress gradients. J. Glaciol., 41(138): 333–344.

Blunier, T., Chappellaz, J., Schwander, J., Barnola, J., Desperts, W., Stauffer, B., and Raynaud, D. 1993. Atmospheric methane record from a Greenland ice core over the last 1000 years. Geophysical Research Letters, 20: 2219–2222.

Budd, W.F. and Warner, R.C. 1996. A computer scheme for rapid calculations of balance-flux distributions. Ann. Glaciol., 23: 21–27.

Budd, W.F. 1971. Stress variations with ice flow over undulations. J. Glaciol., 10(59): 177–195.

Chinn, T.J. and Maze, I. 1983. Hydrology and Glaciology, Dry Valleys, Antarctica. New Zealand Ministry of Works and Development, Christchurch.

Chinn, T.J. 1993. Physical hydrology of the Dry Valleys lakes. In Green, W.J. and Friedman, E.I. (Eds.), Physical and Biogeochemical Processes in Antarctic Lakes, Antarctic Research Series 59. American Geophysical Union, Washington D.C, 1–51.

Christoffersen, P. and Tulaczyk, S. 2003a. Response of subglacial sediments to basal freeze-on, 1. theory and comparison to observations from beneath the West Antarctic Ice Sheet. J. Geophys. Res., 108(B4.2222): 19.1–19.16.

Christoffersen, P. and Tulaczyk, S. 2003b. Thermodynamics of basal freeze-on : Predicting basal and subglacial signatures of stopped ice streams and interstream ridges. Ann. Glaciol., 36: 233–243.

Clarke, G.K.C., Nitsan, U., and Paterson, W.S.B. 1977. Strain heating and creep instability in glaciers and ice sheets. Reviews of Geophysics and Space Physics, 15(2): 235–247.

Clayton, R.N. and Steiner, A. 1975. Oxygen isotope studies of the geothermal system at Warakei, New Zealand. Geochem. Cosmochem. Acta., 39: 1179–1186.

Colinge, J. and Blatter, H. 1998. Stress and velocity fields in glaciers: Part I. finite-difference schemes for higher-order glacier models. J. Glaciol., 44(148): 448–456.

Craig, H., Wharton Jr., R.A., and McKay, C.P. 1992. Oxygen supersaturation in ice-covered Antarctic lakes: Biologic versus physical contributions. Science, 255: 318–321.

Craig, H. 1963. The Isotopic Geochemistry of Water and Carbon in Geothermal Areas. Consiglio Nationale dell Ricerche, Laboratorio de Geologia Nucleare, Pisa.

Cuffey, K., Conway, H., Hallet, B., Gades, A., and Raymond, C. 1999. Interfacial water in polar glaciers and glacier sliding at -17°c. Geophysical Research Letters, 26(6): 751–754.

Cuffey, K., Conway, H., Gades, A., Hallet, B., Lorrain, R., Severinghaus, J., Steig, E., Vaughn, B., and White, J. 2000. Entrainment at cold glacier beds. Geology, 28(4): 351–354.

Dahl-Jensen, D. 1989. Steady thermomechanical flow along two-dimensional flow lines in large grounded ice sheets. J. Geophys. Res., 94(B8): 12,355–10,362.

Dansgaard, W. and Johnsen, S.J. 1969. A flow model and a time scale for the ice core for Camp Century, Greenland. J. Glaciol., 8(53): 215–223.

Fisher, D. and Koerner, R. 1986. On the special rheological properties of ancient microparticle laden Northern Hemisphere ice as derived from bore-hole and core measurements. J. Glaciol., 32(112): 501–510.

Fitzsimons, S.J. 1996. Formation of thrust-block moraines at the margins of dry-based glaciers, south Victorial Land, Antarctica. Ann. Glaciol., 22: 68–74.

Fritsen, C.H., Adams, E.E., McKay, C.P., and Priscu, J.C. 1998. Permanent ice covers of the McMurdo Dry Valleys lakes, Antarctica: Liquid water contents. In Priscu, J.C. (Ed.), Ecosystem Dynamics in a Polar Desert: The McMurdo Dry Valleys, Antarctica. Antarctic Research Series 72. American Geophysical Union. Washington D.C, 269–280.

Gow, A.J. and Langston, D. 1977. Growth history of lake ice in relation to its stratigraphic, crystalline and mechanical structure. US Army CRREL Report, 77(1): 1–24.

Gow, A.J., Ackley, S.F., Buck, K.R., and Golden, K.M. 1987. Physical and structural characteristics of Weddell Sea pack ice. US Army CRREL Report, 87(14): 1–70.

Greve, R. 1997. Application of a polythermal three-dimensional ice sheet model to the Greenland ice sheet: Response to steady-state and transient climate scenarios. J. Climate, 10(5): 901–918.

Hallet, B. 1976. Deposition formed by subglacial precipitation. Geological Society of America Bulletin, 87: 1003–1015.

Hendy, C.H. 2000. The role of polar lake ice as filter for glacial lacustrine sediments. Geografiska Annaler, 82A(2–3): 271–274.

Hindmarsh, R.C.A. and Le Meur, E. 2001. Dynamical processes involved in the retreat of marine ice sheets. J. Glaciol., 47(157): 271–282.

Hindmarsh, R.C.A. 2001. Influence of channelling on heating in ice-sheet flows. Geophys. Res. Lett., 28(19): 3681–3684.

Hooke, R.LeB. 1981. Flow law for polycrystalline ice in glaciers: Comparison of theoretical predictions, laboratory data, and field measurements. Rev. Geophys., 19(4): 664–672.

Hutter, K. 1983. Theoretical Glaciology. Dordrecht, Kluwer Academic Publishers.

Huybrechts, P., Payne, T., and The EISMINT Intercomparison Group, . 1996. The EISMINT benchmarks for testing ice–sheet models. Ann. Glaciol., 23: 1–12.

Huybrechts, P., Rybak, O., Pattyn, F., and Steinhage, D. 2004. Age and origin of the ice in the EPICA DML ice core derived from a nested Antarctic ice sheet model. Geophysical Research Abstracts, 6: EGU04–A–06520.

Huybrechts, P. 1990. A 3-D model for the Antarctic ice sheet: a sensitivity study on the glacial-interglacial contrast. Climate Dyn., 5: 79–92.

Huybrechts, P. 1992. The Antarctic ice sheet and environmental change: a three-dimensional modelling study. Ber. Polarforsch., 99: 1–241.

Huybrechts, P. 2002. Sea-level changes at the LGM from ice-dynamic reconstructions of the Greenland and Antarctic ice sheets during the glacial cycles. Quaternary Science Reviews, 21: 203–231.

Iverson, N. and Souchez, R. 1996. Isotopic signature of debris-rich ice formed by regelation into a subglacial sediment bed. Geophysical Research Letters, 23(10): 1151–1154.

Jean-Baptiste, P., Petit, J.R., Lipenkov, V., Raynaud, D., and Barkov, N. 2001. Helium isotope in deep Vostok ice core (Antarctica): Constraints on hydrothermal processes and water exchange in the subglacial lake. Nature, 411: 460–462.

Jean-Baptiste, P., Petit, J.R., Raynaud, D., Jouzel, J., and Bulat, S. 2003. Helium signature and seismotectonic activity in Lake Vostok. Geophysical Research Abstracts, 5.

Jezek, K. and RAMP Product Team, . 2002. RAMP AMM-1 SAR Image Mosaic of Antarctica. http://nsidc.org/data/nsidc-0103.html, Alaska SAR Facil., Natl. Snow and Ice Data Cent., Boulder, Colo.

Johnson, J. and Fastook, J.L. 2002. Northern Hemisphere glaciation and its sensitivity to basal melt water. Quaternary International, 95–96: 65–74.

Joughin, I.R., Gray, L., Bindschadler, R., Price, S., Morse, D., Hulbe, C., Mattar, K., and Werner, C. 1999. Tributaries of West Antarctic Ice Streams revealed by RADARSAT interferometry. Science, 286(5438): 283–286.

Joughin, I.R., Fahnestock, M., MacAyeal, D., Bamber, J.L., and Gogineni, P. 2001. Observation and analysis of ice flow in the largest Greenland ice stream. J. Geophys. Res., 106(D24): 34,021–34,034.

Jouzel, J. and Souchez, R. 1982. Melting refreezing at the glacier sole and the isotopic composition of the ice. J. Glaciol., 28(98): 35–42.

Jouzel, J., Petit, J.R., Souchez, R., Barkov, N.I., Lipenkov, V.Y., Raynaud, D., Stievenard, M., Vassiliev, N.I., Verbeke, V., and Vimeux, F. 1999. More than 200 meters of lake ice above subglacial Lake Vostok, Antarctica. Science, 286: 2138–2141.

Kapitsa, A., Ridley, J.K., Robin, G. de Q., Siegert, M.J., and Zotikov, I. 1996. A large deep freshwater lake beneath the ice of central East Antarctica. Nature, 381: 684–686.

Killawee, J.A., Fairchild, I.J., Tison, J.L., Janssens, L., and Lorrain, R. 1998. Segregation of solutes and gases in experimental freezing of dilute solutions : Implications for natural glacial systems. Geochimica and Cosmochimica Acta, 62(23–24): 1637–1655.

Knight, P.G. 1997. The basal ice layer of glaciers and ice sheets. Quaternary Science Reviews, 16: 975–993.

Kwok, R., Siegert, M.J., and Carsey, F.D. 2000. Ice motion over Lake Vostok, Antarctica: Constraints on inferences regarding the accreted ice. J. Glaciol., 46(155): 689–694.

Liu, H.X., Jezek, K.C., and Li, B.Y. 1999. Development of an Antarctic digital elevation model by integrating cartographic and remotely sensed data: A geographic information system based approach. J. Geophys. Res., 104(B10): 23199–23213.

Lofgren, G. and Weeks, W.F. 1969. Effect of growth parameters on the substructure spacing in NaCl ice crystals. J. Glaciol., 8(52): 153–164.

Lorrain, R.D., Fitzsimons, S.J., Vandergoes, M.J., and Stievenard, M. 1999. Ice composition evidence for the formation of basal ice from lake water beneath a cold-based Antarctic glacier. Ann. Glaciol., 28: 277–281.

Lythe, M.B. and Vaughan, D.G. 2001. BEDMAP: A new ice thickness and subglacial topographic model of Antarctica. J. Geophys. Res., 106(B6): 11335–11351.

Marshall, S.J. and Clarke, G.K.C. 1997. A continuum mixture model of ice stream thermomechanics in the Laurentide ice sheet. 1. Theory. J. Geophys. Res., 102(B9): 20,599–20,614.

Martinerie, P., Raynaud, D., Etheridge, D.M., Barnola, J.M., and Mazaudier, D. 1992. Physical and climatic parameters which influence the air content in polar ice. Earth and Planetary Science Letters, 112: 1–13.

Martinerie, P., Lipenkov, V.Y., Raynaud, D., Chappellaz, J., Barkov, N.I., and Lorius, C. 1994. Air content paleo-record in the Vostok ice core (Antarctica): a mixed record of climatic and glaciological parameters. Journal of Geophysical Research, 99: 10565–10576.

Mayer, C. and Siegert, M.J. 2000. Numerical modelling of ice-sheet dynamics across the Vostok subglacial lake, central East Antarctica. J. Glaciol., 46(153): 197–205.

Mayer, C., Grosfeld, K., and Siegert, M.J. 2003. Salinity impact on water flow and lake ice in Lake Vostok, Antarctica. Geophys. Res. Lett., 14(1767): doi:10.1029/2003GL017380.

Mayer, C. 1996. Numerische Modellierung der Übergangszone zwischen Eisschild und Shelfeis (numerical modelling of the transition zone between an ice sheet and an ice shelf). Ber. Polarforsch., 214: 1–150.

Moser, H. and Stichler, W. 1980. Environmental isotopes in ice and snow. In Fritz, P. and Fontes, J. (Eds.), Handbook of Environmental Isotope Geochemistry, the terrestrial environment, 1A. Elsevier, Amsterdam, 141–178.

Nedell, S.S., Anderson, D.W., Squyres, S.W., and Love, F.G. 1987. Sedimentation in ice-covered Lake Hoare, Antarctica. Sedimentology, 34: 1093–1106.

Nishio, F., Ishikawa, M., Ohmae, H., Takahashi, S., and Katsushima, T. 1984. A preliminary study of glacial geomorphology in area between Breid Bay and the Sør Rondane Mountains in Queen Maud Land, East Antarctica. Nankyoku Shiryô (Antarct. Rec.), 83: 11–28.

Nishio, F., Uratsuka, S., and Ohmae, K. 1995. Bedrock topography. In Higashi, A. (Ed.), Antarctica, East Queen Maud Land, Enderby Land; Glaciological Folio. Tokyo, Natl Inst. Polar. Res.

Offer, Z.Y., Zangvil, A., and Azmon, E. 1993. Characterization of airborne dust in Sede Boqer area. Israel Journal of Earth Sciences, 41: 239–245.

Oswald, G.K.A. and Robin, G de Q. 1973. Lakes beneath the Antarctic ice sheet. Nature, 245: 251–254.

Paterson, W.S.B. 1994. The Physics of Glaciers. Oxford, Pergamon Press, 3rd edition.

Pattyn, F. and Naruse, R. 2003. The nature of complex ice flow in Shirase Glacier catchment, East Antarctica. J. Glaciol., 49(166): 429–436.

Pattyn, F., De Smedt, B., and Souchez, R. 2004. Influence of subglacial Lake Vostok on the regional ice dynamics of the Antarctic ice sheet: a model study. J. Glaciol., 50: in press.

Pattyn, F., Brabander, S. De, and Huyghe, A. 2005. Basal and thermal control mechanisms of the Ragnhild glaciers, East Antarctica. Ann. Glaciol., 40: accepted for publication.

Pattyn, F. 1996. Numerical modelling of a fast-flowing outlet glacier: Experiments with different basal conditions. Ann. Glaciol., 23: 237–246.

Pattyn, F. 2000. Ice-sheet modelling at different spatial resolutions: Focus on the grounding line. Ann. Glaciol., 31: 211–216.

Pattyn, F. 2002. Transient glacier response with a higher-order numerical ice-flow model. J. Glaciol., 48(162): 467–477.

Pattyn, F. 2003. A new 3D higher-order thermomechanical ice-sheet model: Basic sensitivity, ice-stream development and ice flow across subglacial lakes. J. Geophys. Res., 108(B8, 2382): doi:10.1029/2002JB002329.

Payne, A.J., Huybrechts, P., Abe-Ouchi, A., Calov, R., Fastook, J.L., Greve, R., Marshall, S.J., Marsiat, I., Ritz, C., Tarasov, L., and Thomassen, M.P.A. 2000. Results from the EISMINT model intercomparsion: the effects of thermomechanical coupling. J. Glaciol., 46(153): 227–238.

Payne, A.J., Vieli, A., Shepherd, A.P., Wingham, D.J., and Rignot, E. 2004. Recent dramatic thinning of largest West Antarctic ice stream triggered by oceans. Geophys. Res. Letters, 31(L23401): doi:10.1029/2004GL021284.

Payne, A.J. 1995. Limit cycles in the basal thermal regime of ice sheets. J. Geophys. Res., 100(B3): 4249–4263.

Payne, A.J. 1998. Dynamics of the Siple Coast ice streams, West Antarctica: results from a thermomechanical ice sheet model. Geophys. Res. Letters, 25(16): 3173–3176.

Petit, J.R., Jouzel, J., Raynaud, D., NI, N.I. Barkov, Barnola, J.M., Basile, I., Bender, M., Chappellaz, J., Davis, M., Delaygue, G., Delmotte, M., Kotlyakov, V.M., Legrand, M., Lipenkov, V.Y., Lorius, C., Pepin, L., Ritz, C., Saltzman, E., and Stievenard, M. 1999. Climate and atmospheric history of the past 420,000 years from the Vostok ice core, Antarctica. Nature, 399: 429–436.

Pollard, W.H. and Everdingen, R.O. 1992. Formation of seasonal ice bodies. In Dixon, J.C. and Abrahams, A.D. (Eds.), The Binghampton Symposia in Geomorphology: International Series, 22. Wiley, Chichester, 281–304.

Priscu, J.C., Fritsen, C.H., Adams, E.E., Giovannoni, S.J., Paerl, H.W., McKay, C.P., Doran, P.T., Gordon, D.A., Lanoil, B.D., and Pinckney, J.L. 1998. Perennial Antarctic lake ice: an oasis for life in a polar desert. Science, 280: 2095–2098.

Priscu, J.C., Adams, E., Lyons, W., Voytek, M., Mogk, D., Brown, R., McKay, C., Takacs, C., Welch, K., Wolf, C., Kirshtein, J., and Avci, R. 1999. Geomicrobiology of subglacial ice above Lake Vostok, Antarctica. Science, 286: 2141–2144.

Pye, K. 1987. Aeolian Dust and Dust Deposits. Academic Press, London.

Raymond, C.F. 1983. Deformation in the vicinity of ice divides. J. Glaciol., 29: 357–373.

Raynaud, D., Delmas, R., Ascencio, J.M., and Legrand, M. 1982. Gas extraction from polar ice cores : a critical issue for studying the evolution of atmospheric CO_2 and ice-sheet surface elevation. Ann. Glaciol., 3: 265–268.

Raynaud, D., Chappellaz, J., Barnola, J.M., Korotkevich, Y.S., and Lorius, C. 1988. Climatic and CH_4 cycle implications of glacial-interglacial CH_4 change in the Vostok ice core. Nature, 333: 655–657.

Rippin, D.M., Bamber, J.L., Siegert, M.J., Vaughan, D.G., and Corr, H.F.J. 2003. Basal topography and ice flow in the Bailey/Slessor region of East Antarctica. J. Geophys. Res., 108(F1, 6008): doi:10.1029/2003JF000039.

Ritz, C., Fabre, A., and Letréguilly, A. 1997. Sensitivity of a Greenland ice sheet model to ice flow and ablation parameters: Consequences for the evolution through the last glacial cycle. Climate. Dyn., 13(1): 11–24.

Saito, F., Abe-Ouchi, A., and Blatter, H. 2003. Effects of the first order stress gradients to an ice sheet evaluated by a three-dimensional thermo-mechanical coupled model. Ann. Glaciol., 37: in press.

Saito, F. 2002. Development of a Three Dimensional Ice Sheet Model for Numerical Studies of Antarctic and Greenland Ice Sheet. PhD Thesis, University of Tokyo, Japan.

Sawagaki, T. and Hirakawa, K. 1997. Erosion of bedrock by subglacial meltwater, Soya Coast, East Antarctica. Geografiska Annaler, 79A(4): 223–238.

Schohl, G.A. and Ettema, R. 1986. Theory and laboratory observations of naled ice growth. J. Glaciol., 32(111): 168–177.

Schøtt Hvidberg, C. 1996. Steady-state thermomechanical modelling of ice flow near the centre of large ice sheets with the finite- element method. Ann. Glaciol., 23: 116–123.

Shepherd, A., Wingham, D., and Rignot, E. 2004. Warm ocean is eroding West Antarctic Ice Sheet. Geophys. Res. Letters, 31(L23402): doi:10.1029/2004GL021106.

Shreve, R.L. 1972. Movement of water in glaciers. J. Glaciol., 11(62): 205–214.

Siegert, M.J. and Bamber, J.L. 2000. Subglacial water at the heads of Antarctic ice-stream tributaries. J. Glaciol., 46(155): 702–703.

Siegert, M.J. and Ridley, J.K. 1998. An analysis of the ice-sheet surface and subsurface topography above the Vostok Station subglacial lake, central East Antarctica. J. Geophys. Res, 103(B5): 10,195–10,207.

Siegert, M.J., Dowdeswell, J.A., Gorman, M.E., and McIntyre, N.F. 1996. An inventory of Antarctic subglacial lakes. Ant. Science, 8: 281–286.

Siegert, M.J., Kwok, R., Mayer, C., and Hubbard, B. 2000. Water exchange between the subglacial Lake Vostok and the overlying ice sheet. Nature, 403: 643–646.

Siegert, M.J., Ellis-Evans, J.C., Tranter, M., Mayer, C., Petit, J.R., Salamatin, A., and Priscu, J.C. 2001. Physical, chemical and biological processes in Lake Vostok and other Antarctic subglacial lakes. Nature, 404: 603–609.

Siegert, M.J. 2000. Antarctic subglacial lakes. Earth Science Reviews, 50: 29–50.

Simmons, G. M., Vestal, J.R., and Wharton, R.A. 1993. Environmental regulators of microbial activity in continental Antarctic lakes. In Green, W.J. and Friedmann, E.I. (Eds.), Physical and Biogeochemical Processes in Antarctic Lakes. Antarctic Research Series 59. American Geophysical Union. Washington D.C.

Simoes, J., Petit, J.R., Souchez, R., Lipenkov, V., Angelis, M. De, Jouzel, J., and Duval, P. 2002. Evidence of glacial flour in the deepest 89 m of the glacier ice from Vostok core. Annals of Glaciology, 35: 340–346.

Sleewaegen, S., Lorrain, R., Offer, Z., Azmon, E., Fitzsimons, S., and Souchez, R. 2002. Trapping of aeolian sediments and build-up of the ice cover of a dry-based Antarctic lake. Earth Surface Processes and Landforms, 27: 307–315.

Sleewaegen, S., Samyn, D., Fitzsimons, S., and Lorrain, R. 2003. Equifinality of basal ice facies from an Antarctic cold-based glacier. Annals of Glaciology, 37: 257–262.

Souchez, R. and Jouzel, J. 1984. On the isotopic composition in δD and δ^{18}O of water and ice during freezing. J. Glaciol., 30(106): 369–372.

Souchez, R., Tison, J.L., and Jouzel, J. 1987. Freezing rate determination by the isotopic composition of the ice. Geophysical Research Letters, 14(6): 599–602.

Souchez, R., Lorrain, R., Tison, J.L., and Jouzel, J. 1988. Co-isotopic signature of two mechanisms of basal-ice formation in Arctic outlet glaciers. Ann. Glaciol., 10: 163–166.

Souchez, R., Lemmens, M., and Chappellaz, J. 1995a. Flow-induced mixing in the GRIP basal ice deduced from the CO_2 and CH_4 records. Geophysical Research Letters, 22: 41–44.

Souchez, R., Tison, J.L., Lorrain, R., Flehoc, C., Stievenard, M., Jouzel, J., and Maggi, V. 1995b. Investigating processes of marine ice formation in a floating ice tongue by a high-resolution isotopic study. Journal of Geophysical Research, 100(C4): 7019–7025.

Souchez, R., Jouzel, J., Lorrain, R., Sleewaegen, S., Steivenard, M., and Verbeke, V. 2000a. A kinetic isotope effect during ice formation by water freezing. Geophysical Research Letters, 27: 1923–1926.

Souchez, R., Petit, J.R., Tison, J.L., Jouzel, J., and Verbeke, V. 2000b. Ice formation in subglacial Lake Vostok, Central Antarctica. Earth and Planetary Science Letters, 181: 529–538.

Souchez, R., Vandenschrick, G., Lorrain, R., and Tison, J.L. 2000c. Basal ice formation and deformation in central Greenland: a review of existing and new ice core data. In Maltman, A., Hubbard, B., and Hambrey, M. (Eds.), Deformation of Glacial Materials, volume 176. Geological Society, London, Special publications, 13–22.

Souchez, R., Jean-Baptiste, P., Petit, J.R., Lipenkov, V., and Jouzel, J. 2002. What is the deepest part of Vostok ice core telling us? Earth Science Reviews, 60: 131–146.

Souchez, R., Samyn, D., Lorrain, R., Pattyn, F., and Fitzsimons, S. 2004. An isotopic model for basal freeze-on associated with subglacial upward flow of pore water. Geophysical Research Letters, 31(L02401): doi: 10.1029/2003GL018861.

Spigel, R.H. and Priscu, J.C. 1998. Physical limnology of the McMurdo Dry Valley lakes. In Priscu, J.C. (Ed.), Ecosystem Dynamics in a Polar Desert: The McMurdo Dry Valleys, Antarctica. Antarctic Research Series 72. American Geophysical Union. Washington D.C, 153–187.

Squyres, S.W., Anderson, S.W., Nedell, S.S., and Wharton, R.A. 1991. Lake Hoare, Antarctica: Sedimentation through a thick perennial ice cover. Sedimentology, 38: 363–379.

Stokes, C.R. and Clark, C.D. 1999. Geomorphological criteria for identifying Pleistocene ice streams. Ann. Glaciol., 28: 67–74.

Studinger, M., Bell, R.E., Karner, G.D., Tikku, A.A., Holt, J.W., Morse, D.L., Richter, T.G., Kempf, S.D., Peters, M.E., Blankenship, D.D., Sweeney, R.E., and Rystrom, V.L. 2003. Ice cover, landscape setting, and geological framework of Lake Vostok, East Antarctica. Earth and Planetary Science Letters, 205: 195–210.

Takahashi, S., Naruse, R., Nishio, F., and Watanabe, O. 2003. Features of ice sheet flow in East Dronning Maud Land, East Antarctica. Polar Meteorol. Glaciol., 17: 1–14.

Terwilliger, J.P. and Dizio, S.F. 1970. Salt rejection phenomena in the freezing of saline solutions. Chemical Engineering Science, 25: 1331–1349.

Testut, L., Hurd, R., Coleman, R., Rémy, F., and Legrésy, B. 2003. Comparison between computed balance velocities and GPS measurements in the Lambert Glacier basin, East Antarctica. Ann. Glaciol., 37: 337–343.

Tison, J.L. 1994. Diamond wire-saw cutting technique for investigating textures and fabrics of debris-laden ice and brittle ice. J. Glaciol., 40(135): 410–414.

Tulaczyk, S.M., Kamb, B., and Engelhardt, H.F. 2000. Basal mechanics of Ice Stream B, West Antarctica. II. undrained-plastic-bed model. J. Geophys. Res., 105(B1): 483–494.

Van der Veen, C.J. and Whillans, I.M. 1989. Force budget: I. theory and numerical methods. J. Glaciol., 35(119): 53–60.

Van der Veen, C.J. 1987. Longitudinal stresses and basal sliding: a comparative study. In Van der Veen, C.J. and Oerlemans, J. (Eds.), Dynamics of the West Antarctic Ice Sheet. Dordrecht, Kluwer Academic Publishers, 223–248.

Van der Veen, C.J. 1989. A numerical scheme for calculating stresses and strain rates in glaciers. Math. Geol., 21(3): 363–377.

Vaughan, D.G., Bamber, J.L., Giovinetto, M.B., Russell, J., and Cooper, A.P.R. 1999. Reassessment of net surface mass balance in Antarctica. J. Climate, 12(4): 933–946.

Vimeux, F., Masson, V., Jouzel, J., Stievenard, M., and Petit, J.R. 1999. Glacial-interglacial changes in ocean surface conditions in the Southern hemisphere. Nature, 398: 410–413.

Vimeux, F., Masson, V., Delaygue, G., Jouzel, J., Petit, J.R., and Stievenard, M. 2001. A 420,000 year deuterium excess record from East Antarctica: Information on past changes in the origin of precipitation at Vostok. Journal of Geophysical Research, 106(D3): 31863–31874.

Weertman, J. 1964. The theory of glacier sliding. J. Glaciol., 5: 287–303.

Wettlaufer, J., Worster, M., Wilen, L., and Dash, J. 1996. A theory of premelting dynaics for all power law forces. Physical Review Letters, 76: 3602–3605.

Wharton, R.A., McKay, C.P., and Simmons, G.M. 1989. Perennially ice covered Lake Hoare, Antarctica: Physical environment, biology and sedimentation. Hydrobiologia, 59: 306–320.

Whillans, I.M. and Van der Veen, C.J. 1997. The role of lateral drag in the dynamics of Ice Stream B, Antarctica. J. Glaciol., 43(144): 231–237.

Williams, M.J.M. 2001. Application of a three-dimensional numerical model to Lake Vostok: An Antarctic subglacial lake. Geophys. Res. Lett., 28(3): 531–534.

Wüest, A. and Carmack, E. 2000. A priori estimates of mixing and circulation in the hard-to-reach water body of Lake Vostok. Ocean Modelling, 2: 29–43.